INTRACELLULAR TRAFFICKING AND PLASMA MEMBRANE

MICRODOMAIN DISTRIBUTION OF THE NSP4 ENTEROTOXIN DURING

ROTAVIRUS INFECTION IN EPITHELIAL CELLS

A Dissertation

by

STEPHEN MICHAEL STOREY

Submitted to the Office of Graduate Studies of
Texas A&M University
in partial fulfillment of the requirements for the degree of

DOCTOR OF PHILOSOPHY

December 2006

Major Subject: Veterinary Microbiology

INTRACELLULAR TRAFFICKING AND PLASMA MEMBRANE

MICRODOMAIN DISTRIBUTION OF THE NSP4 ENTEROTOXIN DURING

ROTAVIRUS INFECTION IN EPITHELIAL CELLS

A Dissertation

by

STEPHEN MICHAEL STOREY

Submitted to the Office of Graduate Studies of
Texas A&M University
in partial fulfillment of the requirements for the degree of

DOCTOR OF PHILOSOPHY

Approved by:

Chair of Committee,	Judith M. Ball
Committee Members,	Friedhelm Schroeder
	Julian Liebowitz
	Ellen W. Collisson
Head of Department	Gerald R. Bratton

December 2006

Major Subject: Veterinary Microbiology

ABSTRACT

Intracellular Trafficking and Plasma Membrane Microdomain Distribution of the NSP4

Enterotoxin During Rotavirus Infection in Epithelial Cells. (December 2006)

Stephen Michael Storey, B.S., Texas A&M University

Chair of Advisory Committee: Dr. Judith M. Ball

Rotavirus (RV) nonstructural protein 4 (NSP4) is a multifunctional glycoprotein that induces secretory diarrhea in mouse pups in the absence of other viral proteins. The intracellular transport route(s) and functional mechanism(s) of NSP4 are poorly understood; however, the recent association of the enterotoxin with cellular caveolin-1 may provide a link between NSP4 transport and function. To determine if NSP4 traffics to a specific subset of lipid rafts at the plasma membrane (PM), we isolated caveolae from a PM-enriched fraction with a new method that yielded endoplasmic reticulum (ER)-free caveolae membranes with a unique membrane structure and composition. Comparison of these caveolae with other detergent- and non-detergent-extracted membranes revealed that each caveolae/raft fraction contained caveolae markers; however, only our PM caveolae fraction mimicked the membrane structure and sterol exchange dynamics of intact PM without ER or non-raft PM contaminants. When these PM caveolae were isolated from RV-infected cells, full-length, high-mannose glycosylated NSP4 was present. Confocal imaging showed association of NSP4 with caveolin-1 moving from perinuclear and cytoplasmic sites toward the PM as the infection progressed. Fluorescent imaging also indicated exposure of the NSP4 C-terminus at the exofacial PM surface without transport of the enterotoxin through the Golgi apparatus. Surface-specific biotinylation was used to confirm NSP4 exposure at the surface of infected MDCK cells and to determine that the exposed protein was full-length and high-mannose glycosylated. This study presents an ER contaminant-free PM caveolae isolation methodology, identifies the presence of full-length, high-mannose

glycosylated NSP4 in both PM caveolae and exposed at the cell surface, and confirms the Golgi-bypassing nature of NSP4 ER to PM transport in RV-infected MDCK cells.

TABLE OF CONTENTS

LIST OF FIGURES

LIST OF TABLES

CHAPTER I

INTRODUCTION

Rotaviruses (RV) cause severe and sometimes fatal pediatric gastrointestinal disease. While the mechanisms underlying RV-induced symptoms have yet to be fully characterized, the identification of RV nonstructural protein 4 (NSP4) as the first viral enterotoxin suggested the possibility of a NSP4-induced secretory diarrhea during infection. The presence of NSP4 in lipid rafts, a foci of cellular signaling events, and direct binding of the enterotoxin to caveolin-1, the key structural and functional protein of the caveolar subset of lipid rafts, indicate a potential mechanism/location for NSP4 function during infection.

RV are significant agents of acute diarrhea in children and animals worldwide. Nearly all children have been affected by RV infection by the age of 5 with 2 million cases of severe gastroenteritis and 440,000 deaths annually (Prashar et al., 2003). With the gastroenteritis-induced dehydration often exacerbated by malnutrition and high incidences of co-infection with other gastrointestinal pathogens, children in developing countries account for approximately 82% of these deaths (Cirlet and Estes, 2001; Farthing, 2000). Association of the first licensed RV vaccine with intussusception, an obstruction of the bowel caused by inversion of one segment within another, resulted in the vaccine's removal from the market (Murphy et al., 2001). The disease burden and problematic vaccine issues have resulted in a continued focus on defining the mechanisms of RV-induced diarrhea. The predominant disease mechanism attributed to RV is malabsorption secondary to enterocyte damage; however a secretory component precedes visible tissue damage during infection (Mebus, 1989; Davidson et al., 1977). Elevated levels of prostaglandin induced by RV infection and calcium (Ca^{2+})-mediated sodium secretion induced by NSP4 provide potential clues about the mechanism of RV secretory diarrhea.

_____

This thesis follows the style of *The EMBO Journal*.

At the molecular level, RV is composed of an 11 double-stranded RNA (dsRNA) segmented genome surrounded by concentric protein shells. Expression of RV proteins from the infecting virions is followed by formation of electron dense regions adjacent to the ER, viroplasms, which function as virion assembly sites. Virion cores containing genomic dsRNA and RV-encoded virion proteins (VP) 1, 2, and 3 are encased in VP6 to produce double-layered particles (DLP) in the viroplasm. These particles bud into the ER, gaining both the RV-glycoprotein VP7 and a transient lipid envelope. The mechanism and subcellular site of the final virion maturation are controversial although the transient membrane is removed and replaced with the third/outer protein shell containing VP4 and 7 resulting in an infectious triple-layered particle (TLP). The RV genome also encodes 5 nonstructural proteins (NSP) of which NSP2, 3, and 5 are involved in formation of the viroplasm. NSP4 however appears to play multiple roles during RV infection.

The loss of NSP4 expression and subsequent reduction in yields of infectious virus progeny as a result of transfecting cells with NSP4 small interfering RNA (siRNA) indicates that the nonstructural protein plays a critical role(s) in production of mature TLP (Cuadras et al., 2006; Lopez et al., 2005). This may be due to the receptor function NSP4 plays at the ER. With C-terminal residues 161-175 binding DLPs, NSP4 mediates the budding of these immature particles through the ER membrane into the ER lumen (Meyer et al., 1989). NSP4 also appears to be associated directly with the viroplasm. Early in infection (7 hours post-infection or hpi) NSP4 colocalizes with the viroplasm marker NSP5 and the cellular autophagosome marker microtubule-associated protein 1 light chain 3 (LC3) (Berkova et al., 2006). LC3 has a cytoplasmic localization until it is modified by C-terminal cleavage and lipidation with phosphatidylethanolamine (PE). Once modified, LC3-PE associated with crescent-shaped, potentially ER-derived pre-autophagic membrane vesicles and remains associated with these membranes until destruction of the mature autolysosome (Kabeye, 2000; Kirkegaard et al., 2004). These membrane crescents engulf cytoplasmic contents and form autophagosomes characterized by concentric membrane bilayers surrounding the engulfed material.

Subsequent fusion with lysosome-associated membrane protein (LAMP) 1 and 2-containing endosomes and/or lysosomes results in mature autolysosomes. As NSP4 does not colocalize with LAMP-1, the nonstructural protein is likely associated with either pre-autophagosome membranes or enclosed autophagosomes. While the function of this interaction is still unknown, a similar interaction occurring during polio virus infections has been hypothesized to provide a membrane surface for assembly of the polio virus genomic RNA and virion proteins (Suhy et al., 2000; Lyle et al., 2002). Alternately, down-stream effects of cellular dsRNA-activated protein kinase activation include alteration of cellular translation, apoptosis, and autophagy (Williams, 2001; Talloczy et al., 2002). NSP4 interaction with LC3-positive membranes could protect virion/viroplasm assembly by inhibiting the fusion of the viroplasm-associated autophagic membranes with lysosomes thus avoiding the cellular antiviral response.

NSP4 has also been shown to be transported towards the cell periphery via a Golgi-bypassing mechanism. In NSP4 transfected COS-7 cells, the nonstructural protein redistributes and colocalizes with the ER to Golgi intermediate compartment (ERGIC) marker protein ERGIC-53 and the COP-I-positive transport vesicle marker protein beta-COP (Xu et al., 2000). These proteins colocalize along linear, microtubule-associated tracts that radiate out from the perinuclear area toward the periphery of the cell. In this system, the expressed NSP4 remains glycosylated with EndoH-sensitive glycans suggesting that its carbohydrates have not been processed by Golgi-specific enzymes. In NSP4-enhanced green fluorescent protein (EGFP) transfected HEK293 cells, the nonstructural fusion protein colocalizes with ER-specific marker proteins and is present at the cell periphery, but not within the plane of the PM (Berkova et al., 2006). As with the NSP4 transport in COS-7 cells, the lack of NSP4 colocalization with the Golgi marker protein giantin in HEK293 cells indicates that NSP4 transport to the cell periphery from the ER bypasses the Golgi apparatus. In addition, the punctate pattern of NSP4-EGFP staining and its sensitivity to extracellular Triton X-100 treatment suggest that NSP4 transport to the cell periphery is mediated by a vesicular mechanism. While NSP4 was not found in the PM of transfected cells, a C-terminal NSP4 fragment (aa

112-175) is released from RV-infected MA104 and HT-29 cells (Zhang et al., 2000). The nocodazole-sensitivity and brefeldin A-insensitivity of this secretion suggests that NSP4 ER to PM transport during infection is microtubule-dependent and Golgi-bypassing, respectively.

The ability of NSP4 to induce diarrhea in mouse pups in the absence of other viral proteins indicates that the nonstructural protein can also function as a viral enterotoxin. Exogenous addition of NSP4 or a synthetic NSP4 aa 114-135 peptide to uninfected mouse pups and pup intestinal epithelia induced diarrhea and fluid accumulation with chloride secretion, respectively (Ball et al., 1996). Addition of purified NSP4 to HT-29 cells induces a rapid rise in phospholipase C (PLC)-catalyzed inositiol 1,4,5-triphosphate production resulting in an increased cytoplasmic Ca^{2+} concentration through mobilization of intracellular Ca^{2+} stores and increased Ca^{2+} influx (Dong et al., 1997). Pretreatment of these cells with trypsin or chymotrypsin eliminates the NSP4-induced Ca^{2+} mobilization suggesting that the enterotoxin reacts with an unidentified receptor at the PM. In addition, blocking phosphatidylinositol 4,5-bisphosphate (PIP2) hydrolysis by PLC with U-73122 also results in a loss of the Ca^{2+} mobilization induced by exogenous NSP4. However, in the NSP4-EGFP-transfected HEK293 cells previously described, U-73122 did not block the enterotoxin-induced cytoplasmic Ca^{2+} increase (Berkova et al., 2003). Though both exogenous and endogenous NSP4 result in increased levels of cytoplasmic Ca^{2+}, differences in the underlying signaling mechanisms suggest a unique aspect to the protein's enterotoxic function. The sensitivity of the enterotoxin's presence at the cell periphery to Triton X-100, the identification of NSP4 in Triton X-100-resistant lipid rafts, and the binding of NSP4 and caveolin-1 suggest a unique connection between NSP4-induced signaling and the protein's peripheral localization.

Lipid rafts are membrane microdomains initially defined by their isolation via detergent-insolubility at $4^{o}C$ and light buoyant density on sucrose gradients (Simons and Ikonen, 1997). To determine their makeup, these isolated microdomains have been extensively analyzed for both protein and lipid composition. From these studies a unique

lipid composition was identified for these detergent-resistant membranes (DRM) with an increased concentration of cholesterol, sphingomyelin, and glycolipids relative to the lipids' homogenate levels (Smart et al., 1999). Caveolae are a subset of lipid rafts initially characterized as flask-shaped PM invaginations, but now defined by the presence of the cholesterol-binding caveolin proteins (Murata et al., 1995). While the caveolin proteins provide a marker for determining the enrichment of caveolae in an isolated membrane fraction, comparable non-caveolar raft markers are unavailable. This disparity has led to a wide range in caveolae definitions and a large volume of lipid raft/DRM compositional analysis that is not necessarily applicable to caveolae. A variety of proteins have been found in these membranes including the caveolins, flotillins, glycosylphosphatidylisonitol (GPI)-linked proteins, endothelial nitric oxide synthase, and several cell signaling proteins (Pike, 2003; Pike, 2004; Anderson, 1998). The partitioning of PIP2, IP3-receptors, and the PM Ca^{2+} pump into rafts/caveolae suggest that these microdomains may function in Ca^{2+}-mediated signaling and cellular Ca^{2+} homeostasis (Fujimoto et al., 1992; Fujimoto, 1993; Hope and Pike, 1996; Pike and Casey, 1996). While the enrichment of lipid rafts in arachidonic acid appears to be independent of caveolin-1 expression, cyclooxygenase-1 (COX-1), whose function is essential in arachidonic acid conversion to prostaglandin, is present in isolated raft/caveolae membranes, coimmunoprecipitates with the caveolin protein, and colocalizes with the caveolin protein in HEK293 cells (Pike et al., 2002; Marnett et al., 1999; Cha et al., 2004). This is of particular interest for RV infection as infection of Caco-2 cells increases prostaglandin secretion and inhibition of COX-1 function reduces infection by 85% as assayed by foci reduction with anti-RV immunofluorescent assay (Rossen et al., 2004). Also of interest is the intracellular ER to PM trafficking of caveolin-1. Two distinct pathways have been defined experimentally: in a soluble caveolin-1-containing complex and via membrane trafficking following the secretory transport pathway to the trans Golgi network (TGN) where caveolin-1 buds in caveolae-like vesicles for subsequent transport to the PM. The soluble complex, composed of caveolin, heat shock protein 56, cyclophilin 40, cyclophilin A, and cholesterol,

transports newly synthesized cholesterol directly from the ER to PM caveolae (Uittenbogaard et al., 1998).

Biosynthesis of sphingomyelin in the early Golgi and its segregation with cholesterol results in the genesis and clustering of lipid rafts in the TGN (van Vliet et al., 2003). At the TGN, caveolin-1 associates with these clustering rafts and buds in a caveolae-like vesicle which traffics to the PM. With synthesis of both sphingomyelin and lipid rafts in the Golgi, it is unknown if rafts or mature caveolae are present in the ER. Anterograde movement of Golgi-derived caveolin-1-containing raft-like vesicles has not been documented, but recycling of caveolin-1 in caveolae internalized at the PM to the ER through the caveolae to ER to Golgi (CERGA) pathway and internalization via a chaperone complex with annexin II, cyclophilin 40, cyclophilin A, and HDL-derived cholesteryl ester has been observed (Liu et al., 1999; Uittenbogaard et al., 2002). The association of RV virions and NSP4 with lipid rafts, the colocalization and binding of NSP4 with caveolin-1, and the absence of RV proteins in the Golgi suggest a unique and potentially caveolin-1/caveolae-mediated transport pathway for the virus and/or NSP4. To define the function of NSP4 interaction with caveolin-1 and potentially caveolae, the enterotoxin's presence and microdomain distribution at the PM as well as its intracellular trafficking mechanism must first be characterized.

CHAPTER II
STRUCTURE AND CHOLESTEROL DYNAMICS OF CAVEOLAE/RAFT AND NON-RAFT PLASMA MEMBRANE DOMAINS

SYNOPSIS

Despite recognition that the plasma membrane (PM) is comprised of lipid raft domains that are key organizing sites of multiple signaling pathways and other cell functions, limited information is available regarding the structure and function in sterol dynamics of these microdomains. To begin to resolve these issues, Madin Darby Canine Kidney (MDCK) membranes were subfractionated by three different techniques to obtain: (i) detergent-resistant membranes (DRM) and detergent-soluble membranes (DSM), (ii) non-detergent caveolae/rafts (NDCR), (iii) non-detergent, affinity-purified caveolae/rafts (ACR) and non-caveolae/non-rafts (NR). ACR exhibited the least cross-contamination with other PM domains or intracellular membranes, in marked contrast to DRM that contained the highest level of cross-contaminants. Spectral properties of dehydroergosterol (DHE), a naturally-occurring fluorescent sterol, showed that ACR, NDCR, and NR did not contain crystalline sterol—consistent with the lack of crystalline sterol in PM of intact cells. In contrast, DRM contained significant levels of crystalline sterol. Fluorescence polarization of membrane probes showed that ACR were the least fluid, had the highest transbilayer fluidity gradient, most liquid ordered phase, and most responsive sterol dynamics to sterol carrier protein-2 (SCP-2). In contrast, DRM had structural properties similar to those of NR, anomalous (very fast) spontaneous sterol dynamics, and sterol-dynamics unresponsive to SCP-2. Differences in the DRM structural and functional properties when compared to the non-detergent preparations (ACR, NDCR) were not due to the presence of detergent. A non-detergent, affinity purified (ACR) lipid domain fraction isolated from MDCK cells for the first time revealed unique structural (non-crystalline sterol, liquid-ordered, high transbilayer fluidity gradient) and functional (cholesterol dynamics) properties of lipid rafts as compared to non-rafts (NR). In summary, this study showed membrane microdomains

(rafts/caveolae) isolated by three different methodologies have unique structural, functional and organizational characteristics.

INTRODUCTION

Despite recognition that the plasma membrane (PM) is comprised of lipid raft domains that are key organizing sites of multiple signaling pathways and other cell functions, limited information is available regarding the structure and function in sterol dynamics of these microdomains. To begin to resolve these issues, MDCK membranes were subfractionated by three different techniques to obtain: (i) detergent-resistant membranes (DRM) and detergent-soluble membranes (DSM), (ii) non-detergent caveolae/rafts (NDCR), (iii) non-detergent, affinity-purified caveolae/rafts (ACR) and non-caveolae/non-rafts (NR). ACR exhibited the least cross-contamination with other PM domains or intracellular membranes, in marked contrast to DRM that contained the highest level of cross-contaminants. Spectral properties of dehydroergosterol (DHE), a naturally-occurring fluorescent sterol, showed that ACR, NDCR, and NR did not contain crystalline sterol - consistent with the lack of crystalline sterol in PM of intact cells. In contrast, DRM contained significant levels of crystalline sterol. Fluorescence polarization of membrane probes showed that ACR were the least fluid, had the highest transbilayer fluidity gradient, most liquid ordered phase, and most responsive sterol dynamics to sterol carrier protein-2 (SCP-2). In contrast, DRM had structural properties similar to those of NR, anomalous (very fast) spontaneous sterol dynamics, and sterol-dynamics unresponsive to SCP-2. Differences in the DRM structural and functional properties when compared to the non-detergent preparations (ACR, NDCR) were not due to the presence of detergent. A non-detergent, affinity purified (ACR) lipid domain fraction isolated from MDCK cells for the first time revealed unique structural (non-crystalline sterol, liquid-ordered, high transbilayer fluidity gradient) and functional (cholesterol dynamics) properties of lipid rafts as compared to non-rafts (NR). In summary, this study showed membrane microdomains (rafts/caveolae) isolated by three

different methodologies have unique structural, functional and organizational characteristics.

Increasing evidence indicates that cholesterol-rich domains/lipid rafts provide a nexus for organizing not only reverse cholesterol transport (Frolov et al., 2000; Smart, 2005)*,* but also many physiological processes at the plasma membrane (PM), including receptor-effector coupling, signaling, immune function, transcytosis, and cell recognition (Schroeder et al., 2005). Cholesterol-rich lipid rafts/caveolae also serve as entry portals for microorganisms, including bacteria (and associated toxins such as cholera toxin, Shiga toxin, Shiga-like toxin), viruses (for example Ebola, Marburg, Echovirus, and HIV), and parasites (malaria) (Schroeder et al., 2005).

Despite the putative importance of cholesterol-rich domains/lipid rafts in cellular function, their existence in the PM of living cells has only recently been addressed. A variety of techniques using tagged proteins or tagged lipids have been utilized to visualize lipid rafts enriched in the respective markers (Schroeder et al.., 2005), yet these studies have failed to directly visualize sterol in the PM. Recent studies utilizing real-time multiphoton imaging and pattern distribution analyses of dehydroergosterol (DHE) for the first time detect the existence of sterol-rich and –poor domains/rafts in the PM of living cells (McIntosh et al., 2003; Zhang et al., 2005). Although it is recognized that DHE is not identical to cholesterol, DHE is a naturally-occurring fluorescent sterol (yeast, Red Sea sponge), readily replacing endogenous sterol in cultured cells, and exhibiting structural as well as functional properties closely resembling those of cholesterol (McIntosh et al., 2003; Schroeder, 1984; Schroeder and Nemecz, 1990; Schroeder et al., 1991; Schroeder et al., 1996; Hale and Schroeder, 1982; Delseth et al., 1979; Sica et al., 1982; Schroeder et al., 2001a; Bergeron and Scott, 1982a and 1982b; Gimpl and Fahrenholz, 2000). Thus, it would appear that cholesterol-rich rafts do exist in living cells and are not just an artifact induced by subcellular fractionation protocols or non-physiological probe molecules.

Elucidation of the biochemical and structural characteristics of cholesterol-rich domains/lipid rafts also has been difficult. To date the majority of biochemical characterizations have been performed on detergent-resistant membrane (DRM)-enriched fractions and there remain concerns as to whether DRM equate with lipid rafts as well as whether such domains reflect the biological nature of intact cells (Skwarek, 2004; Schnitzer et al., 2003; Foster et al., 2003). Fluorescence probes indicate that the physical state of lipids in DRM isolated from model membranes is in a liquid ordered state, intermediate between the liquid crystalline and gel states (Schroeder et al., 2005; McIntosh et al., 2003; Zhang et al., 2005). Likewise, fluorescence and electron spin resonance techniques show that the lipids of DRM isolated from cultured cells are also in a liquid ordered state (Ge et al., 1999). Although the liquid ordered state is not due to the presence of detergents within the DRM, detergent extraction itself may induce the formation of the liquid ordered state (Skwarek, 2004; Schnitzer et al., 2003). Despite the limitations of DRM, however, this approach has focused attention on and significantly contributed to our understanding of lipid rafts, as evidenced by the appearance of a great number of publications using this technique over the past decade. Simultaneous to the development of DRM, other investigators focused on techniques avoiding the use of detergents (Schroeder et al., 2005; Smart et al., 1995), yet almost nothing is known regarding the structural or functional properties of these preparations. To date only a single report has appeared examining the physical structure of lipids in lipid rafts isolated without the use of detergents (Gallegos et al., 2004). The latter study showed that lipid rafts isolated from L-cell fibroblasts using a classical non-detergent method (Smart et al., 1995) are in a liquid ordered state. While the physiological significance of these observations to intact cells is not completely clear, a recent study using two-photon microscopy of a synthetic fluorescent molecule (Laurdan) revealed microscopically-visible liquid ordered lipid domains in macrophages and fibroblasts in culture (Gaus et al., 2003). The size of the liquid ordered domains (183-800 nm) detected by Laurdan in PM of living cells is in the same range as the size of sterol-rich domains imaged by three-photon microscopy of DHE (Zhang et al., 2005).

Despite reports that cholesterol-rich domains have important functions in reverse cholesterol transport (Smart et al., 2005; Schroeder et al., 2005; McIntosh et al., 2003), little is known regarding structure, cholesterol dynamics and cholesterol responsiveness to intracellular cholesterol binding proteins (e.g. sterol carrier protein-2). To begin to address these questions, four types of lipid domain fractions were isolated from MDCK cells: DRM obtained with Triton X-100, non-detergent caveolae/rafts (NDCR), non-detergent affinity-purified caveolae/rafts (ACR), and non-caveolae/non-raft (NR).

RESULTS

Purification of Caveolae/Raft Enriched Plasma Membrane Fractions: Detergent Resistant Membranes (DRM), Non-Detergent Caveolae/Raft Domains (NDCR), and Affinity-Purified Caveolae/Raft Domains (ACR). Western blotting and densitometric analysis of DRM (Fig. 1A, top row) indicated that the DRM (lane 3) were enriched nearly 10- and 4.3-fold in caveolin-1, a caveolae/raft marker, as compared to MDCK cell homogenate (lane 1) and detergent-soluble membranes (DSM, lane 2), respectively. The DRM fraction exhibited low contamination with calnexin, a marker for ER (Fig. 1C, top row), which was reduced 2.5-fold and 1.6-fold (lane 3) as compared to that in the MDCK cell homogenate (lane 1) and DSM fraction (lane 2). In contrast, DRM were slightly enriched 1.2-fold in the non-raft (NR) PM marker Na^+/K^+ ATPase (Fig. 1B, top row) as compared to MDCK cell homogenate (lane 1) and enriched nearly 10-fold when compared to DSM (lane 2). Thus, although DRM appeared enriched in caveolae/raft marker, they also contained endoplasmic reticulum (ER) contaminant and essentially no diminution of the NR PM domain marker.

DSM (Fig. 1A, top row, lane 2) contained 4.3-fold less caveolin-1 than the DRM fraction isolated from MDCK cells (lane 3). It was noted that two distinct and as yet uncharacterized, forms of caveolin-1 found in all membrane fractions analyzed, potentially due to a difference in prosphorylation state. The DSM fraction had 1.6-fold less ER marker calnexin (Fig. 1 C, top row, lane 2) than the MDCK cell homogenate (lane 1). However, the DSM contained 8- and 10-fold less NR marker Na^+/K^+ATPase

(Fig. 1B, top row, lane 2) than the MDCK cell homogenate (lane 1) and DRM (lane 3). Thus, DSM appeared depleted of caveolae/raft marker as compared to DRM, but they had also lost the NR marker Na^+/K^+ ATPase.

Western blotting and densitometric analysis indicated that NDCR (Fig. 1A, middle row) were enriched 1.4-fold in caveolin-1 as compared to MDCK cell homogenate (lane 1). In confirmation, dot blotting and densitometric analyses showed that NDCR (Fig. 1D, middle row) were enriched 1.9-fold in GM1 as compared to MDCK cell homogenate (lane 1). However, response to anti-calnexin antisera (Fig. 1 C, middle row) indicated essentially the same content of this ER marker in NDCR (lane 3) as in MDCK cell homogenate (lane 1). Finally, the Na^+/K^+ATPase marker (Fig. 1B, middle row) was enriched 3.7- and 3.7-fold in NDCR domains (lane 3) as compared to MDCK cell homogenate (lane 1) and in unfractionated PM (lane 2). Thus, the NDCR were enriched in the caveolae/raft marker, but exhibited no reduction in ER contaminant or NR marker as compared to the unfractionated PM or cell homogenate.

Western blotting and densitometric analysis of caveolae/rafts isolated by use of the detergent-free Concanavalin A-sepharose affinity chromatography (i.e. ACR) revealed a caveolae/raft enriched fraction. Anti-caveolin-1 western blotting (Fig. 1A, bottom row) detected caveolin-1 in the ACR isolated from MDCK cells (lane 4). While this was congruent with the ACR fraction being caveolae/rafts, the ACR was not specifically enriched in caveolin-1, most likely due to the presence of high amounts of caveolin-1 in other cellular compartments (e.g. cytoplasmic chaperone complexes, etc.). In contrast, anti-GM1 dot blotting (Fig. 1E) showed that the ACR isolated from MDCK cells were enriched about 2.7-fold in GM1 (lane 3). In contrast, the ER marker, calnexin (Fig. 1C, bottom row, lane 3) and the NR PM domain marker, Na^+/K^+ ATPase (Fig. 1B, bottom row, lane 3) were not detectable in the ACR. Thus, the ACR contained in appropriate caveolae/lipid raft markers and, in contrast to DRM and NDCR, were significantly reduced in ER and non-caveolae/non-raft PM markers.
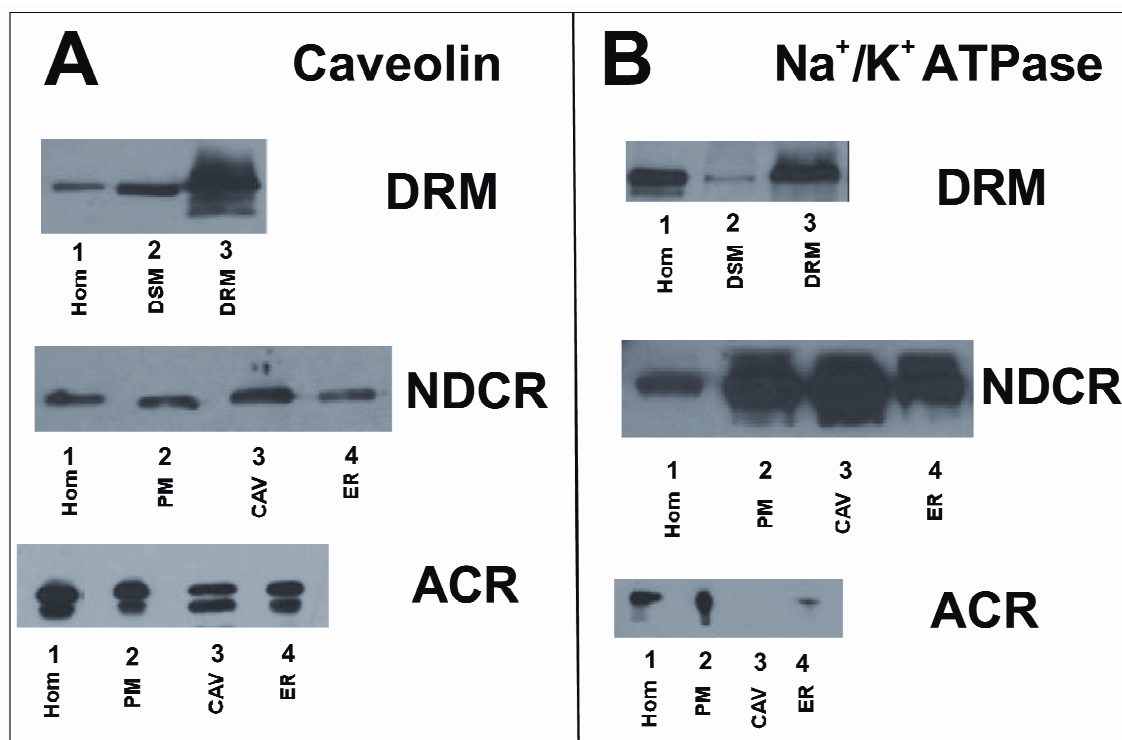
Fig 1. Western Blotting of Protein Markers in Caveolae/Lipid Raft Preparations. Immunoblots were probed with (**A**) anti-caveolin-1, a marker for caveolae, or (**B**) anti-Na$^+$/K$^+$ ATPase, a non-caveolae/non-raft marker. Cell homogenate (homog), detergent-soluble membranes (DSM), detergent-resistant membranes (DRM) (upper row, lanes 1-3 respectively), homog, PM, non-detergent caveolae/rafts (NDCR), ER (middle row, lanes 1-4 respectively), and homog, PM, affinity-purified caveolae/rafts (ACR), ER (lower row, lanes 1-4 respectively) were loaded at 5 μg of total protein per lane.
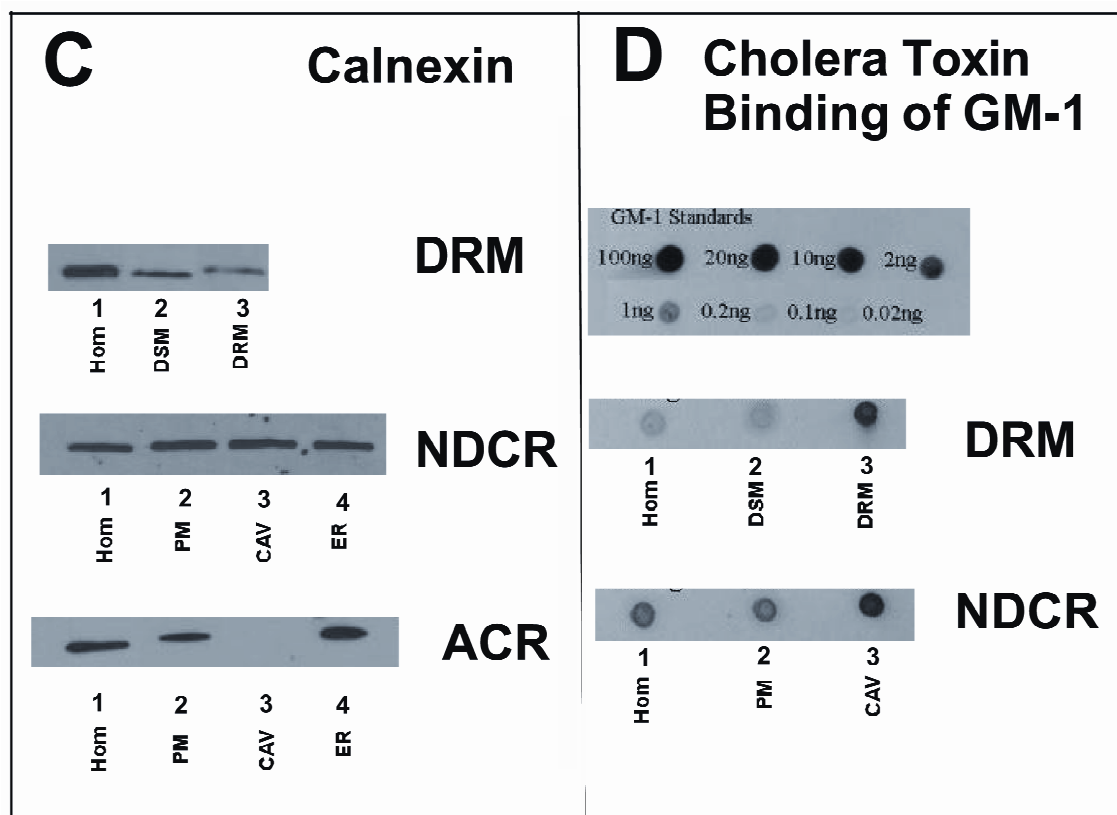
Fig 1. cont. Immunoblots were probed with (**C**) anti-Calnexin, an endoplasmic reticulum marker. For panel C, the cell homogenate (homog), detergent-soluble membranes (DSM), detergent-resistant membranes (DRM) (upper row, lanes 1-3 respectively), homog, PM, non-detergent caveolae/rafts (NDCR), ER (middle row, lanes 1-4 respectively), and homog, PM, affinity-purified caveolae/rafts (ACR), ER (lower row, lanes 1-4 respectively) were loaded at 5 µg of total protein per lane. Panel D shows a dot-blot probed with cholera toxin B subunit (CTB) and anti-CTB, for the caveolae marker ganglioside M1 (GM-1). The GM-1 standards (upper rows) for homog, DSM, and DRM (middle row, spotted respectively) as well as the homog, PM, and NDCR (lower row, spotted respectively) are the same, yielding a curve fit of $r^2 = 0.995$.

E   Cholera Toxin Binding of GM-1

GM-1 Standards

100 ng   20 ng   10 ng   2 ng

1 ng   0.2 ng   0.1 ng   0.02 ng

1   2   3   **ACR**

Hom   PM   CAV
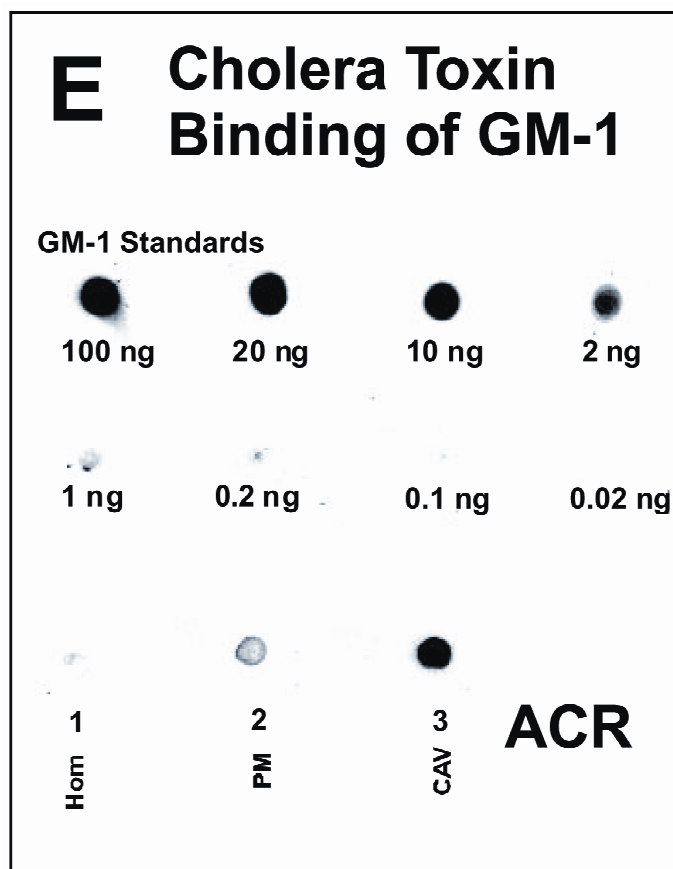
Fig. 1 cont. Panel E also shows a dot-blot probed with cholera toxin B subunit (CTB) and anti-CTB, for the caveolae marker ganglioside M1 (GM-1).GM-1 standards (upper rows) for the homog, PM, and ACR (lower row spotted respectively) were performed separately, but also resulted in a curve fit of $r^2 = 0.995$.

In summary, western blotting and dot blotting of protein markers indicated that the ACR fraction contained the appropriate caveolae/raft markers while concomitantly

being lowest in non-raft markers of any fraction examined.

Sterol Structural Properties in Caveolae/Rafts Enriched Membrane Fractions: DHE. We and others have shown that DRM, NDCR, and membranes similar to ACR are highly enriched in cholesterol (Smart et al., 1995; Gallegos et al., 2004; Atshaves et al., 2003; Eckert et al., 2003; Pike et al., 2002). Although model membrane studies suggest that at such high cholesterol contents the cholesterol may separate into a crystalline phase (McIntosh et al., 2003), little is known regarding the structural phase properties of the cholesterol within DRM or the non-detergent isolates of caveolae/raft domains. Therefore, the fluorescence emission spectral differences in monomeric (maxima near 356 and 375 nm) vs. crystalline (maxima near 403 and 426 nm) DHE phase (McIntosh et al., 2003) were used to determine structural properties of sterol in DRM, NDCR, and ACR. The fluorescence emission spectra of DHE in DRM exhibit highest intensity maxima near 356 and 375 nm, consistent with the presence of monomeric DHE (Fig. 2A). However, additional maxima with approximately half the intensity are noted in the range of 400-453nm, indicating the presence of significant amounts of DHE in the crystalline phase in DRM (Fig. 2A). Taking into account the relative differences in quantum yield, the proportion of crystalline DHE was calculated as described earlier (McIntosh et al., 2003), showing that 7-10% of the sterol within the DRM was in the crystalline state while 90-93% was in the monomeric state. In contrast, the spectra of DHE in the NDCR (Fig. 2B) and ACR (Fig. 2C) exhibited only the emission maxima consistent with the presence of monomeric sterol with no detectable crystalline sterol.
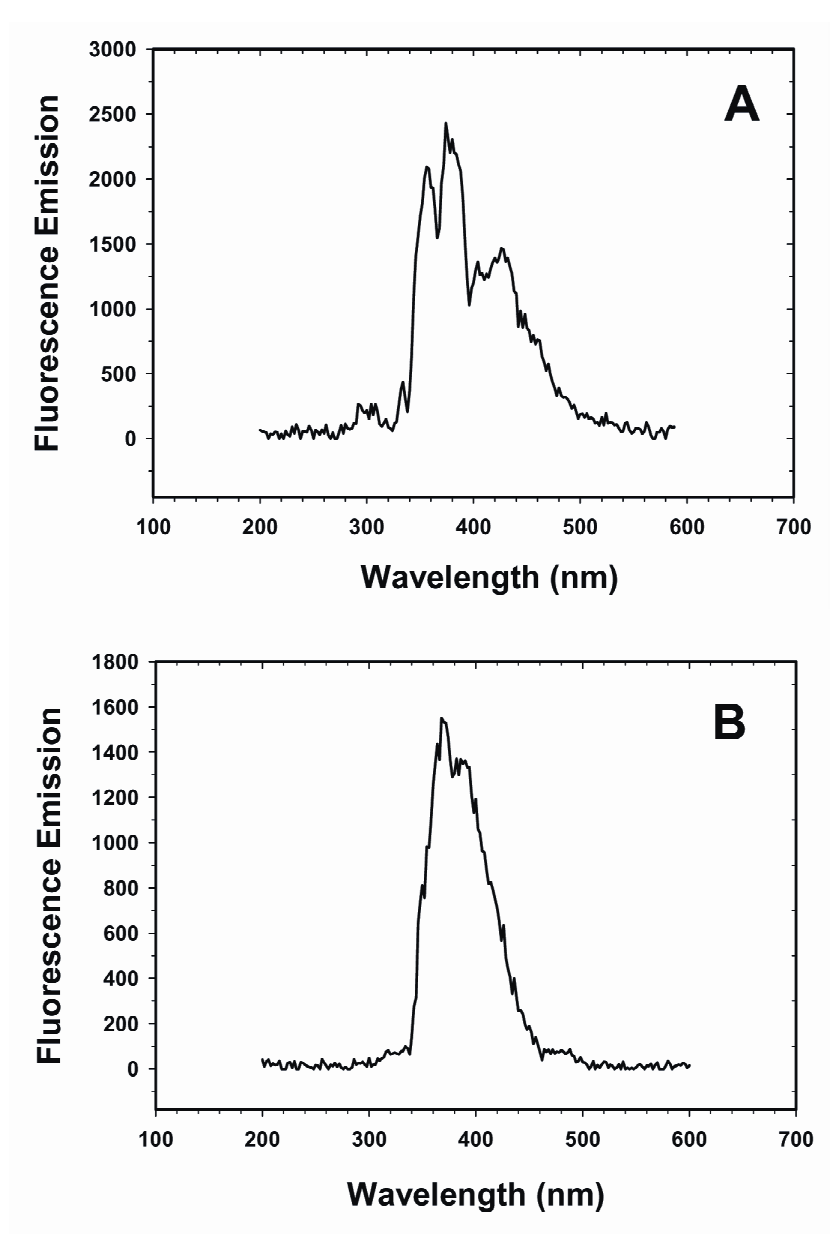
Fig. 2. Fluorescence Emission Spectra of Dehydroergosterol (DHE) in DRM and Caveolae/Raft Enriched Fractions. (**A**) Emission spectrum of DRM in PIPES buffer (3.5 μg/2 ml). Excitation wavelength was set at 320 nm. (**B**) Emission spectrum of non-detergent caveolae/lipid rafts in PIPES buffer (3.5 μg /2 ml). Excitation wavelength was set at 324 nm.
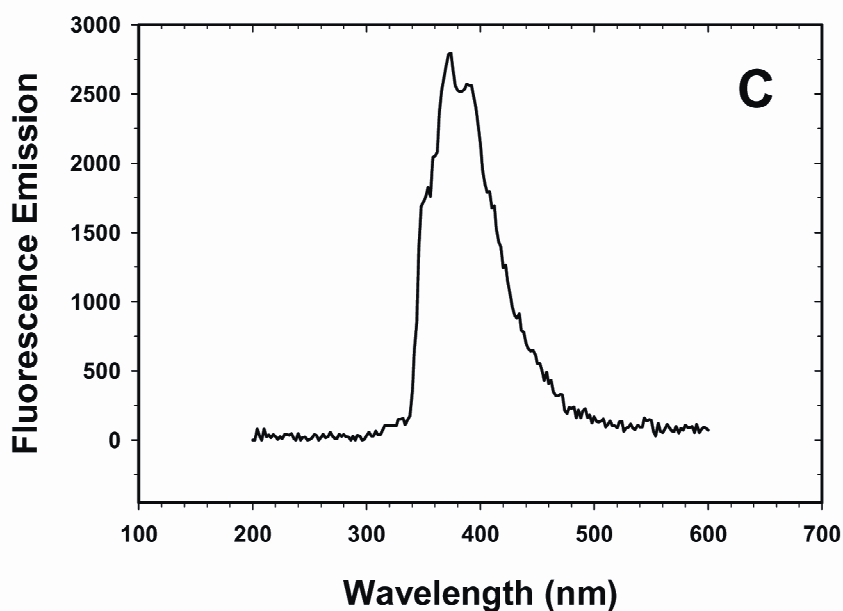
Fig. 2 cont. (**C**) Emission spectrum of affinity-purified caveolae/lipid rafts in PIPES buffer (3.5 μg/2 ml). Excitation wavelength was set at 324 nm.

To determine the relative fluidity of the microenvironment wherein the sterol resided in the DRM, NDCR, and ACR, the fluorescence polarization of DHE (present at low, non-self quenching concentration) was determined. The fluorescence polarization of DHE in DRM was 0.3120 ± 0.0011, significantly ($p<0.05$) lower than that of DHE in NDCR and ACR (Table 1). In contrast, the fluorescence polarization of DHE in DRM, NDCR, and ACR were all significantly higher than in NR.

These data indicated the bulk of DRM sterols are present in a mobile, less ordered microenvironment in spite of the presence of significant amounts (7-10%) of crystalline sterol. Further, the rank order of DHE fluorescence polarization was: ACR (most rigid) > NDCR > DRM > NR (most fluid). Since 'mobility' is inversely proportional to polarization, the sterol mobility was lowest not in the DRM, but in the preparations not utilizing detergents, in particular ACR. In summary, these data showed that sterol organization of caveolae/lipid rafts is highly dependent on the method of isolation.

Fluorescence Polarization of Other Lipidic Probe Molecules That Preferentially Localize in Lipid Rafts: DiI C_{18} vs. DiI C_1. To confirm whether the higher fluidity sensed by DHE in DRM was unique to this probe, fluorescence polarization studies were performed with DiI probes, in particularly DiI $C_{18,}$ which partitions preferentially into lipid rafts (Thomas et al., 1994). The fluorescence polarization of the long alkyl chain length DiI C_{18} exhibited the following order of fluorescence polarization: ACR>NDCR>DRM>NR (Table 1). Thus, while the fluorescence polarization of the long alkyl chain length DiI C_{18} was significantly higher in DRM than in NR, nevertheless it was significantly lower than either of the other lipid raft preparations, i.e. NDCR or ACR (Table 1). Unlike DiI $C_{18,}$ which is anchored deep in the bilayer, the short alkyl chain DiI C_1 is anchored close to the phospholipid head group/water interface and does not show preference for lipid rafts vs. non-raft domains in lipid bilayers (Thomas et al., 1994). Nevertheless, the overall pattern of DiI C_1 fluorescence polarization in the membrane fractions was basically similar to DiI C_{18} (Table 1).

Taken together, both the lipid raft selective DiI C_{18} and the non-selective DiI C_1 indicated that the acyl chain environments (both deep in the bilayer and closer to the surface, respectively) of the PM ACR domains was the most rigid while the NR domains were the most fluid, with the DRM and other non-detergent caveolae/raft preparations being intermediate. This pattern was very similar to that exhibited by DHE in the various membrane domain preparations shown in the preceding section. Thus, the highest polarization/rigidity obtained was characteristic of the most highly purified caveolae/raft fractions, i.e. ACR > NDCR > DRM.

Table 1. Structural Parameters of Lipidic Probes That Preferentially Distribute in Caveolae/Raft Domains: Dehydroergosterol (DHE) and DiI.[a]

Membrane	Polarization[b]
DHE	
DRMs	$0.3120 \pm 0.0011^{+}$
non-detergent caveolae/rafts	$0.3343 \pm 0.0021 *^{+}$
affinity-purified caveolae/rafts	$0.3472 \pm 0.0019*^{+}$
non-caveolae/non-rafts	$0.3078 \pm 0.0041 *$
DiI C_{18}	
DRMs	$0.3381 \pm 0.0032^{+}$
non-detergent caveolae/rafts	$0.3428 \pm 0.0040*^{+}$
affinity-purified caveolae/rafts	$0.3479 \pm 0.0029*^{+}$
non-caveolae/non-rafts	$0.3257 \pm 0.0053 *$
DiI C_{1}	
DRMs	$0.3379 \pm 0.0023^{+}$
non-detergent caveolae/rafts	$0.3397 \pm 0.0017^{+}$
affinity-purified caveolae/rafts	$0.3466 \pm 0.0037*^{+}$
non-caveolae/non-rafts	$0.3255 \pm 0.0046*$

[a] Lipids were incorporated at low, non-self quenching levels into purified membrane fractions as described in Methods.
[b] Fluorescence polarization values represent the mean $\pm$ SD (n=7)
* $p < 0.05$ vs. DRMs
+ $p < 0.05$ vs. non-caveolae/non-rafts

Fluorescence Polarization of Probe Molecules That Preferentially Distribute in 'Solid/Gel' or 'Fluid/Liquid-Crystalline' Lipid Phases: Parinaric acids, NBD-stearic acid, DiI C18. Long (i.e. 18 carbon) straight chain lipidic fluorescence probes such as *trans*-parinaric acid or NBD-stearic acid, as well as DiI_{18} preferentially partition into solid gel-phases rather than fluid liquid-crystalline phases in the lateral plane of the lipid bilayer (Schroeder and Soler-Argilaga, 1983; Spink et al., 1990). C*is*-parinaric acid exhibits no selectivity for either phase.

All the straight-acyl chain fatty acid probes (i.e. *trans*-parinaric acid, NBD-stearic acid) detected the same or even lower fluorescence polarization in DRM than in NR domains (Table 2). In contrast, fluorescence polarizations of the two straight-chain fatty acid probes [i.e. *trans*-parinaric acid, NBD-stearic acid (Table 2)] were significantly lower ($p<0.05$) in DRM than in NDCR or ACR. For the kinked-acyl chain probe, *cis*-parinaric acid (Table 2), fluorescence polarization pattern in the various membrane fractions was in the order: ACR > NDCR > DRM > NR ($p<0.05$). Comparison of the fluorescence polarization of *cis*-parinaric acid and *trans*-parinaric acid (Table 2) showed that in general the fluorescence polarization of *cis*-parinaric acid was lower than that of *trans*-parinaric acid in the same membrane fraction. This was consistent with the fact that *cis*-parinaric acid exhibits equal selectivity for either solid/gel or fluid liquid-crystalline phases. Since polarization is lower in fluid liquid-crystalline phases, the average polarization of *cis*-parinaric acid was predicted to be lower than that of *trans*-parinaric acid in solid/gel phases. The data supported this prediction.

In summary, qualitative analysis of fluorescence polarization for the straight-chain 18-carbon straight-chain fluorescent fatty acid probes did not detect higher polarization in DRM vs. NR domains. While the kinked-chain *cis*-parinaric acid detected slightly higher polarization in DRM vs. NR domains, this polarization was still much lower than that in ACR. Thus, in general the fluorescence polarization the respective probes was dependent on the type of membrane fraction examined in the order: ACR (least fluid) > NDCR > DRM $\geq$ NR (most fluid).

Fluorescence Polarization and Emission Intensity of Diphenylhexatriene (DPH). The above polarization data (Tables 1 and 2) suggested that: (i) both gel- and liquid-crystalline phases were more rigid in ACR, NDCR, and DRM; and/or (ii) the probes sensed an intermediate lipid phase enriched in the various lipid raft preparations as compared to NR. This possibility was further examined through use of DPH, a probe molecule that preferentially distributes in and detects the 'intermediate liquid ordered' lipid phase. Since DPH has no preference for coexisting in gel vs. fluid liquid-

crystalline phases, the fluorescence polarization of DPH has been used to show the extent to which acyl chains in caveolae isolated by use of detergents (DRM) are organized in the liquid-ordered phase (Florine-Casteel and Feigenson, 1988; London and Brown, 2000; Simon and Vas, 2004).

Table 2. Lateral Structure of Caveolae/Raft Domains and Plasma Membrane: Selectively Probing 'Solid' Vs. 'Fluid' Domains with *Trans-* and *Cis-* Fatty Acids.[a]

Membrane	Polarization[b]
Trans-parinaric Acid	
DRMs	0.3267 ± 0.0036
non-detergent caveolae/rafts	0.3398 ± 0.0016*[+]
affinity-purified caveolae/rafts	0.3416 ± 0.0019*[+]
non-caveolae/non-rafts	0.3245 ± 0.0022
Cis-parinaric Acid	
DRMs	0.3076 ± 0.0014[+]
non-detergent caveolae/rafts	0.3201 ± 0.0016*[+]
affinity-purified caveolae/rafts	0.3429 ± 0.0013 *[+]
non-caveolae/non-rafts	0.3021 ± 0.0044*
NBD-stearic acid	
DRMs	0.3199 ± 0.0025[+]
non-detergent caveolae/rafts	0.3225 ± 0.0027
affinity-purified caveolae/rafts	0.3392 ± 0.0017*[+]
non-caveolae/non-rafts	0.3287 ± 0.0031 *

[a] *Trans*-parinaric acid, *cis*-parinaric acid, and NDB-stearic acid were incorporated at low, nonself-quenching levels into purified membrane fractions as described in Methods
[b] Fluorescence polarization values represent the mean $\pm$ SD (n=7)
* $p < 0.05$ vs. DRMs
[+] $p < 0.05$ vs. non-caveolae/non-rafts

To determine whether this was also true for NDCR and ACR, DPH polarization was measured not only in DRM but also in NDCR, ACR, and NR. To assure that DPH itself did not perturb the lipid structures, the various membrane fractions were incubated with DPH at a low ratio of DPH to membrane protein (i.e. 0.1µg/100µg) to maximally incorporate the probe as described in Methods. The data showed that the DPH polarization was lowest in NR, but significantly higher in the various lipid raft preparations in the order: ACR>NDCR>DRM (Table 3). These data were consistent with the presence of disordered liquid phase in all three lipid raft preparations, especially in the ACR and NDCR, but less so in DRM (Table 3).

Fluorescence Polarization of Probe Molecules That Preferentially Distribute Into Outer and Inner Leaflets of the Membrane: DPH-TMA and DPH-Pro. Previous studies with other cell lines show that the DPH polarization is lower in the outer (exofacial) leaflet than in the inner (cytofacial) leaflet of the PM; this has been interpreted as indicating the outer leaflet acyl chains are more fluid than those of the inner leaflet (Sweet and Schroeder, 1988a; Schroeder et al., 2001b; Dudeja et al., 1991). Due to its positive charge, DPH-TMA appears to selectively localize in the outer leaflet which is enriched in positively charged but essentially devoid of negatively charged lipids. The negatively charged DPH-Pro appears to localize in the PM inner leaflet which contains predominantly negatively charged lipids (Schroeder et al., 2001b; Daleke and Lyles; 2000).

Table 3. Transbilayer Structure of Caveolae/Raft Domains and Plasma Membranes: Diphenylhexatriene Probes (DPH, TMA-DPH, DPH-Propionic Acid).[a]

Membrane	Polarization[b]
Diphenylhexatriene	
DRMs	$0.2912 \pm 0.0036^{+}$
non-detergent caveolae/rafts	$0.3032 \pm 0.0028^{*+}$
affinity-purified caveolae/rafts	$0.3177 \pm 0.0019^{*+}$
non-caveolae/non-rafts	$0.2873 \pm 0.0026^{*}$
DPH-TMA	
DRMs	$0.2784 \pm 0.0034^{+}$
non-detergent caveolae/rafts	$0.2688 \pm 0.0028^{*}$
affinity-purified caveolae/rafts	$0.2711 \pm 0.0024^{*+}$
non-caveolae/non-rafts	$0.2680 \pm 0.0061^{*}$
DPH-Propionic Acid	
DRMs	$0.2844 \pm 0.0045^{@}$
non-detergent caveolae/rafts	$0.2902 \pm 0.0026^{*+@}$
affinity-purified caveolae/rafts	$0.3011 \pm 0.0028^{*+@}$
non-caveolae/non-rafts	$0.283\,8 \pm 0.0017^{@}$

[a] DPH, TMA-DPH, and DPH-propionic acid were incorporated at low, nonself-quenching levels into purified membrane fractions as described in Methods
[b] Fluorescence polarization values represent the mean $\pm$ SD (n=7)
[*] $p < 0.05$ vs. DRMs
[+] $p < 0.05$ vs. non-caveolae/non-rafts

The fluorescence polarization of the outer-leaflet selective probe was lowest in NR (0.2873 ± 0.0026, Table 3). Polarization of DPH-TMA was significantly higher (p<0.050) in all lipid raft preparations as compared to NR in the order: ACR > NDCR> DRM > NR. Thus, the outer leaflet of ACR appeared least fluid while that of DRM was most fluid.

In contrast to the above results, DPH-Propionic Acid polarization was lowest in NR, i.e. 0.2838 ± 0.0017, essentially equivalent to that in DRM, i.e. 0.2844 ± 0.0034 (Table 3). Polarization of DPH-Propionic Acid was significantly higher (p<0.050) only

in the NDCR and ACR in the order: ACR > NDCR> DRM, NR. Since fluidity is inversely related to polarization, the inner leaflet of the NDCR and ACR appeared less fluid as compared to that of DRM and NR.

Comparison of the DPH-TMA (outer leaflet probe) and DPH-Propionic acid (inner leaflet probe) in each of the membrane fractions suggested the presence of a transbilayer fluidity gradient in each of the various membrane fractions. Qualitatively, the fluorescence polarization values of the DPH-Propionic acid probe were higher than those of the DPH-TMA probe in all cases (Table 3), indicating that the outer leaflet is more fluid than the inner leaflet in each respective membrane fraction. However, quantitative analysis showed that the difference in polarization (P), defined as PDPH-Propionic acid - PDPH-TMA, was markedly dependent on the membrane fraction being examined in the following order: ACR (P=0.0300)> NDCR (P=0.0214)> NR (P=0.0158)>DRM (P=0.0060). Thus, the DRM exhibited the smallest transbilayer fluidity difference, nearly 2.6-fold less than that of NR. In contrast, the NDCR and ACR showed the highest transbilayer fluidity differences, both of which were greater (1.4- and 1.9-fold, respectively) than that of NR. Thus, among the various lipid raft preparations, the NDCR and ACR showed the highest transbilayer fluidity differences (3.6- and 5-fold, respectively) as compared to DRM.

These findings were consistent with earlier studies indicating that the PM inner leaflet fluidity is less than that of the outer leaflet. The above data demonstrated for the first time that this is the case not only for the entire PM, but also for the lipid raft vs. non-lipid raft domains therein (Sweet and Schroeder, 1988a). The transbilayer fluidity difference as compared to the NR appeared greater for the two membrane fractions not utilizing detergents (i.e. NDCR and ACR). In contrast, the transbilayer fluidity difference in DRM was markedly less than any other membrane fraction examined, including the NR. Appendix A shows a graphic summary of the isolated membrane structural analyses.

Contribution of Detergent to Structure and Fluidity. Because detergents, such as Triton X-100, are known to solubilize membranes, the possibility was considered that

some of the differences in the structural and cholesterol dynamic properties of DRM vs. NDCR and ACR may be due to the presence of Triton X-100 in the DRM. To test this hypothesis, the absorbance spectra of all three membrane preparations and Triton X-100 in TNE buffer were obtained (Fig. 3). The absorbance spectrum of the detergent Triton X-100 in TNE buffer demonstrated a major peak with maximum near 224 nm and a minor doublet with maxima near 270 and 280 nm (Fig. 3A). The limit of detection of Triton-X-100 was 63 nM and was determined by the method as described earlier (Berthouex and Brown, 1994a and 1994b). It is noteworthy that the absorbance spectrum of Triton X-100 in ethanol (not shown) was very similar to that taken in aqueous solvent. The absorbance spectrum of DRM did not reveal any of the peak maxima typical of Triton X-100 (Fig. 3B). As expected, the absorbance spectra of the caveolae/lipid raft domains isolated by the detergent-free methods also contained no absorbance peaks typical of Triton X-100: NDCR (Fig. 3C); ACR (Fig. 3D).

Thus, the significant differences in structure and fluidity of DRM as compared to NDCR, ACR, and NR of PM were not due to residual detergent in the DRM.

Spontaneous and SCP-2 –Mediated Sterol Transfer from DRM and DSM. Although the above data indicate that the structure (crystalline vs. monomeric) and fluidity (polarization under non-self quenching conditions) of DHE in DRM differed significantly from those of NDCR and ACR, nothing is known regarding the effect of these differences on: (i) spontaneous sterol transfer from DRM as compared to that in the other caveolae/lipid raft preparations, or (ii) the response of DRM vs. other caveolae/lipid raft preparations to intracellular sterol carrier protein-2. To begin to resolve these issues, a previously-established fluorescent DHE exchange assay was utilized as described in Methods.
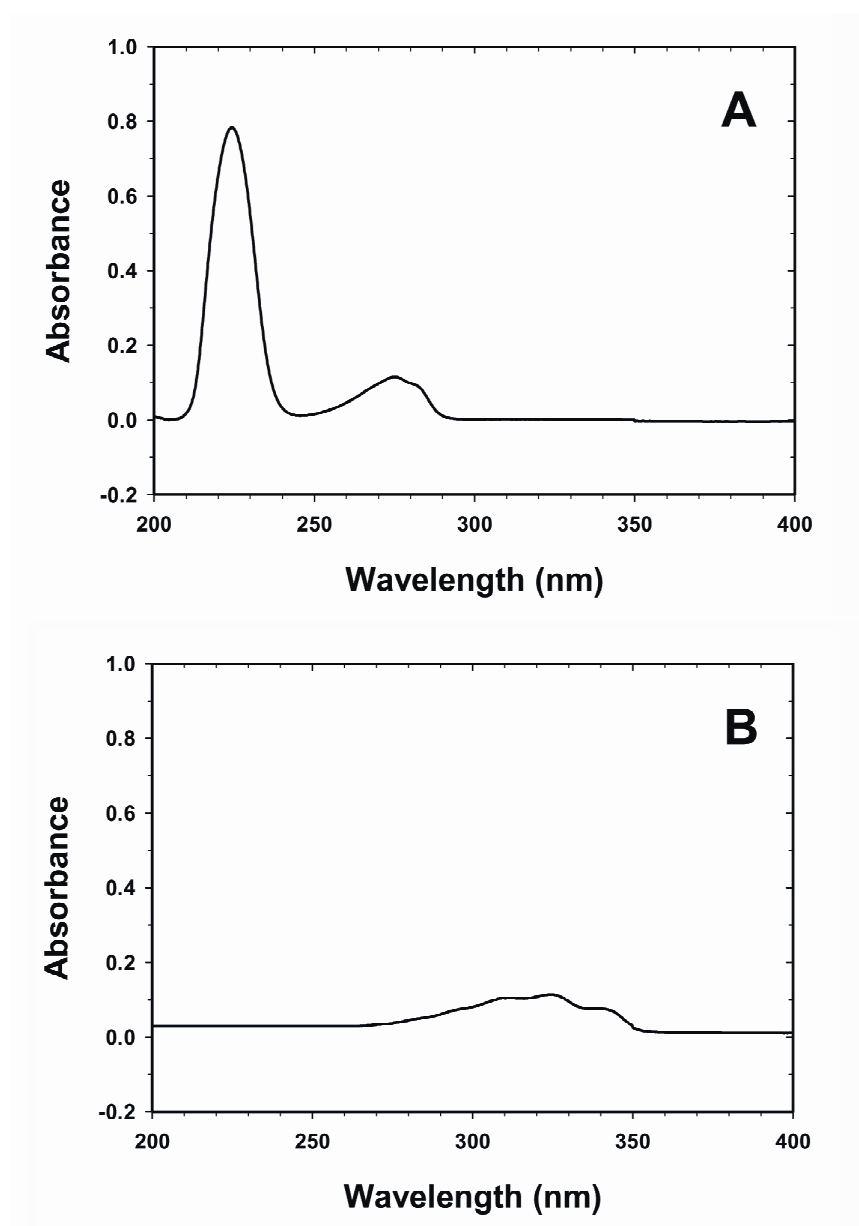
Fig. 3. Detection of Detergent Triton X-100: Absorbance Spectra of Triton X-100 and Caveolae/Raft Enriched Membrane Fractions. (**A**) Absorbance spectrum of Triton X-100 in PIPES buffer (2 ml, 5% solution). (**B**) Absorbance spectrum of DRM in PIPES buffer (3.5 μg/2 ml).
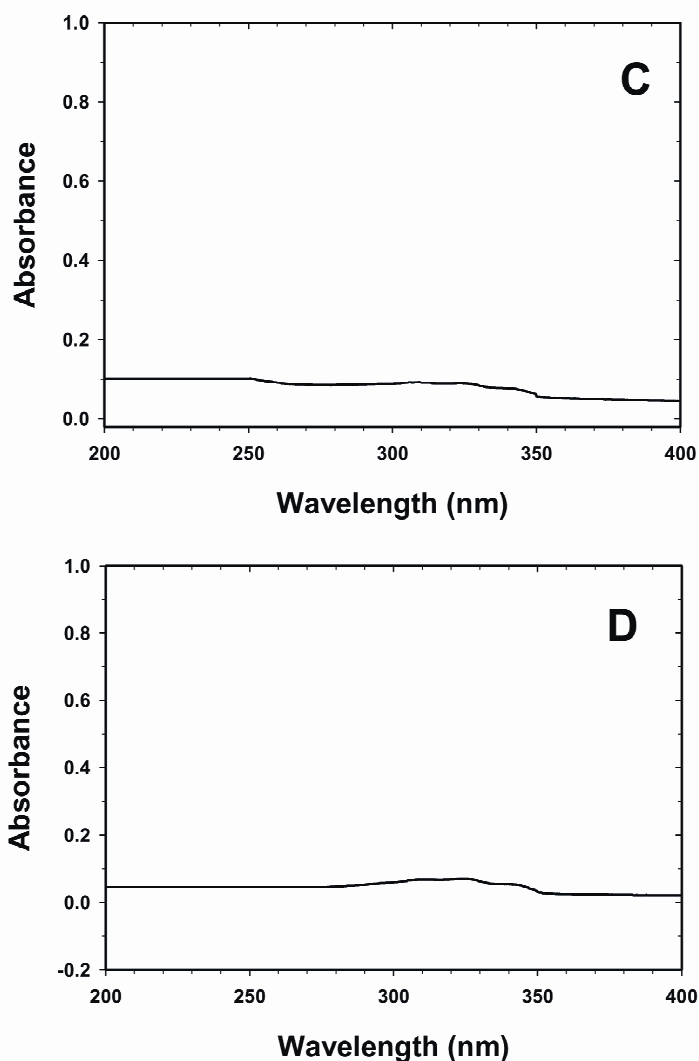
Fig. 3 cont. (**C**) Absorbance spectrum of non-detergent caveolae/lipid rafts in PIPES buffer (3.5 µg/2 ml). (**D**) Absorbance spectrum of affinity-purified caveolae/lipid rafts in PIPES buffer (3.5 µg/ml).

The initial polarization of DHE in the donor DRM was 0.1153 ± 0.0016, consistent with self-quenching due to the presence of high levels of DHE (Fig. 4A, open circles). In the absence of acceptor DRM, DHE polarization in DRM donors did not significantly change over several hours (Fig. 4A, upside-down triangles). However, surprisingly, addition of 10-fold excess acceptor DRM elicited a fast increase in polarization, consistent with release from self-quenching due to exchange of DHE

(donor) and cholesterol (acceptor). From a starting polarization of 0.1146 ± 0.0024, the polarization of DHE exhibited a nearly linear increase and did not saturate until reaching a polarization near 0.45 (Fig. 4A, open circles). The initial rate of spontaneous molecular sterol transfer from DRM, calculated as described in Methods, was 0.387 ± 0.072 pmol/min (Table 4). Since the spontaneous exchange was approximately linear over the entire time period examined, the exchangeable fraction (f1) for spontaneous sterol exchange was set to unity (Table 4).

To determine if sterol transfer from DRM was responsive to a sterol transfer protein, i.e. sterol carrier protein-2 (SCP-2), the sterol exchange was monitored in the presence of SCP-2 as described in Methods. SCP-2 is a protein present in all mammalian tissues examined to date, which enhances sterol transfer between a majority of membranes, with erythrocytes being a rare exception (Kavecansky et al., 1994). Therefore, SCP-2 was used to probe sterol dynamics of DRM and DSM. Addition of SCP-2 to donor alone failed to significantly alter DHE polarization (not shown) consistent with earlier studies of model and biological membranes (Thomas et al., 1994). The SCP-2 – mediated exchange of sterol between DRM donors (DHE-containing) and DRM acceptors resulted in release from self-quenching and increased DHE fluorescence polarization (Fig. 4A, closed circles). The shape of the 4 hr SCP-2 mediated sterol exchange curve was consistent with a more rapid and saturable process as compared to the spontaneous exchange between DRM which was still linear over this time period.

Since the SCP-2 –mediated exchange curve reached a maximal polarization of 0.3382 ± 0.0042 by 4 hr, while the spontaneous exchange was still linear (polarization near 0.3600) at 4 hr, suggesting SCP-2 acted to enhance sterol transfer at early time points, but slightly inhibited sterol exchange at later time points. The initial rate of SCP-2 mediated sterol transfer 0.619 ± 0.037 pmol/min, was 1.6-fold faster than that of spontaneous sterol transfer from DRM (Table 4). Since kinetic analysis of the SCP-2 mediated sterol exchange was unable to resolve more than one exchangeable domain, the exchangeable fraction (f_1) for each exchange was set to unity (Table 4).

In contrast to the DRM, the spontaneous sterol exchange curve for the DSM was essentially unchanged over the 4 h time period examined (Fig. 4B, open circles). The initial polarization of DHE near 0.1163 ± 0.0034 was essentially unaltered during spontaneous exchange between donor DSM (containing DHE) and acceptor DSM over the 4 h incubation (Fig. 4B, open circles).

The initial rate of spontaneous sterol transfer from DSM was calculated to be 0.024 ± 0.009 pmol/min, 14-fold slower than spontaneous sterol transfer from DRM (Table 4). SCP-2 elicited a slight change in fluorescence polarization, but the resulting polarization curve did not have a steep slope (Fig. 4B, closed circles), in contrast to that observed with SCP-2 and DRM (Fig. 4A, closed circles). The initial rate of SCP-2 mediated sterol transfer from DSM was 0.087 ± 0.041 pmol/min, 3.6-fold faster than for spontaneous sterol transfer from DSM, but still nearly 4-fold slower than SCP-2 mediated sterol transfer from DRM (Table 4). Kinetic analysis of the spontaneous sterol exchange between DSM as described in Methods resolved a long half-time, $t_{1/2} = 755 \pm 55$ min, and an exchangeable fraction, $f_1 = 0.229 \pm 0.021$ (Table 4). For the SCP-2 – mediated sterol exchange from DSM, kinetic analysis resolved 2-fold faster $t_{1/2} = 382 \pm 34$ min, but an essentially unaltered exchangeable fraction, $f_1 = 0.251 \pm 0.028$.

In summary, spontaneous sterol transfer from DRM, but not DSM, was rapid and essentially not saturable during the 4 h time period of the exchange. Because spontaneous sterol transfer from DRM was so rapid, SCP-2 elicited only a modest increase in sterol transfer. In contrast, spontaneous sterol transfer from DSM was comparatively slow and relatively unresponsive to SCP-2. As discussed above, these properties of DRM (Fig. 3B) and DSM (not shown) were not due to contamination with residual Triton X-100. If one assumed that DRM are enriched in caveolae/lipid rafts, as indicated by the western blots (Fig. 1), while DSM are enriched in non-rafts, these data suggest that spontaneous sterol transfer from lipid rafts may be rapid while that from non-rafts are very slow in comparison.
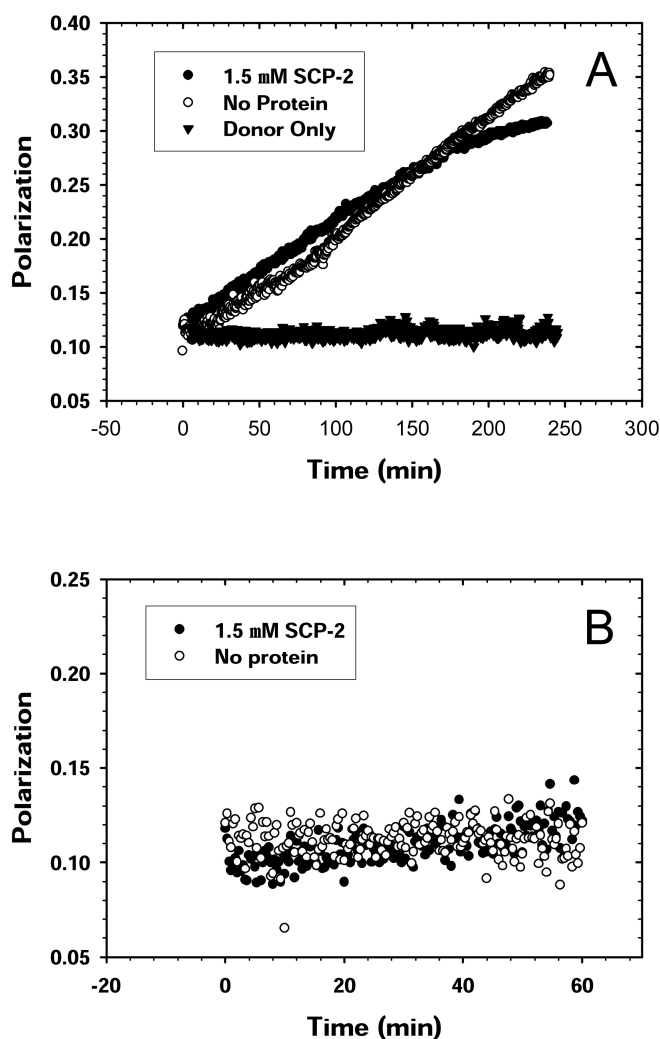
Fig. 4. Sterol Transfer from Detergent-Resistant Membranes (DRM) and Detergent-Soluble Membranes (DSM). Effect of SCP-2 on sterol exchange between DRM. (**A**) Dehydroergosterol (DHE) exchange between DRM donors (1.75 μg protein/ml) and DRM acceptors (17.5 μg/ml) was measured by monitoring polarization as described in Methods. Open circle shows the spontaneous sterol exchange after addition of 10-fold excess acceptor DRM. The solid circles show the effect of SCP-2 (1.5 μM) on the sterol exchange between donor and acceptor DRM. For comparison, a donor-only polarization curve is shown (solid triangles). (**B**) Effect of SCP-2 on sterol exchanger between DSM. DHE exchange was measured as in Panel A, except that DSM donor and DSM acceptor membranes were used as described in Methods. Open circle shows the spontaneous sterol transfer from donor DSM after addition of 10-fold excess acceptor DSM. The solid circles show the effect of 1.5 μM SCP-2 on the sterol exchange between donor DSM and acceptor DSM**.**

Table 4. Initial Rates and Kinetic Multi-Exponential Analysis of Molecular Sterol Exchange: Effect of Sterol Carrier Protein-2.[a,c]

Donor-Acceptor	Protein Added	Initial Rate (pmol/min)	$t_{1/2}$ (min)[b]	f_1[b]	f_2[b]
DRM	None	$0.3\,87 \pm 0.072^+$	-	1.000	-
	SCP-2	$0.619 \pm 0.037^{*+}$	-	1.000	-
DSM	None	0.024 ± 0.009	755 ± 55	0.229 ± 0.021	0.771 ± 0.034
	SCP-2	0.087 ± 0.041	$382 \pm 34^*$	0.251 ± 0.028	0.749 ± 0.028
non-detergent caveolae/rafts	None	0.127 ± 0.037	194 ± 24	0.421 ± 0.021	0.579 ± 0.004
	SCP-2	0.163 ± 0.025	$131 \pm 17^*$	$0.520 \pm 0.027^*$	0.480 ± 0.041
affinity-purified caveolae/rafts	None	0.105 ± 0.028	172 ± 15	0.472 ± 0.033	0.528 ± 0.029
	SCP-2	$0.234 \pm 0.021\ ^{*+}$	$121 \pm 26^*$	$0.583 \pm 0.022^{*+}$	0.417 ± 0.031
non-caveolae/ non-rafts	None	0.024 ± 0.009	412 ± 32	0.371 ± 0.041	0.629 ± 0.025
	SCP-2	0.032 ± 0.005	384 ± 47	0.401 ± 0.031	0.599 ± 0.032

[a] Fluorescence polarization exchange curves for DHE sterol transfer from isolated membrane donors (DHE-loaded) to isolated membrane acceptors (without DHE) were measured in the absence or presence of SCP-2 (1.5 µM) followed by determination of initial rates and kinetic analysis as described in Methods
[b] unless otherwise stated, half times ($h_{1/2}$) were in minutes, while f_1 and f_2 represent fractions due to the exchangeable and non-exchangeable components respectively
[c] values represent the mean $\pm$ SD (n=3-4)
[*] $p < 0.05$ vs. no protein added
[+] $p < 0.05$ vs. non-detergent caveolae/rafts

Spontaneous and SCP-2–Mediated Sterol Transfer from NDCR. To resolve if the high spontaneous rate of sterol transfer from DRM was a unique property of this lipid raft enriched fraction, the above experiments were repeated with NDCR isolated as described in Methods. Since the NDCR isolation method did not produce a comparable DSM fraction, it was not possible to directly obtain the sterol exchange dynamics from this membrane domain. The initial polarization of DHE in donor NDCR was near 0.14 (Fig. 5), consistent with self quenching of the DHE therein. In the absence of acceptor NDCR, DHE polarization was not altered over the 4 h time frame of exchange (not

shown). In contrast, in the presence of acceptor NDCR, slow spontaneous sterol transfer was detectable as an increase in DHE polarization (Fig. 5, open circles). The initial rate of spontaneous molecular sterol transfer from NDCR was 0.127 ± 0.037 pmol/min, nearly 3-fold slower than that exhibited by DRM (Table 4). Kinetic analysis resolved a half-time of spontaneous sterol transfer for the NDCR near 194 ± 24 min (Table 4) and an exchangeable fraction, $f_1 = 0.421 \pm 0.021$, which was 2.4-fold smaller than that for DRM (Table 4).

Sterol transfer from NDCR was more responsive to the sterol carrier protein SCP-2. When SCP-2 was added to NCDR donors alone, a change in DHE fluorescent polarization was observed (not shown). However, when SCP-2 was added to NCDR donors with a 10-fold excess of acceptor membranes, there was a more rapid and extensive increase in DHE polarization (Fig. 5, closed circles). These results indicated that SCP-2 enhanced sterol transfer from the NCDR membranes. The initial rate of SCP-2-mediated sterol exchange between NDCR was 0.163 ± 0.025 pmol/min, 1.3-fold faster than that of spontaneous sterol exchange from NDCR (Table 4). Kinetic analysis of SCP-2-mediated sterol transfer curves from the NDCR indicated that SCP-2 decreased the $t_{1/2}$ of the exchangeable sterol pool by 32% from 194 ± 24 to 131 ± 17 ($p<0.05$) and increased the size of the exchangeable sterol pool by 1.23-fold from 0.421 ± 0.021 to 0.520 ± 0.027 ($p<0.05$) (Table 4).

In summary, the spontaneous molecular transfer of sterol from NDCR was significantly slower (i.e. nearly 3-fold) than that exhibited by DRM. Furthermore, SCP-2 increased sterol transfer from NDCR, but the initial rate of SCP-2 mediated sterol transfer from NDCR was still 3.8-fold slower than that mediated by SCP-2 in DRM. Thus, both the spontaneous and SCP-2 mediated sterol dynamics of NDCR differed markedly from those of DRM.
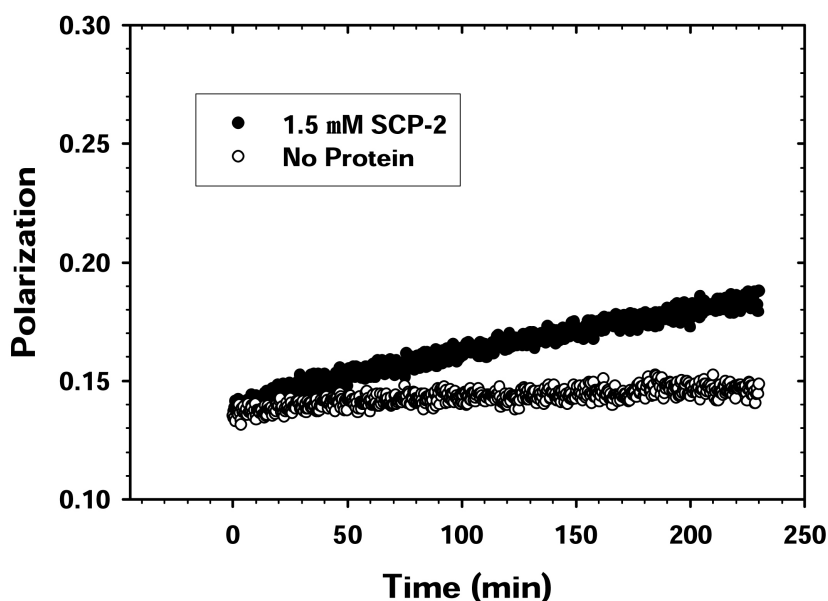
Fig. 5. Sterol Transfer from Non-detergent Caveolae/Rafts. Dehydroergosterol (DHE) exchange between non-detergent caveolae/raft donor (1.75 µg protein/ml) and non-detergent caveolae/raft acceptor (17.5 µg protein/ml) was measured by monitoring DHE polarization as described in Methods. Open circles show the spontaneous sterol exchange between donor non-detergent caveolae/rafts after addition of 10-fold excess acceptor non-detergent caveolae/rafts. The solid circles show the effect of 1.5 µM SCP-2 on the sterol exchange between donor and acceptor non-detergent caveolae/rafts.

Spontaneous and SCP-2 –Mediated Sterol Transfer from ACR. Concanavalin A–sepharose binding affinity chromatography was used to simultaneously fractionate ACR, the adherent fraction, and NR, the non-adherent fraction (equivalent to DSM), from purified PM vesicles isolated from MDCK cells as described in Methods. Spontaneous sterol transfer from ACR was slower than that exhibited by DRM. Consistent with DHE self-quenching, the initial fluorescence polarization of DHE in donor ACR was 0.1327 $\pm$ 0.0046 (Fig. 6A, open circles). In the absence of acceptor, ACR was unaltered over the 4 h time frame of exchange (not shown). Upon addition of 10-fold excess acceptor ACR, DHE spontaneously transferred from the donor to acceptor membranes as indicated by increased polarization (Fig. 6A, open circles). The initial rate of spontaneous molecular sterol transfer from ACR was 0.105 $\pm$ 0.028 pmol/min, 3.7-fold slower than from DRM

(Table 4). Kinetic analysis as described in Methods showed that the exchange curves for spontaneous molecular sterol transfer from ACR best fit two components: an exchangeable sterol pool with $t_{1/2}$ of 172 ± 15 min and fraction f1 = 0.472 ± 0.033 of total sterol, which was 2.1-fold smaller than that exhibited by DRM (Table 4). In addition, ACR domains contained a very slow ($t_{1/2}$ of days), essentially non-exchangeable sterol pool representing 0.528 ± 0.029 of total ACR domain sterol (Table 4). The size of the non-exchangeable sterol pool was similar to that observed in NDCR, which did not contain a detectable non-exchangeable pool, but significantly different than the sterol organization of DRM. When sterol transfer from donor to acceptor ACR domains was probed with SCP-2, the DHE polarization increased markedly (Fig. 6A, solid circles). SCP-2 enhanced the initial rate of molecular sterol transfer from ACR essentially 2-fold from 0.105 ± 0.028 to 0.234 ± 0.021 pmol/min, p<0.05 (Table 4).

Kinetic analysis of the SCP-2 mediated sterol exchange curves showed that SCP-2 enhanced the sterol transfer from ACR domains by: decreasing the $t_{1/2}$ of exchange by nearly 30% from 172 ± 15 to 121 ± 26 min, p<0.05; and by increasing the fraction of exchangeable sterol by 24% from 0.472 ± 0.033 to 0.583 ± 0.022, p<0.05 (Table 4). Thus, SCP-2 altered the sterol dynamics of ACR domains significantly more than in either DRM or NDCR. In contrast, NR exhibited markedly slower spontaneous sterol transfer (Fig. 6B, open circles) and lacked responsiveness to SCP-2 (Fig. 6A, closed circles). The initial rate of molecular DHE transfer from NR was 0.024 ± 0.009 pmol/min, 4.4-fold slower than from ACR (Table 4). The half-time of spontaneous sterol transfer from NR $t_{1/2}$ was slow, 412 ± 32 min which was 2.4-fold slower than that from ACR (Table 4). The fractional contribution of exchangeable sterol domain in NR was 0.371 ± 0.041, which was 22% smaller than that exhibited by ACR (Table 4). SCP-2 did not significantly alter any of the parameters of sterol dynamics in NR indicating NR contained both exchangeable and non-exchangeable sterol domains.
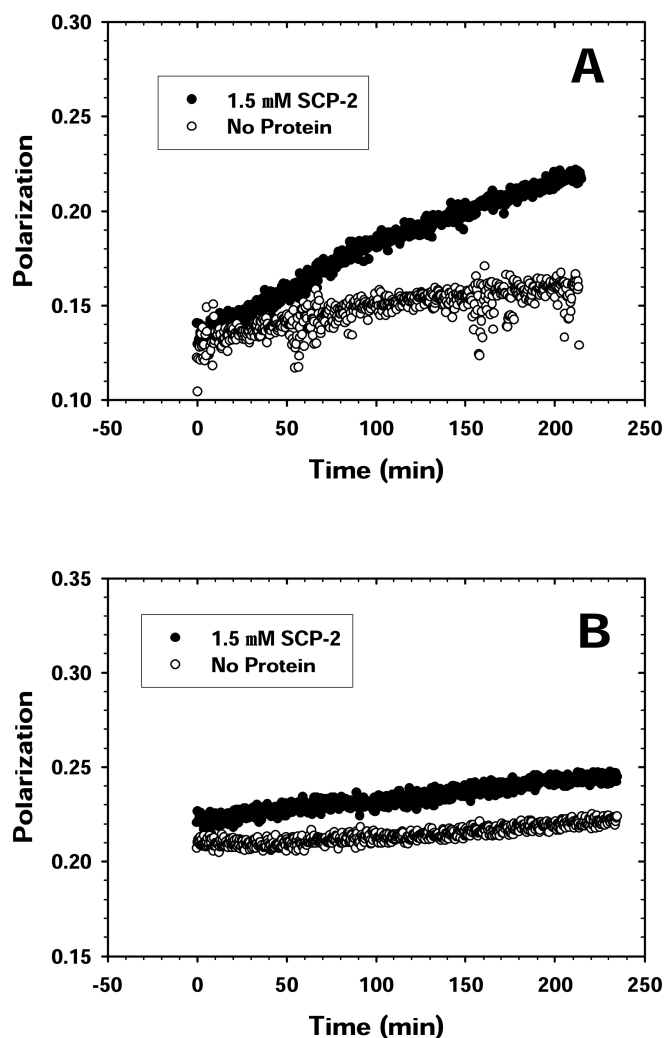
Fig. 6. Sterol Transfer from Affinity-Purified Caveolae/Rafts. (**A**) Effect of SCP-2 on sterol exchange between affinity-purified caveolae/rafts. Dehydroergosterol (DHE) exchange between affinity-purified caveolae/raft donors (1.75 µg protein/ml) and affinity-purified caveolae/raft acceptors (17.5 µg protein/ml) was measured by monitoring DHE polarization as described in Methods. Open circle shows the spontaneous sterol exchange between donor and acceptor affinity-purified Caveolae/rafts. The solid circles show the effect of 1.5 M SCP-2 on the sterol exchange between donor and acceptor affinity-purified caveolae/rafts. (**B**) Effect of SCP-2 on sterol transfer from affinity-purified caveolae/raft domains which did not bind the Concanavalin A-sepharose affinity column. DHE exchange was measured as in Panel A. Open circles show the spontaneous sterol transfer from donor caveolae/raft membranes after addition of 10-fold excess acceptor caveolae/raft membranes. The solid circles show the effect of 1.5 µM SCP-2 on the sterol transfer from donor caveolae/raft membrane to 10-fold excess acceptor caveolae/raft membrane.

In summary, although ACR exhibited the slowest initial rate of spontaneous sterol transfer of any of the examined lipid raft-enriched membrane fractions, it was still more than 4-fold faster than spontaneous sterol transfer from NR. The NR had the largest fraction of non-exchangeable sterol domain and was unresponsive to SCP-2.

DISCUSSION

There has been paucity in information regarding the structural organization of cholesterol, fluidity, transbilayer structure, and cholesterol dynamics of caveolae/raft domains (Schroeder et al., 2005). Further, there has been an ongoing debate as to what constitutes a lipid raft/caveolae (Skwarek, 2004; Schnitzer et al., 2003). These studies also indicated that the use of detergents can alter the nature/composition of the resultant isolated rafts. To begin to address these issues, this study utilized three distinct methods to obtain caveolae/rafts from MDCK cells: (i) a Triton X-100-based method to obtain detergent-resistant membranes (DRM) and detergent-soluble membranes (DSM); (ii) a non-detergent isolation based on the Percoll and the OptiPrep gradients to first isolate plasma membrane (PM) and then fractionate caveolae/lipid rafts according to density (Smart et al., 1995); and (iii) an affinity chromatography based method wherein PM are first isolated by sucrose density fractionation and then separated into Affinity-purified Caveolae/lipid rafts (ACR) and Non-caveolae/non-rafts (NR) by use of Concanavalin A-sepharose affinity chromatography (Atshaves et al., 2003). However, it is important to emphasize that these techniques do not distinguish caveolar lipid rafts from non-caveolar lipid raft. The data presented herein demonstrate for the first time that the function (cholesterol exchange dynamics) and structure (lipid fluidity) of DRM share qualitative, but not quantitative, properties exhibited by caveolae/lipid rafts isolated from MDCK cells by non-detergent methods in the order: DRM < Non-detergent Caveolae/rafts (NDCR) < ACR. The key findings of this study are enumerated below.

First, it was shown for the first time that the structural form of sterol (monomeric vs. crystalline) in DRM differed markedly from that of all other examined MDCK PM fractions. DRM, but not NDCR or ACR, contained a significant amount of

crystalline sterol (i.e. near 10%). This was unexpected as previous compositional analysis of isolated PM and multiphoton images of sterol in the PM of living cells detected very little crystalline sterol, generally near 1% (McIntosh et al., 2003). In contrast, crystalline sterol is associated primarily with lysosomes (McIntosh et al., 2003; Tabas, 1997). These data suggest that the appearance of significant amounts of crystalline sterol in DRM arise during the preparation. Since DRM are isolated from whole cells, the crystalline sterol in DRM may arise in part by selective retention of cholesterol from lysosomes. Alternatively, as the detergents used in DRM isolation selectively extract certain phospholipids, the resulting high sterol/phospholipid ratio could lead to phase separation of sterol into crystalline form (Eckert et al. 2003, Pike et al., 2002). It has been shown that the sterol phase separates into crystalline sterol at high molar ratio of cholesterol/phospholipid in model membranes (McIntosh et al., 2003).

Second, the sterol fluidity in DRM was shown to differ markedly from that of the other MDCK PM fractions using DHE. Although synthetic sterol probe molecules may have deleterious effects on membrane structure-function, such as NBD-cholesterol, sterol-phenol or nitroxide-cholesterol, to our knowledge there is no data demonstrating toxic or adverse effects of DHE added to cultured cells or fed to animals (Schroeder, 1984; Schroeder and Nemecz, 1990; Schroeder et al., 1991; Schroeder et al., 1996). However, DHE is a natural component of membranes in other eukaryotic organisms, including yeast and sponges (Schroeder, 1984; Hale and Schroeder, 1982; Delseth et al., 1979; Sica et al., 1982). When DHE is simply fed to cultured cells or animals, it is readily incorporated into membranes or lipoproteins in the absence of additional chemicals, catalysts or experimental manipulations (McIntosh et al., 2003; Delseth et al., 1979; Schroeder et al., 2001a; Bergeron and Scott, 1982a and 1982b). Incorporation of DHE to up to 80-90% of total membrane sterol has no adverse effects on sterol-phospholipid ratio, fatty acid composition, sterol distribution or receptor-effector interactions sensitive to sterols or sterol structure (Hale and Schroeder, 1982; Gimpl and Fahrenholz, 2000).

The fluorescence polarization of DHE in DRM was higher than that of NDCR. Consistent with this observation, electron spin resonance studies comparing spin-labeled cholestane mobility in model membranes with that in DRM isolated from RBL-2H3 cells also conclude a less fluid sterol environment in the DRM (Ge et al., 1999). However, quantitative analysis indicated that the fluorescence polarization of DHE in DRM was the highest of any of the lipid raft-enriched PM fractions examined: DRM > NDCR > ACR. Since fluorescence polarization provides a relative measure of mobility/fluidity of the probe, these data suggested that the sterol in DRM was significantly less mobile as compared to NR fraction, but more mobile than in any of the other lipid raft-enriched fractions of the PM in the following order: NR > DRM > NDCR > ACR. The physical basis for the uniquely lower fluidity of sterol in DRM and other caveolae/lipid raft preparations is not clear, but several possibilities may be considered: (i) Contaminating detergent may increase the fluidity of sterol in DRM as compared to other caveolae/lipid raft preparations. However, the data showed that DRM did not contain detergent Triton X-100, consistent with earlier studies which also demonstrated the absence of detergent in DRM (Brown and London, 1998); (ii) Crystalline sterol in DRM may contribute to the higher fluidity/mobility of sterol in DRM; (iii) Sterol may partition into a liquid ordered phase in DRM, NDCR, and ACR. Consistent with the latter possibility, electron spin resonance of spin-labeled cholestane in model membranes and DRM isolated from RBL-2H3 cells suggested that the sterol partitioned into a liquid ordered phase in DRM (Gallegos et al., 2004). If the results obtained with the naturally-occurring fluorescent sterol DHE and the spin labeled sterol cholestane both report on the same type of sterol environment, then these data further indicate that the degree of order in the liquid ordered phase sensed by the sterols was lowest in DRM, intermediate in NDCR, and highest in ACR. These data implied that the physical state of the liquid ordered phase in DRM is unique or that the relative amount of liquid ordered phase in lipid raft enriched PM fractions is highly dependent on the method used for isolation.

Third, as compared to NR the fluidity of lipid acyl chains detected by fluorescent polarization of lipidic probes in NDCR and ACR (but not DRM) was lower, consistent with a liquid disordered state. In general the polarizations of DiI C_{18} and *cis*-parinaric acid (but not DPH, *trans*-parinaric acid, or NBD-stearic acid) appeared significantly higher in DRM than in NR. In contrast, the fluorescence polarizations of all five lipidic probes were higher in NDCRs and ACR than in NR. Model membrane studies show that DPH polarization in the non-fluid gel phase and in the liquid crystalline phase is 0.381 and 0.095, respectively, while that in the liquid disordered phase is intermediate (Schroeder et al., 1994). As shown herein, the fluorescence polarization of DPH in ACR was 0.3177 + 0.0019 (Table 3), well within the range of DPH in the liquid ordered phase of model membranes (Schroeder et al., 1994). With regard to the other lipid raft preparations, DPH polarization in NDCR was also higher (but not as high as in ACR) than in NR, consistent with the presence of liquid disordered phase. The average DPH polarization in DRM was slightly higher than in NR, but did not achieve statistical significance. This was in contrast to earlier fluorescence and electron spin resonance studies of DRM from model membranes and other cell types suggesting a liquid disordered phase therein (Ge et al., 1999; Schroeder et al., 1994). Taken together, the acyl chain environment of a variety of non-sterol lipidic fluorophores suggested that the liquid ordered phase is either: (i) more prevalent in ACR > NDCR >DRM, or (ii) the degree of order in equivalent concentrations of liquid ordered phase is higher in ACR > NDCR >DRM.

Fourth, the fluorescence polarizations of the leaflet selective DPH-TMA (exofacial leaflet) and DPH-Pro (cytofacial leaflet) fluorophores were used to examine the relative fluidity of the outer and inner leaflets of lipid raft membranes. Mammalian cell membranes contain transport proteins (phospholipid flippases and translocases) that actively transport negatively charged phospholipids to the cytofacial leaflet (Daleke and Lyles, 2000). Consequently, phosphatidylserine and phosphatidylinositol are on the cytofacial leaflet while other phospholipids remain in the outer leaflet. Just as the other negatively charged phospholipids, the negatively charged DPH-Pro is expected to be

found on the cytofacial leaflet. Hence, DPH-TMA (zwitterionic or non-negative) is expected to be found on the outer leaflet just as other zwitterionic phospholipids, non-negative (phosphatidylcholine, sphingomyelin) phospholipids. The difference in DPH-TMA polarization and DPH-Pro polarization is a measure of the transbilayer fluidity gradient between the two membrane leaflets (Sweet and Schroeder, 1988a; Schroeder et al., 2001b; Dudeja et al., 1991).

Although in all membrane fractions examined the exofacial leaflet appeared more fluid, the fluidity gradient was markedly dependent on the membrane fraction being examined with DRM being the smallest: DRM (P=0.0060) < NR (P=0.0158) < NDCR (P=0.0214) < ACR (P=0.0300). Thus, the DRM were unique in exhibiting a 2.6-fold smaller transbilayer fluidity gradient when compared to that of NR. In contrast, the NDCR and ACR had the highest transbilayer fluidity differences, 1.4- and 1.9-fold greater, respectively, than NR. While the exact basis for the DRM exhibiting such a small transbilayer fluidity difference (even lower than in NR) is not known, there are three possible causes: (i) detergents are known to selectively extract certain phospholipids species (Brown and London, 1998); (ii) DRM may be comprised of a mixture of right-side-out and inside-out orientations (Radeva and Sharom, 2004); (iii) Since DRM are isolated from whole cells, they may be composed not only of PM constituents but also of other intracellular membrane components that contain significant amounts of cholesterol (e.g. lysosomes, ER). In contrast, a previous study showed that ConA-Sepharose-affinity purified membranes were oriented right-side-out (Wood et al., 2002). It is important to note that transbilayer fluidity gradients function in modulating the activity of transbilayer coupled receptors and transporters in the PM (Sweet and Schroeder, 1988b). Taken together, the data presented herein indicated that the transbilayer fluidity gradient in lipid raft enriched membrane fractions were more clearly defined and greater in ACR and NDCR than NR, while that in DRM is actually less than in the other PM-enriched fractions.

Fifth, it was shown for the first time that spontaneous sterol transfer from NR and DSM was slow and essentially unresponsive to SCP-2. These findings supported current

studies with intact cells indicating that sterol transfer is mediated through proteins localized in the PM (i.e. SRB 1, P-glycoprotein, ABC-A1) and within the cell (i.e. SCP-2, caveolin-1) (Smart, 2005; Schroeder et al., 2005; Schroeder et al., 1998).

Sixth, both spontaneous and SCP-2-mediated sterol transfer from lipid raft enriched PM fractions were highly dependent on the type of preparation used. Although spontaneous sterol transfer from DRM was very rapid (polarizations approached the theoretical limit), SCP-2 did not enhance the already very rapid sterol transfer from DRM. Since SCP-2 did not enhance sterol transfer from DRM, much less DSM and NR, these data do not account for the significant SCP-2 mediated enhancement of sterol transfer from isolated PM vesicles noted earlier (Gallegos et al., 2001b). In contrast to these observations with DRM, spontaneous sterol transfer from NDCR and ACR was moderately faster than from DSM and NR and highly responsive to SCP-2. SCP-2 enhanced the initial rate, decreased the half-time, and increased the size of the exchangeable sterol domain in NDCR and ACR, but not DRM or NR. Notably the slow spontaneous sterol transfer from all PM fractions (except DRM) was not due to slow transbilayer sterol migration. Transmembrane cholesterol flip-flop across both model membranes and PM is fast (min) (Schroeder and Nemecz, 1990; John et al., 2002; Boesze-Battaglia et al., 1996). Intact cells have evolved very rapid (1-2 min) protein-mediated (i.e. SCP-2, caveolin-1) and somewhat slower (10-20 min) vesicular intracellular cholesterol trafficking pathways to and from the PM (Frolov et al., 2000; Atshaves et al., 2000). An example of the potential importance of cholesterol transfer by sterol-binding proteins is the movement of sterols from hepatocyte basolateral PM to the bile canilicular region, which occurs by non-vesicular pathways (Fuchs et al., 2001). Identifying these pathways, the PM domains involved, and protein mediators may provide valuable insight into the function of caveolae/rafts in sterol trafficking. Taken together, these data on spontaneous and SCP-2 mediated sterol dynamics from lipid raft enriched fractions isolated without the use of detergents (i.e. NDCR and even more so ACR) vs. sterol dynamics from NR more closely resembled sterol dynamics from the PM of intact cells than DRM.

Despite the recognition that PM are comprised of multiple types of domains, i.e. rafts vs. non-rafts, little is known regarding the fluidity, transbilayer structure, and sterol dynamics of these functionally distinct domains. Although most studies have focused largely on DRM, recent reports in the literature have questioned the purity of lipid rafts prepared from whole cells by use of detergents (Foster et al., 2003) and have postulated that DRM may not necessarily be equivalent to caveolae/lipid rafts in cells or may represent a different fraction of caveolae/lipid rafts than those isolated by methods not using detergents (Schroeder et al., 2005; Skwarek, 2004; Schnitzer et al., 2003; Pike et al., 2002; Radeva and Sharom, 2004). Therefore, the present investigation was undertaken to isolate both non-raft and raft types of domains from MDCK PM using two classical techniques (DRM, NDCR) and a newly developed method that simultaneously resolves ACR and NR without the use of detergents. These data showed that DRM, NDCR, and ACR qualitatively share several (but not all) structural properties, but differ functionally. For example, ACR had no crystalline sterol, were the least fluid, had the highest transbilayer fluidity gradient, and exhibited the most liquid ordered phase. NDCR also had no crystalline sterol, but were intermediate in the other properties. In contrast, DRM contained significant amounts of crystalline sterol, were the most fluid, had the least transbilayer fluidity gradients, had the largest amount of liquid ordered phase, and most closely resembled NR. Functionally, spontaneous and SCP-2 mediated sterol dynamics of ACR and NDCR were most like those reported for PM and intact cells (Fuchs et al., 2001). Again NDCR were intermediate in these properties while DRM appeared anomalous. We postulate that the latter may be due to the presence of more non-raft contaminating membranes in DRM. Although an exhaustive panel of markers was not examined, based on the representative markers used, the DRM appeared the least pure while the ACR appeared the most pure of the three lipid raft preparations. In contrast to ACR and NDCR, DRM exhibited significant contamination from both intracellular membrane fractions (e.g. ER). Consistent with these data showing the presence of NR proteins in DRM, a recent proteomics/mass spectrometry approach identified nearly 1/3 of DRM proteins as being nonspecific

contaminants (Foster et al., 2003). One possible reason for the elevated level of contaminating membranes in the DRM fraction is the isolation of DRM from whole MDCK cells, rather than from a pre-purified PM fraction. In contrast, NDCR and ACR were prepared from pre-purified PM isolated from the MDCK cells. However, the presence of contaminating intracellular membranes alone does not completely account for the anomalous spontaneous and SCP-2 mediated sterol dynamics of DRM. Intracellular membranes (lysosomes, mitochondria, ER) exhibit slow, rather than fast, spontaneous sterol transfer (Schroeder et al., 2001a). Furthermore, sterol transfer from intracellular membranes is enhanced by SCP-2 (Schroeder et al., 2001a). These data would suggest that the structure and sterol dynamics of DRM are at least in part either a product of the detergent isolation procedure or that DRM comprise a distinct lipid raft domain significantly different from those obtained without the use of detergents. Although it would be difficult to claim that any raft preparation is identical to that of lipid rafts in the plasma membranes of intact cells, the non-detergent, ACR protocol described herein yielded raft membrane fractions that contained the fewest intracellular organelle contaminants based on select intracellular markers, demonstrated cholesterol exchange dynamics similar to that of intact cells (Schroeder et al., 2005; Schroeder et al., 2001c), and lacked crystalline sterols (McIntosh et al., 2003), which are absent in intact, viable cells (*4*). Whether these findings can be extended to other cell types remains to be shown.

In summary, there are many types of preparations for lipid rafts, each with proven value that has provided insights into multiple fields of study. Data obtained with different preparations may reflect not only the purity of the lipid raft isolate, but also different populations of lipid rafts isolated from different cells. These results indicate that the methodology selected for raft/caveolae isolation should be carefully considered. Further, care should be taken when interpreting results from DRM and other methods of raft/caveolae isolation.

MATERIALS AND METHODS

Materials and Marker Antibodies. Cholesterol (99[+]% pure) and ergosterol (99[+]% pure) were purchased from Steraloids (Wilmington, NH). EDTA, Tris-base, sucrose, phosphate-buffered saline (PBS), phenylmethylsulfonyl fluoride (PMS-F) and Percoll were obtained from Sigma Chemical (St. Louis, MO). Optiprep was purchased from Accurate Chemical Scientific Corporation (Westbury, N.Y.). Lipid-soluble fluorophores including 1,6-diphenyl-1,3,5-hexatriene (DPH), 1,6-diphyenyl-1,3,5-hexatrienyl-trimethylammonium (DPH-TMA), 3(1,6-diphenyl-1,3,5-hexatrienyl)-propionic acid (DPH-Pro), 9Z,11 E,13E,15Z-octatetradecanoic acid (*cis*-parinaric acid), 9E,11 E,13E,15E-octatetradecanoic acid (*trans*-parinaric acid), 12-(N-methyl)-N-[(7-nitrobenz-2-oxa-1,3-diazol-4-yl)amino]-octadecanoic acid (NBD-stearic acid), 1,1',3, 3, 3', 3'-hexamethyl-indodicarbocyanine iodide (DiI1), and 1,1'-dioctadecyl-3, 3, 3', 3'-tetramethylindocarbocyanine perchlorate (DiI18) were obtained from Molecular Probes (Eugene, OR). All solutions in which water was used contained milliQ/deionized water.

Mouse anti-sheep sodium/potassium-ATPase alpha subunit was obtained from Affinity BioReagents, Inc. (Golden, CO), rabbit anti-canine calnexin peptide (aa 575-593) was purchased from Stressgen Biotechnologies (Victoria, BC Canada), mouse anti-flotillin-1 peptide (aa 312-428) were from BD Transduction Laboratories (Lexington, KY), and both goat anti-rabbit IgG*HRP and goat anti-mouse IgG*HRP antisera were obtained from Southern Biotechnologies Associates, Inc (Birmingham, AL). Rabbit anti-human caveolin-1 peptide (aa 2-31) antibodies were raised in rabbits against a 29 aa peptide, deduced from the human caveolin-1 sequence, cross-linked to KLH with gluteraldehyde.

Dehydroergosterol Synthesis. Although dehydroergosterol (DHE) occurs naturally in yeast and Red Sea sponge, DHE utilized herein was chemically synthesized from ergosterol (99[+]% pure) by a method developed in our laboratory (McIntosh et al., 2003; Fisher et al., 1985). This method yielded DHE with a high degree of purity (99[+]%), as ascertained by high performance liquid chromatography (Gallegos et al., 2004; Atshaves et al., 2003).

Cell Culture. MDCK (American Type Culture Collection) cells were grown in high-glucose (4.5 g/L) Dulbecco's Modification of Eagle's media (D-MEM) (Cellgrow/Mediatech, Herndon, VA) supplemented with the following: 2 mM L-glutamine (BioWhittaker/Canbrex, East Rutherford, NJ); 1 mM sodium pyruvate (BioWhittaker/Canbrex); 0.1 mM non-essential amino acids (Cellgrow/Mediatech); 100 U/L penicillin, 100 μg/L streptomycin, and 0.25 μg/L Fungizone (BioWhittaker/Cambrex); 43.9 mM sodium bicarbonate (Gibco/Invitrogen, Carlsbad, CA); 5% fetal bovine serum and 5% Serum Supreme (BioWhittaker/Cambrex). Cells stocks, maintained in 175 cm^2 flasks (Sarstedt, Newton, NC), were expanded into 500 cm^2 trays (Corning, NY) and grown to 85% confluency for membrane isolations.

Cell Culture for Bioincorporation of Fluorescent Sterol (DHE). For measurement of fluorescent sterol dynamics in purified membrane fractions (see below), MDCK cells were cultured with equivalent amounts of DHE to obtain donor membrane fractions, as described previously for other cell lines (McIntosh et al., 2003; Hale and Schroeder, 1982; Schoer et al., 2000). Since DHE supplementation does not alter the sterol content of the membrane fractions, this ensured that the exchange assay determined sterol exchange, rather than net transfer down a concentration gradient (Hale and Schroeder, 1982; Schoer et al., 2000). Briefly, to prepare fluorescent sterol containing donor membrane fractions for sterol exchange assays, the MDCK cells were cultured as above for 72 h, the medium removed, the cells were washed with PBS, followed by the addition of serum-free medium containing DHE (20 μg/ml serum-free medium). DHE was freshly prepared as a concentrated stock solution in 95% ethanol containing 1 mol % butylatedhydroxytoluene (BHT) and stored at -80$^°$C. DHE was then added to the serum-free culture medium (20 μg/ml serum-free medium) such that the final concentration of ethanol was <0.3%. Since cells rapidly metabolize ethanol and cells were incubated with the DHE for 18 h, the low level of ethanol (<0.3%) initially added to the culture medium had no effect on cell growth, membrane cholesterol distribution, or membrane biochemical properties (Hale and Schroeder, 1982). Acceptor membrane fractions were obtained similarly except that the MDCK cells were cultured

in serum-free maintenance medium without DHE. At the end of 18h culture, the cells were subjected to subcellular fractionation techniques described below.

Isolation of Detergent-Resistant Membranes (DRM) and Detergent-Soluble Membranes (DSM) from MDCK Cells. DRM and DSM were isolated from MDCK cells as previously described for other polarized cell lines (Sapin et al., 2002). Cultures were washed twice in PBS, scraped twice with 2 ml (4 ml final volume) of TNE buffer (20 mM Tris-HCl pH 7.4, 150 mM NaCl, 1 mM EDTA, 0.2 μM PMS-F and 1% Triton X-100), and passed 10 times through a 22-gauge needle. The resulting homogenate was incubated at 4°C for 30 minutes and mixed with 2.5 M sucrose to a density of 40% as part of a discontinuous sucrose density gradient (40%/35%/5%). After ultracentrifugation at 180,000 X g, 4°C for 18 h with an SW41Ti rotor and Optima LE-80k Ultracentrifuge (Beckman Instr., Fullerton CA), DRM were recovered from the 35%/5% interface. For Western blot analysis and sterol exchange assay, the DRM (35%/5% interface) and Triton X-100 soluble material, referred to as DSM (40% gradient layer), were further processed by ultracentrifugation (190,000 X g, 1.5 h, Beckman SW41Ti rotor) in Tris buffer (10 mM Tris, 1 mM EDTA) and suspended in PBS for protein quantification (Pierce Micro BCA assay) or in PBS containing 0.2 μM PMS-F and 1 μl/ml protease inhibitor cocktail set III (Calbiochem) for storage at -80°C. The final purified DRM and DSM were aliquoted in 3.5 μg protein aliquots for donors and 35 μg protein quantities for acceptors.

Isolation of Non-detergent Caveolae/raft Domains (NDCR) from Purified Plasma Membrane Vesicles Isolated from MDCK Cells. First described by Smart et al.. (1995), this procedure utilizes differential (Percoll) centrifugation to first isolate purified PM, followed by subfractionation of the PM vesicles on OptiPrep density gradients. The originally reported method was modified by first culturing MDCK cells with and without DHE as described above and isolated as follows. Four 500cm^2 trays of MDCK cells cultured with the respective sterols were grown to approximately 6x10^7 cells per tray (~85% confluency), washed twice with PBS, scraped twice with 4 ml (8 ml final volume) of PBS containing 0.2 μM PMS-F, and sedimented by

ultracentrifugation at 1000 X g room temperature (RT) for 5 minutes in a model GR4.11 Jouan centrifuge (Jouan, SA, Cedex, France). The cells were suspended in 2 ml ice-cold 0.25 M sucrose, 1 mM EDTA, 20 mM Tris-base, pH 7.8 and sonicated on ice with a cuphorn for four 30 second bursts at 30 second intervals (Misonix 3000, Misonix Inc., Farmingdale, NY) set to power level 3. The nuclei were sedimented at 1,000 X g RT for 10 minutes. The resulting post nuclear supernatant (PNS) was layered onto 30% Percoll (Amersham Biosciences Corp., Piscataway, NJ) and centrifuged at 84,000 X g for 30 minutes at 4°C in a Beckman SW41Ti rotor. The opaque protein band near the middle of the gradient (PM-enriched fraction) was removed (~2 ml total volume) and sonicated on ice with six 30 second bursts at 30 second intervals on ice with a cuphorn (Misonix, Inc.). The PM-enriched fraction was diluted with 50% (weight per volume) OptiPrep to a final concentration of 23% OptiPrep. A continuous gradient of 10% and 20% OptiPrep (1:1, volume per volume) was layered onto the membrane fraction, and the procedure continued exactly as described. Then, 0.2 µM PMS-F and 1 µl/ml protease inhibitor cocktail set III were added to the Non-detergent Caveolae/rafts (NDCR) before storage at -80°C in aliquots of 3.5 µg protein quantities for donors (i.e. containing DHE) and 35 µg quantities for acceptors (lacking DHE).

Isolation of Concanavalin A Affinity-Purified Caveolae/Raft Domains (ACR) and Non-Caveolae/Non-Rafts Domains (NR) from Purified Plasma Membrane Vesicles Isolated from MDCK Cells. PM-derived Affinity-purified Caveolae/rafts (ACR) and Non-caveolae/non-rafts were isolated using a modification of a previously established concanavalin A-based affinity method (Frolov et al., 2000; Schnitzer et al., 2003, Atshaves et al., 2003). All centrifugation steps utilized a Beckman SW41Ti rotor and Optima LE-80k Ultracentrifuge. PM was first isolated by sucrose gradient centrifugation to remove intracellular contaminants, followed by Concanavalin A-based affinity chromatography of PM vesicles to obtain ACR and NR. Briefly, MDCK cells cultured in 500 cm^{2} trays with or without DHE were pelleted as described above. The cells were suspended in 2 ml 0.25 M sucrose, 1 mM EDTA, 20 mM Tris-base, pH 7.8, homogenized by nitrogen gas cavitation (15 minutes at 40 psi), and the nuclei removed

by centrifugation as above. The resulting PNS was floated on a discontinuous sucrose density gradient (0.5 ml 55%, 1.5 ml 40%, 1.5 ml 35%, 1.5 ml 32%, 1.5 ml 29%, 1.5 ml 27%, 1.5 ml 20%, and 0.5 ml 8.3%; w/v in Tris buffer) and centrifuged at 192,000 X g 4^oC for 90 minutes. The PM fractions at the 27%/29% and 29%/32% interfaces were sonicated on ice with three one-second bursts at ten second intervals using a Misonix Sonicator 3000 with a cuphorn and then added to a Concanavalin A-Sepharose 4B slurry (equivalent to 25 ml pre-swollen 4B material; 10-16 mg ConA/ml drained medium) in buffer A (0.14 M KCl, 0.01 M HEPES, 1 mM MgCl2, 1 mM MnCl2, pH 7.8 with KOH). The sample slurry was mixed by lightly bubbling nitrogen through the solution for 2 minutes, incubated for 10 minutes at RT for binding, then transferred to a glass preparative column and allowed to settle for 15 minutes. The flow-through was collected in 14 ml increments, centrifuged at 111,000 X g, 4^oC for 14 h, and the resulting non-caveolar/raft (NR) protein pellets suspended in small volumes of buffer A for protein quantification by BCA. After an additional wash with 25 ml of buffer A, 14 ml volumes of buffer B (0.5 M -methyl-mannosidase in buffer A) were added to the column and mixed with nitrogen bubbling for 10 minutes. Six volumes of buffer B were collected, centrifuged at 111,000 X g, 4^oC for 14 h, and the resulting ACR protein pellets were suspended in small volumes of buffer A for protein quantification or buffer A containing 0.2 µM PMS-F and 1 µl/ml protease inhibitor cocktail set III for storage at -80^oC as above.

Western Blotting to Determine Purity of Purified Membrane Fractions. A series of Western blots were used to detect the presence of specific markers for PM domains or intracellular organelles (e.g. endoplasmic reticulum). Protein concentrations were calculated from a BSA standard curve of absorbance at 280 nm with a Cary100 UV/Visible spectrophotometer (Varian, Palo Alto, CA), then 5 µg/lane of total protein from each fraction was resolved by 12% SDS-PAGE and electroblotted onto nitrocellulose filters (GE Osmonics Inc., Minnetouka, MN). The filters were blocked in 10% weight per volume non-fat dry milk in PBS (10% blotto) for 1 h RT and blotted with the primary antibody (1° Ab) in 2.5% blotto for 14 h at 4^oC. Reactive bands were

visualized by the addition of horseradish peroxidase (HRP)-conjugated IgG and SuperSignal® West Pico chemiluminescent substrate (Pierce) followed by exposure to Kodak X-OMAT film (Parr and Ball, 2003).

Incorporation of Fluorescent Probes for Measurement of Fluorescence Polarization in Purified Membrane Fractions. All fluorophores were prepared as stock solutions in 200 proof anhydrous ethanol with 2% wt/vol butylated hydroxytoluene as an antioxidant. The fluorescent probes were: DHE, DiI C18, DiI C1, *trans*-parinaric acid, *cis*-parinaric acid, NBD-stearic acid, diphenylhexatriene (DPH), DPH-TMA, and DPH Propionic Acid. DHE was bioincorporated into MDCK cells prior to isolation of purified membrane fractions basically as described in the preceding sections, except that the DHE concentration was 10-fold lower in concentration than used for sterol exchange assays to avoid self-quenching. All other fluorescence probes were directly incorporated into purified membrane fractions. In brief, purified stock membrane fractions from several isolations were pooled together, then washed two times with 10 mM Tris buffer (pH 7.4) and subjected to centrifugation at 30,000 rpm for 45 min at $4^{o}C$ in a SW40Ti rotor in an XL90 Ultracentrifuge (Beckman Instr.). Fluorescent probes were incorporated into purified membrane fractions by first placing 35 µg protein of the respective membrane fraction (acceptor, i.e. not containing DHE) in 2 ml of 10 mM, 7.4 pH PIPES buffer. Fluorescent probes were added at a ratio of 1000 µg protein: 1 µg fluorophore such that final ethanol concentrations were maintained at <25 mM. Ethanol concentrations <25 mM have no effect on membrane structure or interaction of lipid binding proteins with ligands (Colles et al., 1995; Schroeder et al., 1995). Finally, such low amounts of ethanol fail to induce fluorescent sterol self-aggregation and formation of crystalline sterol in lipid rafts either *in vitro* or in intact cells (McIntosh et al., 2003). After incubation for 30 min at RT to assure maximal probe incorporation, fluorescence polarization data were acquired as described in the following section.

Measurement of Membrane and Detergent Buffer by Absorbance Spectroscopy. All absorbance measurements to determine detergent concentrations and protein levels

were performed using a Cary 100 Scan UV/Visible spectrophotometer (Varian, Palo Alto, CA). The spectrophotometer has a sample and reference channel; 2 ml samples were measured in 2 cm quartz cuvettes (Fisher Scientific, Pittsburgh, PA). For measurements involving membranes, 10mM PIPES buffer was used as reference. The concentration of Triton X-100 was determined with a method (Crabb and Persinger, 1964; Greff et al., 1965) outlined by the supplier (Sigma Chemical, St. Louis, MO).

Measurement of the Steady State Fluorescence Polarization in Purified Membrane Fractions. All measurements of steady-state fluorescence polarization were determined using a PC1 spectrofluorometer with photon-counting electronics (ISS Instruments, Inc., Champaign, IL) exactly as described earlier (Gallegos et al., 2004). Any residual light scatter contribution to the polarization data with the membrane fractions was corrected by converting polarization to anisotropy according to the relation r = 2P/(3-P), and subtracting the residual fluorescence anisotropy from all experimental data. In order to avoid artifacts due to inner filter effects, absorbance of sample solutions at the excitation wavelengths were kept below 0.15. While we recognize that polarization/anisotropy measurements are comprised of both static (limiting anisotropy) and dynamic (rotational rate) parameters, earlier studies from our laboratories showed that agents which fluidize membranes (ethanol, anesthetics) primarily alter the static (i.e. limiting anisotropy), but not dynamic (rotational), components of polarization/anisotropy measurements (Colles et al., 1995; Schroeder et al., 1995; Schroeder et al., 1988; Sweet and Schroeder, 1986a and 1986b; Sweet et al., 1987). Since alterations in limiting anisotropy are a measure of the cone-angle of fluorescence probe rotation in lipid bilayers, limiting anisotropy and consequently, polarization of the above probe molecules (at very low, non-self quenching concentrations) are useful as relative measures of membrane 'fluidity'.

Measurement of Membrane Sterol Exchange: DHE Release from Self-Quenching Fluorescence Polarization Assay. Sterol exchange between the isolated membrane fractions was determined by using a fluorescent sterol (DHE) exchange assay previously developed by our laboratory (Gallegos et al., 2001a). DHE was used as a

probe for cholesterol transfer because it: (i) is a naturally-occurring fluorescent sterol, (ii) is a close structural analogue of cholesterol, (iii) exhibits the same exchange kinetics as cholesterol in both model membranes and biological membranes, (iv) is taken up by cultured L-cells such that >80% of endogenous sterol is replaced by DHE without altering membrane lipid composition or sterol-sensitive enzymes, (v) co-distributes with cholesterol in model and biological membranes, and (vi) is non-toxic to cultured cells or animals (McIntosh et al., 2003; Schroeder, 1984; Schroeder and Nemecz, 1990; Schroeder, 1991; Schroeder et al., 1996; Hale and Schroeder, 1982; Delseth et al., 1979; Sica et al., 1982; Schroeder et al., 2001a; Bergeron and Scott, 1982a and 1982b; Gimpl and Fahrenholz, 2000; Gallegos et al., 2001a). The underlying premise of the DHE exchange assay is that fluorescence self-quenching of DHE occurs in the donor membrane, which contains high levels of DHE. This results in low DHE fluorescence polarization values for the donor. However, upon addition of 10-fold excess acceptor membranes, the donor membrane DHE exchanges sterols one-for-one with acceptor membranes, thereby resulting in release from self-quenching of DHE. This results in an increase in DHE polarization.

In all sterol exchanges, DHE fluorescence polarization of the donor membrane fraction sample was measured for 20 minutes in 2 ml of 10 mM PIPES buffer to ensure a stable signal baseline and to obtain an initial value for the fluorescence polarization. This was followed by addition of a 10-fold excess of acceptor (i.e., no DHE) membrane. The protein concentration of the donor membrane fractions was 1.5 μg/ml 10 mM PIPES buffer (2 ml total volume), whereas

the protein concentration of the acceptor membrane fraction was 15.0 μg/ml in the 2 ml sample. The DHE polarization was subsequently recorded during 20 s intervals for 3 or 4 h to monitor sterol transfer between membranes.

Standard Curves for the Sterol Exchange Assay. We note that DRM, NDCR, and ACR obtained from all three isolation methods are relatively lipid-rich, and cholesterol-rich compared to the PM (Eckert et al., 2003; Pike et al., 2002; Smart et al., 1995; Gallegos et al., 2004; Atshaves et al., 2003). Also, the ratio of sterol/phospholipid

in caveolae/raft domains isolated by detergent-free methods is basically similar to that of PM (McIntosh et al., 2003; Eckert et al., 2003; Pike et al., 2002; Gallegos et al., 2001b). The standard curve that calculates the fraction of DHE remaining in the donor membrane fraction during an exchange is a polynomial equation involving polarization P of the exchange in the form of:

$$P = \Sigma\ b_n \cdot X_d^n \qquad \text{(Eq. 1)}$$

where X_d is the mole fraction of DHE left in the donor.

For sterol exchange between donor membrane fraction and acceptor membrane fraction, a polynomial with two terms yielded a fit with $r^2 = 0.9999$, i.e. Equation 2:

$$P(x) = b_0 + b_1 X_d + b_2 X_d^2 \qquad \text{(Eq. 2)}$$

where $b_0 = 0.3261$, $b_1 = 0.016$ and $b_2 = -0.144$.

Calculation of the Initial Rate of Sterol Transfer. The initial rate of DHE exchange between donor and acceptor membrane fractions was estimated from the first 10 minutes of exchange data by using the standard curve described above in Equation 2 (Gallegos et al., 2001b). In essence, Equation 2 is the definitive relation that describes the exchange between donor and acceptor membranes. Taking the time derivative of Equation 2 yields:

$$(dP/dt) = b_1\ (dX_d/dt) + 2b_2 \cdot X_d \cdot (dX_d/dt) \qquad \text{(Eq. 3)}$$

As $t \to 0$, $X_d \to 1$ (i.e., initial rate criteria) and rearranging Equation 3, then the following expression is obtained:

$$(1/(b_1+2b_2)) \cdot (dP/dt)|_{t \to 0} = (dX_d/dt)|_{t \to 0} \qquad \text{(Eq. 4)}$$

To obtain the molar transfer rate of DHE (d[DHE]/dt) from donor membrane fraction to acceptor membrane fraction, dX_d/dt was transformed into d[DHE]/dt by factoring in the initial donor membrane fraction protein concentration (1.5 μg protein/ml), the total sterol/protein concentration in the donor membrane fraction (1011.02 pmol total sterol / μ g protein), and the values of b_1 (0.016) and b_2 (-0.144). Combining this information with Equation 4 yielded Equation 5:

$$(d[DHE]/dt)|_{t \to 0} = -2253\ \text{pmol} \cdot (dP/dt)|_{t \to 0} \qquad \text{(Eq. 5)}$$

The initial rate of DHE transfer was directly estimated by substituting the initial measured rate of fluorescence polarization change per unit time (i.e. minutes) for $(dP/dt)|_{t \to 0}$.

Calculation of the Kinetic Parameters of Sterol Exchange. The kinetic parameters of exchange between membrane fraction donor/acceptor pairs were determined by use of the standard curve equation, i. e. Equation 2, and the equation for a one-exponential exchange:

$$X = f_1 \cdot \exp(-k \cdot t) + f_2 \qquad \text{(Eq. 6)}$$

where f_1 and f_2 are the exchangeable and non-exchangeable fractions, respectively, of the sterol in the exchange assay, and k is the rate constant of the exchange. The expression for X in Equation 6 was substituted into Equation 2 to obtain the expression describing the exchange:

$$P(x) = b_0 + b_1 \cdot [f_1 \cdot \exp(-k \cdot t) + f_2] + b_2 \cdot [f_1 \cdot \exp(-k \cdot t) + f_2]^2 \qquad \text{(Eq. 7)}$$

The exchange curves were fit to Equation 8 with r^2 values varying from 0.97 to 0.99. The halftime, $t_{1/2,}$ of the exchanges was defined by the following equation:

$$t_{1/2} = (\ln 2) / k \qquad \text{(Eq. 8)}$$

Data and Statistical Analyses. All curve-fitting and data analyses herein were performed by use of SigmaPlot (Jandel Scientific, San Rafael, CA) scientific data analysis and graphing software.

CHAPTER III

FULL-LENGTH, GLYCOSYLATED NSP4 TRAFFICS TO PLASMA MEMBRANE CAVEOLAE IN ROTAVIRUS-INFECTED CELLS

SYNOPSIS

Rotavirus NSP4, initially characterized as an ER intracellular receptor, is a multifunctional viral enterotoxin that induces diarrhea in murine pups. The route(s) and mechanism(s) of NSP4 intracellular transport vary in different assays and cell lines with reports of secretion of a cleaved fragment, transport in LC3-positive autophagosomes, and association with raft membranes and microtubules. To determine if NSP4 traffics to a specific subset of rafts at the plasma membrane, we isolated caveolae from plasma membrane-enriched material that yielded caveolae membranes free of ER and non-raft plasma membrane markers. Analyses of the newly isolated caveolae from rotavirus-infected MDCK cells revealed full-length, high-mannose glycosylated NSP4. Lack of Golgi-specific processing of the caveolar NSP4 glycans support studies showing NSP4 bypasses the Golgi. Confocal imaging showed colocalization of NSP4 with caveolin-1 early and late in infection, elucidating the temporal and spatial NSP4-caveolin-1 association during infection. This study presents an ER contaminant-free caveolae isolation protocol, the presence of full-length, endoglycosidase H-sensitive NSP4 in plasma membrane caveolae and a final plasma membrane destination for Golgi-bypassing NSP4 transport.

INTRODUCTION

Rotaviruses (RV) are the leading viral etiologic agents of severe pediatric gastroenteritis worldwide affecting nearly all children before the age of 5 with 2 million cases resulting in 444,000 deaths annually (Prashar et al., 2003). RV non-structural protein 4 (NSP4) was initially characterized as an endoplasmic reticulum (ER) transmembrane glycoprotein due to the protein's high mannose glycosylation and its critical function as an intracellular receptor for translocation of subviral particles into the

ER during virion morphogenesis (Erison et al., 1982; Au et al., 1989; Bergmann et al., 1989). However, the identification of NSP4 and NSP4 amino acids (aa) 114-135 (NSP4$_{114-135}$) as enterotoxic and the redistribution of RV-encoded proteins upon NSP4 silencing led to a re-evaluation of NSP4 function(s) and subcellular localization(s) (Ball et al., 1996; Lopez et al., 2005).

A cleaved NSP4 fragment, aa 112-175, is secreted from RV-infected epithelial cells implicating that some portion of NSP4 traffics from the ER to the plasma membrane (PM) (Zhang et al., 2000). Colocalization of NSP4$_{114-135}$ and the extracellular matrix proteins laminin-β3 and fibronectin at the basement membrane of small intestinal epithelia from RV EDIM-infected mouse pups also supports NSP4 transport to the PM during host infection (Boshuizen et al., 2004). While both studies demonstrate that at least a fragment of NSP4 leaves the ER of infected cells, neither confirms the presence of full-length protein at the PM nor reveals the PM lipid microdomain in which the viral glycoprotein localizes. However detection of NSP4 in Triton X-100-resistant 'lipid rafts' isolated from RV-infected Caco-2 cells indicates the viral enterotoxin may be a resident of cellular lipid rafts during infection (Sapin et al., 2002; Cuadras and Greenberg, 2003).

The biophysical structure and composition of cellular lipid rafts remain controversial as they are primarily defined operationally as a collection of cellular membranes insoluble in non-ionic detergents at 4°C. These detergent-resistant membranes or DRM have a unique lipid composition enriched in cholesterol, sphingomyelin, and glycolipids producing a liquid-ordered or gel-phase 'raft' with a light buoyant density on sucrose gradients (Simons and Ikonen, 1997; Smart et al., 1999). Ganglioside M1 (G$_{M1}$), glycerophosphatidylinositol-anchored proteins, flotillin, and caveolins have been used as markers for measuring enrichment of DRM after isolation from cell lysates or membrane fractions (Palandino et al., 2004; Schnitzer et al., 1995; Bickel et al., 1997). Yet the ability of detergents to both cluster and remove cellular membrane proteins illustrate that DRM do not represent the actual composition

of all rafts in the cell (Mayer and Maxfield, 1995; Edidin, 2003; Sot et al., 2002; Heerklots et al., 2003).

Caveolae are a subset of lipid rafts defined by the presence of caveolin proteins (caveolin-1, -2, or -3) (Song et al., 1996; Scherer et al., 1997; Scheffele et al., 1998). Despite the recent use of detergent-free isolations, caveolae composition is nearly as controversial as that of rafts due to the confusing and often conflicting data resulting from the use of different cell types and isolation procedures (Pike 2003). Using a high pH sodium carbonate homogenization buffer and sucrose gradient to isolate caveolae from myocytes yields a caveolin-3-enriched fraction without detectable clathrin, Na/K-ATPase (non-raft PM marker) and mannosidase II (Golgi marker) (Yarbrough et al., 2004). Whereas utilizing the same protocol with a PM-enriched material yields a caveolin-1-enriched fraction that contains both clathrin and Na/K-ATPase (Gustavsson et al., 1999). Other caveolae isolation protocols, such as anti-caveolin affinity chromatography and density gradient fractionation of caveolae sheared from silica-coated PM successfully extract caveolin-containing membranes, but these fractions have yet to be assayed for a similar range of organelle- and vesicle-specific markers (Souto et al., 2003; Schnitzer et al., 1995; Smart et al.., 1995).

We have reported that NSP4 may specifically partition into caveolae during infection. NSP4 and NSP4$_{114-135}$ preferentially interact with highly-curved model membranes enriched in cholesterol and anionic phospholipids (Huang et al., 2001, 2004). Specific secondary structure alterations (increased helical content) upon interacting with different model membranes demonstrate NSP4 and NSP4$_{114-135}$ associate with membranes that mimic caveolae (Huang et al., 2004). Whereas that study utilized vesicles lacking proteins, we also show colocalization of NSP4 with caveolin-1 at both intracellular sites and at the periphery of RV-infected MDCK and Caco-2 cells, and a direct interaction between NSP4 and caveolin-1 by yeast two-hybrid, *in vitro* binding, and co-immunoprecipitation assays (Parr et al., 2006). From these data, we hypothesize full-length NSP4 traffics from the ER to PM caveolae during RV infection of epithelial cells. To examine this hypothesis, we generated a detergent-free isolation method

optimized to produce a PM caveolae-enriched fraction from epithelial cells that contained caveolae markers and were devoid of detectable Golgi, ER, clathrin-coated pit, and liquid-phase (non-raft) PM markers. Analysis of the PM caveolae isolated in this manner from RV-infected cells revealed that full-length NSP4 was present and was double-glycosylated with high-mannose glycans.

RESULTS

Triton X-100-Resistant Lipid Rafts (DRM). A previous report shows NSP4 expression at 12hpi in both Triton X-100 detergent-resistant and -soluble fractions isolated from RV-infected Caco-2 cells (Sapin et al., 2002). For DRM to approximate PM caveolae/rafts, the resistant fraction must contain caveolae-specific markers without detectable ER or non-raft PM markers. The presence of even a trace of ER contamination, a known reservoir of NSP4 during RV infection, in the raft/caveolae fraction could introduce NSP4 as an artifact of the isolation methodology. For analyses of the detergent-resistant and -soluble (DSM) membrane fractions isolated from MDCK cells, DRM were extracted using Triton X-100. Equivalent amounts of lysate, DRM, and DSM proteins (Fig. 7, lanes 1-3 respectively) were resolved by SDS-PAGE and assayed by Western or dot blot for each caveolae/raft and non-caveolar maker described in Table 5. Fig. 7 shows that caveolae markers caveolin-1 (A), flotillin-1 (B), and G_{M1} (C) were present in the DRM fractions. As noted earlier, two distinct forms of caveolin-1 were found in each of the membrane fractions. Two forms of flotillin-1 were also present in the CSC-isolated membranes and, while as yet uncharacterized, may also be due to differences in protein phosphorylation state. Densitometry analysis of the caveolin-1 bands indicated that this key caveolae protein is enriched approximately 3.5 fold in the DRM fractions when compared to lysate levels (data not shown). However the contaminant marker profiles revealed calnexin (ER marker, Fig. 7D) and Na/K-ATPase α (non-raft PM marker, Fig. 7E) also were present in the DRM fraction. The presence of ER and non-raft PM markers preclude use of DRM for determining if full-length NSP4 reaches PM caveolae.

Table 5. Protein and Lipid Markers for Specific Subcellular Membranes.

Marker	Distribution	Comments	References
Caveolin-1	Caveolae, ER, Golgi	Defining caveolae marker, hairpin confirmation inserted into membrane	Smart et al., 1995; Souto et al., 2003; Rothberg et al., 1992
Flotillin-1	Lipid rafts, caveolae[*]	[*]potential caveolae localization, peripheral membrane association	Bickel et al., 1997; Souto et al., 2003; Morrow et al., 2002
Ganglioside M1	PM, caveolae	Glycolipid, primary cholera toxin receptor	Palandino et al., 2004; Parton, 1994; Fra et al., 1995
Calnexin	ER	Integral membrane protein	Rajagopalan et al., 1994; Jackson et al., 1990; Drenan et al., 2004
Giantin	Cis/medial Golgi	Integral membrane protein	Linstedt and Hauri, 1993
Golgin-97	Trans Golgi network (TGN)	Peripheral membrane association	Lu et al., 2004; Drenan et al., 2004
Na/K-ATPase α	Non-raft PM[*]	[*]potential cardiac caveolae localization, integral membrane protein	Gustavsson et al., 1999; Lisanti et al., 1994; Ovchinnikov et al., 1988
Clathrin heavy chain	Coated PM pits, TGN, endosomes	Peripheral membrane association	Schmid, 1997; Kirchhausen, 2000; Stoorvogel et al., 1996
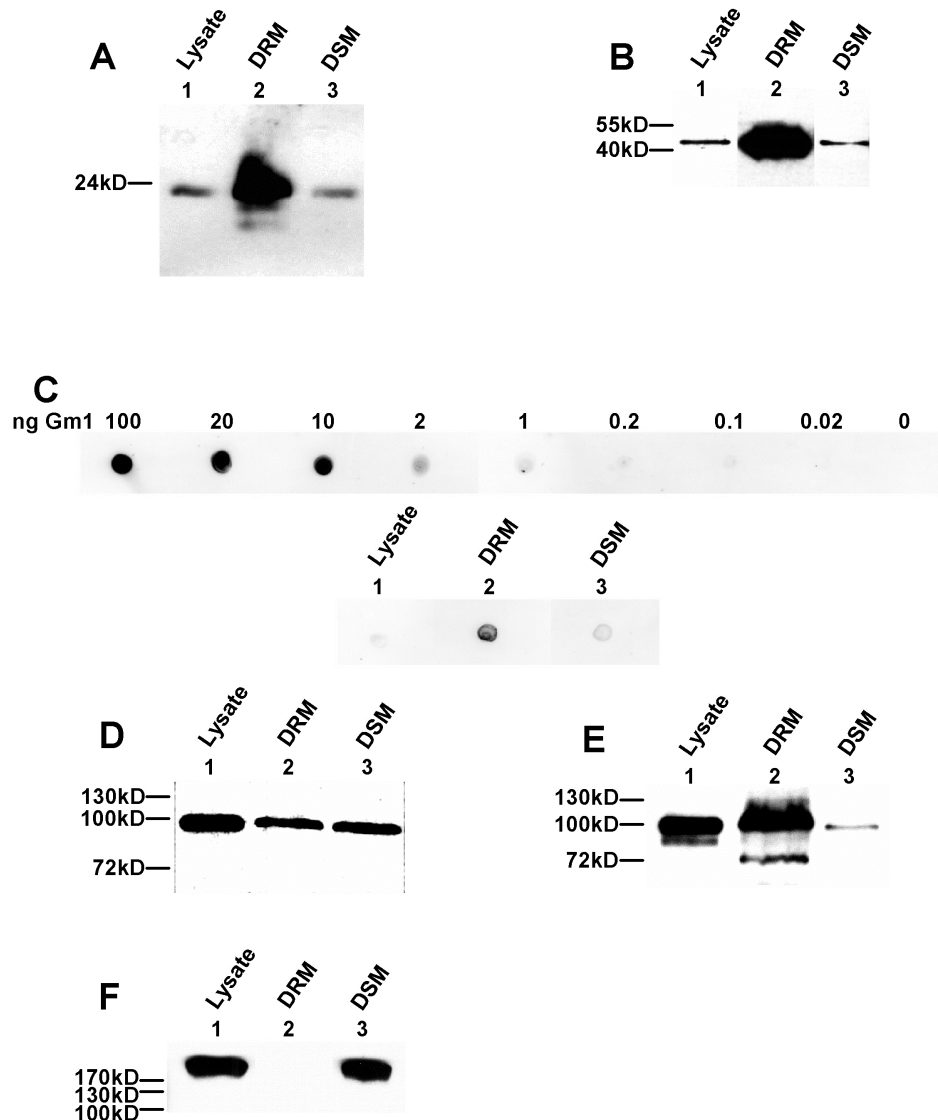
Fig. 7. Distribution of Intracellular Protein and Lipid Markers in Triton X-100-Extracted (DRM) Membrane Fractions. Equivalent amounts of total protein from the cell lysate, detergent-resistant (DRM) and -soluble material (DSM) fractions of MDCK cells (lanes 1, 2, and 3 respectively) were assayed for the presence of specific cellular markers (Table I) by Western blot. Peptide-specific antisera were used to detect (**A**) caveolin-1 and (**B**) flotillin-1. (**C**) Cholera toxin B subunit (CT-B) and CT-B-specific antisera were used to detect the caveolae-localized lipid ganglioside M1 (G_{M1}) levels by dot blot. Marker-specific antisera identified the distribution of contaminating (**D**) ER membrane (calnexin), (**E**) non-lipid raft PM (Na/K-ATPase α subunit) and (**F**) clathrin coats (clathrin heavy chain).

Isolation of PM-Enriched Caveolae in the Absence of ER Marker from Epithelial Cells. Isolation of PM-enriched material was optimized for MDCK cells based on nitrogen cavitation and sucrose gradient fractionation (Gallegos et al., 2001b). Following cell homogenization, the nuclei were pelleted and the post-nuclear supernatant (PNS) was fractionated on discontinuous sucrose gradients. Equivalent volumes of sequential fractions from the gradient were resolved by SDS-PAGE and examined by Western blot for the presence of caveolin-1, Na/K-ATPase α, and calnexin (data not shown). The resulting marker profiles indicated that the gradient layers between the 27% and 29% sucrose interface and the 32% and 35% sucrose interface were enriched in both caveolae and PM markers with a minimal amount of ER marker. This PM-enriched material was briefly sonicated to disrupt large membrane sheets, further purified by ConA affinity chromatography, tested for caveolae and non-caveolae markers, and designated cavitation-sucrose-chromatography (CSC) caveolae.

Differential Protein Composition and Membrane Structure in DRM and CSC Caveolae Fractions. To determine if the global protein composition of the CSC caveolae fraction was similar to that of DRM, equivalent amounts of Triton X-100-extracted and CSC-isolated membrane fractions were resolved by SDS-PAGE and examined by silver staining. As anticipated, there were distinct banding patterns for both DRM and CSC caveolae with unique and similar bands at different molecular weights (mol wt) (Fig. 8). The predominant DRM bands were present at 24 kD and above, while the major bands of CSC caveolae were below 24 kD. Hence there was a striking difference in the overall protein content of the DRM and CSC caveolae.

EM images of CSC caveolae showed vesicular membrane structures (Fig. 9A) with an average diameter of 99 nm (n=61). Separation of these objects into 10 nm diameter groups showed that a majority of these isolated membranes were within the expected range of intact caveolae (50-100 nm diameter) or appeared to be broken structures of smaller size (Fig. 9B).
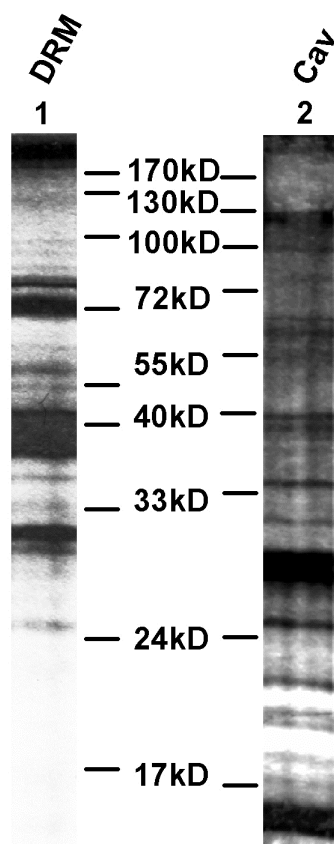
Fig. 8. Silver Stain Analysis of DRM and CSC Caveolae. Equal amounts of total protein from Triton X-100 extracted DRM (lane 1) and isolated CSC caveolae (Cav, lane 2) were resolved by 12% SDS-PAGE and evaluated by silver stain.

A

Negative Stained CSC Caveolae

Frequency Histogram of Discrete CSC Caveolae

B
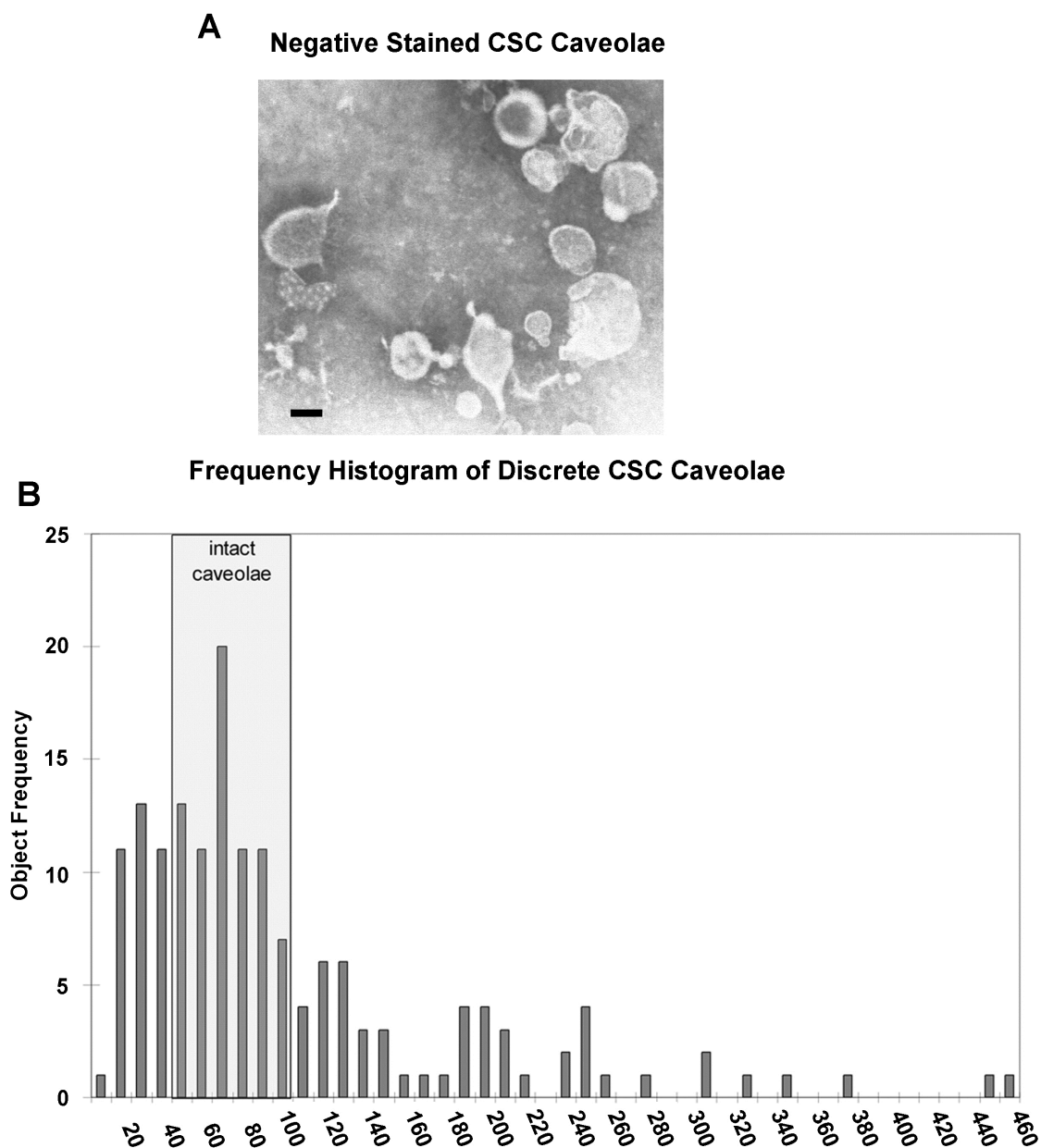
Fig. 9. EM Imaging and Analyses of CSC Caveolae. CSC caveolae were negatively stained with 2% phosphotungstic acid and imaged by EM. (**A**) Three-fold digital magnification was used to resolve the ultrastructure of the membranes to a resolution of 1.52 pixels per nm (inserted bar indicates 100 nm). (**B**) Manual separation of discrete objects and analysis of maximal object diameter by Feret's function resulted in the quantification of the diameter contained in the CSC caveolae fraction. The diameter values were segregated into 10 nm groups and plotted against the number of objects observed within that diameter range. Analyses of 161 discrete objects revealed the size distribution of the membranes in CSC caveolae.

CSC-Isolated Caveolae Contained Caveolae Markers in the Absence of Detectable ER and Non-Raft PM Markers. To examine the presence of caveolae, ER and non-raft PM in the CSC caveolae, equivalent amounts of homogenate, PNS, ER, PM, and CSC caveolae fractions were resolved by SDS-PAGE and analyzed by Western or dot blot for the corresponding cellular markers (Table 5). Specific bands corresponding to caveolin-1 and flotillin-1, and specific spots for G_{M1} confirmed the presence of each caveolae marker in the CSC caveolae (Fig. 10A-C). The contaminant marker profiles (Fig. 10D-F) showed that the protein composition of CSC caveolae differed from that of DRM isolated from the same cells (Fig. 7A-F). The absence of calnexin in CSC caveolae (Fig. 10D) demonstrated that this isolation method lacked detectable ER contamination endemic to DRM. Thus the CSC caveolae preparation was more suitable for our studies to detect NSP4 in PM caveolae. The relatively intense bands corresponding to Na/K-ATPase α and clathrin in the CSC PM fraction and the absence of detectable amounts of either protein in CSC caveolae indicated that these non-caveolar protein markers were absent in the final CSC caveolae isolated from the PM material (Fig. 10E and F).

RV Infection did not Affect Marker Distributions in CSC Caveolae. To ensure that the presence of NSP4 in CSC caveolae was not due to redistribution of ER or non-raft membranes into the caveolae fraction by viral infection, CSC fractions were isolated from RV-infected MDCK cells at 24 hpi and analyzed by Western blot for the same protein markers (Table 5). The caveolae marker profiles showed that the infected CSC caveolae contained both caveolin-1 and flotillin-1 (Fig. 11A and B), but lacked calnexin (C). Since Na/K-ATPase α and clathrin also were absent in the infected CSC caveolae fraction (Fig. 11D and E), RV infection did not introduce redistribution of intracellular organelles or non-raft PM membranes into the CSC caveolae at the time points examined. These data indicate if NSP4 was present in the infected CSC caveolae, its presence would not be from cross-contamination of other intracellular organelles, but transport of NSP4 to PM caveolae.
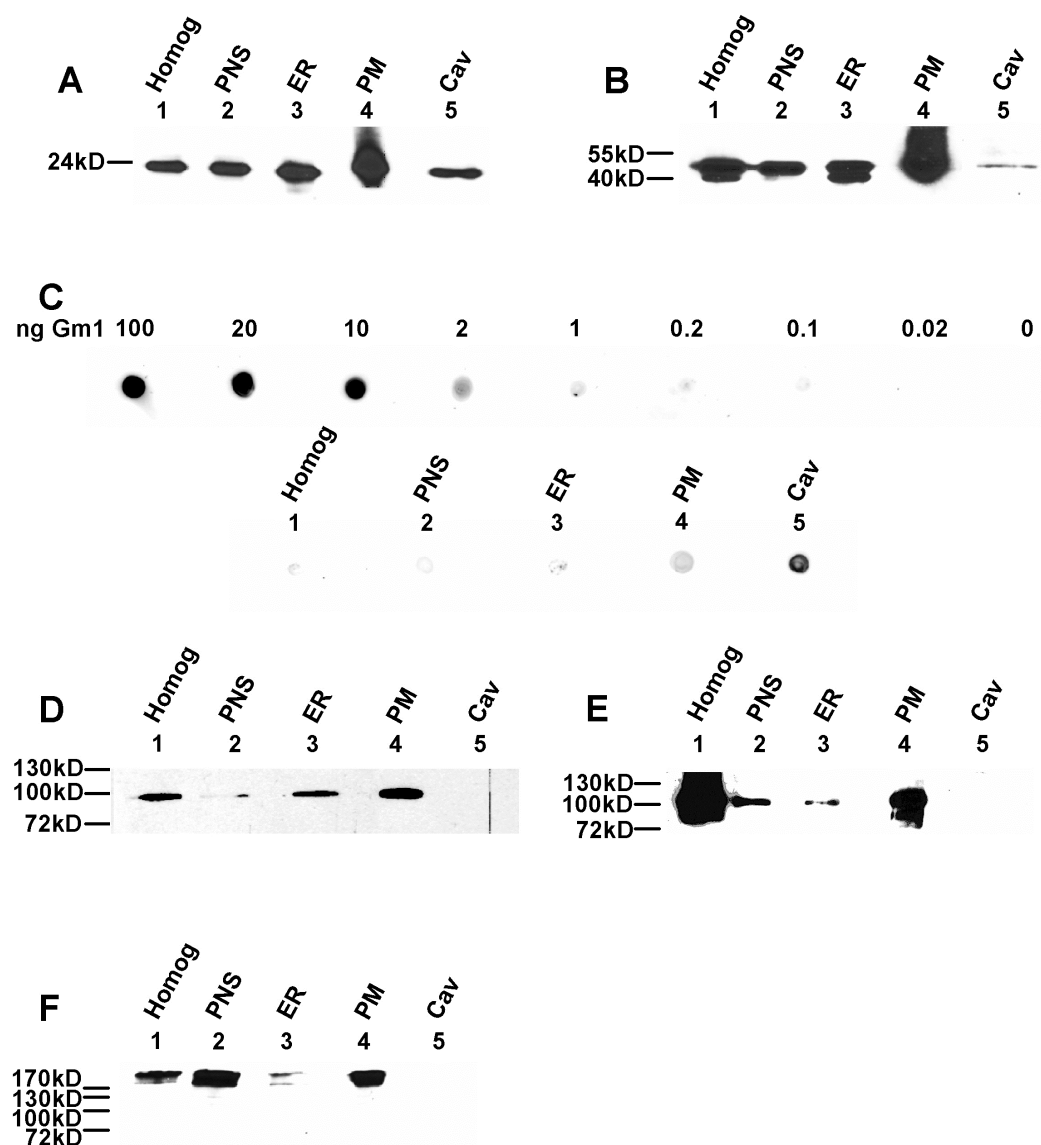
Fig. 10. Distribution of Intracellular Protein and Lipid Markers in CSC-Isolated Membrane Fractions. Equivalent amounts of total protein from homogenate (Homog), post-nuclear supernatant (PNS), ER, PM, and caveolae (Cav) fractions isolated from MDCK cells by CSC isolation (lanes 1-5 respectively) were assayed for the presence of the corresponding markers (Table I). Peptide-specific antisera were used to detect (**A**) caveolin-1 and (**B**) flotillin-1 by Western blot. (**C**) CT-B and CT-B-specific antisera were used to detect the caveolae-localized lipid G_{M1} levels by dot blot. Marker-specific antisera and western blots identified the distribution of contaminating (**D**) ER membrane (calnexin), (**E**) non-lipid raft PM (Na/K-ATPase α subunit), and (**F**) clathrin-coated membranes (clathrin heavy chain) in each of the membrane fractions.
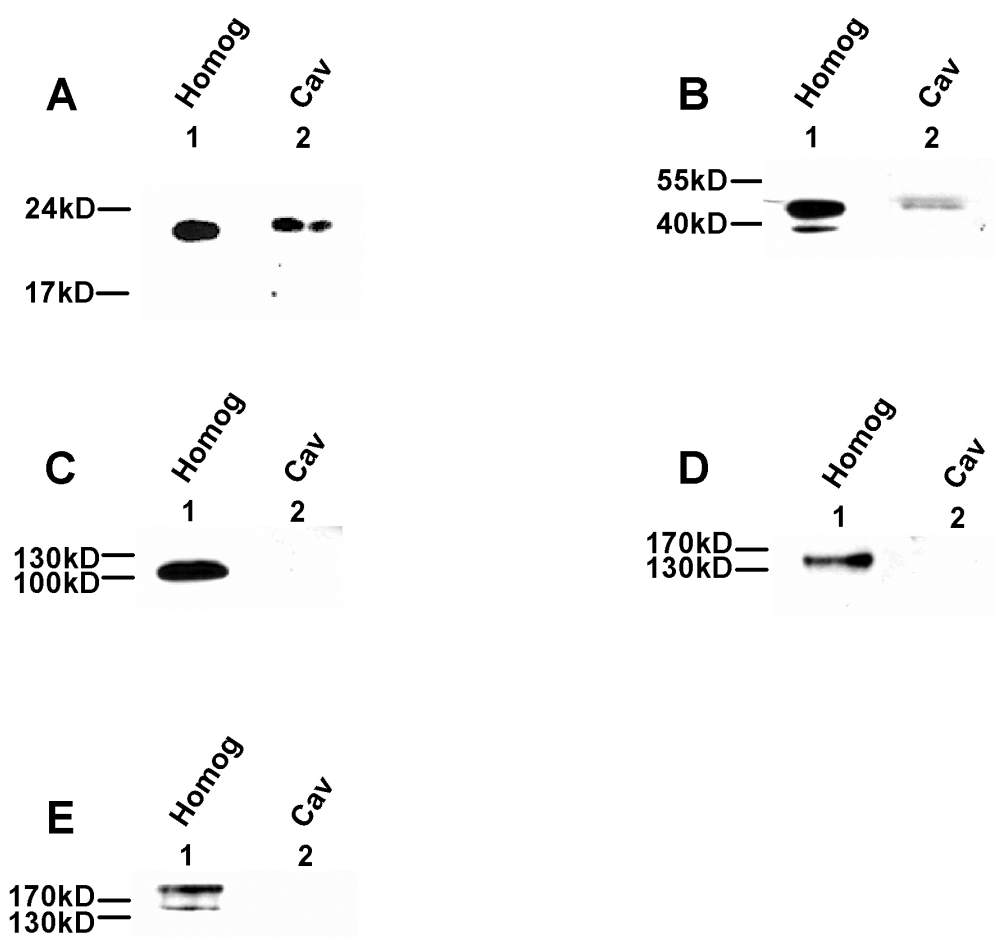
Fig. 11. Distribution of the Intracellular Markers in CSC Caveolae from RV-infected Cells. Equal amounts of total protein from homogenate (Homog, lane 1) and caveolae (Cav, lane 2) fractions isolated from RV-infected MDCK cells were assayed for a panel of cellular markers (Table I). Peptide-specific antisera were used to detect (**A**) caveolin-1 and (**B**) flotillin-1 by Western blot. Marker-specific antisera and western blots were used to identify the distribution of contaminating (**C**) ER membrane (calnexin), (**D**) non-lipid raft PM (Na/K-ATPase α subunit), and (**E**) clathrin-coated membranes (clathrin heavy chain) in each membrane fraction.

Full-Length, EndoH-Sensitive NSP4 was Present in CSC Caveolae Isolated from RV SA11-Infected Epithelial Cells. To evaluate the presence of NSP4 in PM caveolae during RV infection, CSC fractions were isolated from mock or RV-infected MDCK cells, resolved by SDS-PAGE, and analyzed by Western blot. NSP4-specific bands were

present at 28, 24, and 20 kD, the expected mol wt of double-, single- and unglycosylated full-length enterotoxin (Ericson et al., 1982), in the homogenate and enriched in the ER and PM fractions (Fig. 12A, lanes 6, 8, 9 respectively). Of these, only the 28 kD NSP4 was present in CSC caveolae (Fig. 12A, lane 10). There was also a NSP4-specific band of approximately 16 kD observed in all CSC fractions, including CSC caveolae when the blot was overexposed (Fig. 12A, lane 11). While this protein has yet to be fully characterized, its reaction to carboxyl-terminus specific NSP4 antibodies and its appearant mol wt indicate that it may be a NSP4 aa 42-175 (transmembrane domain-to-carboxyl terminus) fragment or a dimer of the previously identified 7.5 kD NSP4 aa 112-175 fragment (Zhang et al., 2000).

EndoH-sensitivity of NSP4 was used to verify the 28 and 20 kD bands were due to the multiple glycosylation states of NSP4 and that both termini of NSP4 were present, the N-terminus by the presence of glycosylation (glycosylation sites at aa 8 and 18; Both et al., 1983) and the C-terminus by using a C-terminal peptide-specific antibody (anti-NSP4$_{150\text{-}175}$). EndoH pretreatment of the infected homogenate resulted in a loss of the 28kD NSP4-specific band with a coinciding increase in the intensity of the 20kD (unglycosylated) NSP4 band (Fig. 12B, lanes 5 and 6). EndoH pretreatment of the CSC caveolae also resulted in a shift of the NSP4 28kD band to the unglycosylated 20 kD form (Fig. 12B, lanes 7 and 8). Absence of the single-glycosylated NSP4 and presence of the non-glycosylated 16 kD fragment in the CSC caveolae indicated that inclusion of full-length, double-glycosylated NSP4 in the PM caveolae was not due to NSP4 glycans simply binding ConA.

NSP4 Associates with Caveolin-1, but not Golgi-Localized Proteins at Early and Late Stages of Infection. The EndoH-sensitivity of NSP4 in CSC caveolae isolated from MDCK cells at 24 hpi suggested the enterotoxin bypassed the endomannosidase-rich Golgi apparatus during transport from the ER. Confocal imaging demonstrated the association of NSP4 with caveolin-1 and lack of association with Golgi at different times post infection. Specificity of each antibody set was tested using mock infected cells, as well as primary and secondary antibody controls (Fig. 13A and B).
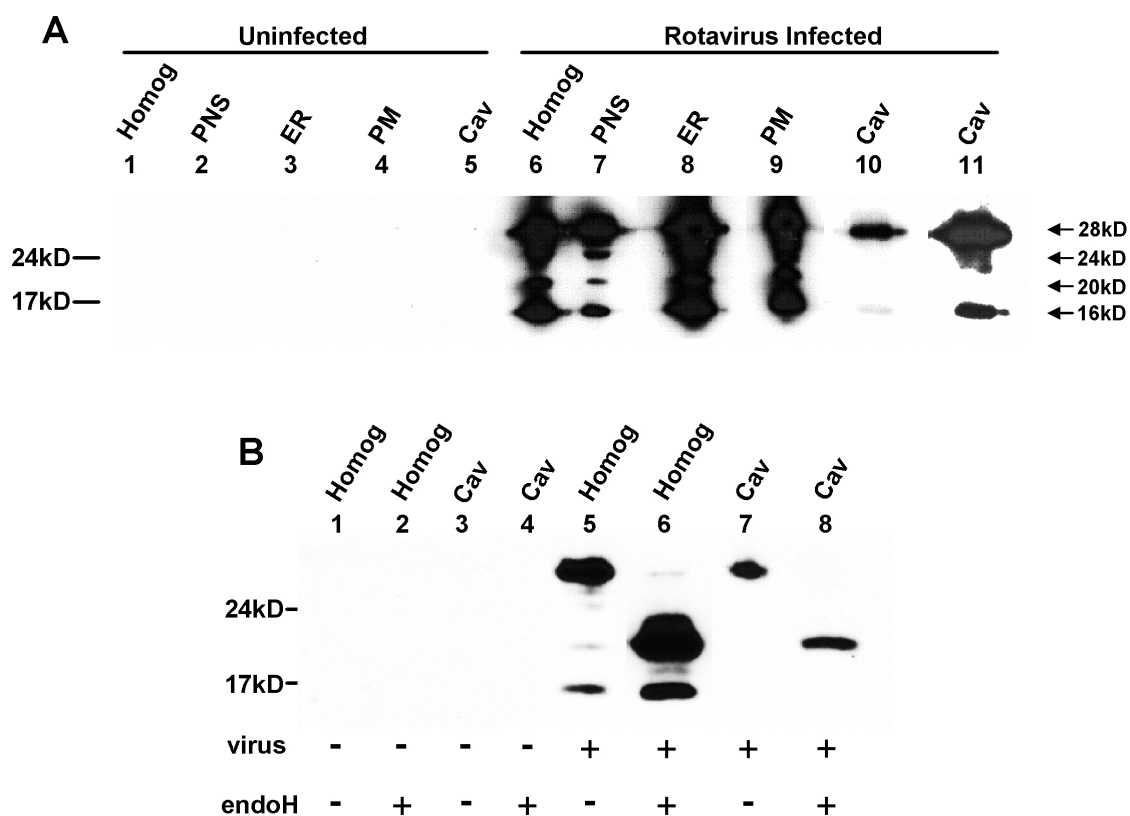
Fig. 12. Detection of Full-Length, EndoH-Sensitive NSP4 in CSC Caveolae Isolated from RV-Infected Epithelial Cells. (**A**) Equal amounts of total protein in homogenate (Homog), post-nuclear supernatant (PNS), ER, PM, and CSC caveolae (Cav) isolated from mock (lanes 1-5) or RV-infected MDCK cells (lanes 6-10) were assayed for the presence of NSP4 with NSP4$_{150-175}$-specific antisera. Homog, PNS, ER and PM fractions show NSP4-specific banding profiles consistent with full-length, double-, single-, and unglycosylated NSP4 (28, 24, and 20 kD respectively) in addition to a ~16 kD band that may be a dimer of the NSP4 cleavage fragment (aa 112-175). CSC caveolae contained predominately the doubly-glycosylated 28 kD form of NSP4 with a relatively small amount of the 16kD band. (**B**) The homogenate (lanes 1 and 2) and PM caveolae (lanes 3 and 4) fractions from uninfected cells were mock (lanes 1 and 3) or EndoH (lanes 2 and 4) treated to determine if the enzyme treatment altered the specificity of NSP4 staining observed in panel A. The homogenate (lanes 5 and 6) and PM caveolae (lanes 7 and 8) from RV-infected MDCK cells were similarly mock (lanes 5 and 7) or EndoH treated (lanes 6 and 8) to confirm that the multiple mol wt forms of NSP4 were due to differences in the glycosylation state of the full-length protein and the absence of Golgi mannosidase trimming.

Captured NSP4 and caveolin-1 images (Fig. 13C center and left panels, respectively) showed significant signal overlap with greater than 50% of NSP4 colocalizing with the cellular caveolae marker at 24 hpi. Analyses of the overlap for pixels wherein both signals were of equivalent relative fluorescent intensity indicated that the NSP4-caveolin-1 association at 24 hpi occurred at the cell periphery, but also perinuclear sites and in vesicular-like cytoplasmic structures (Fig. 13C right panel). The absence of overlapping (Fig. 13D right panel) NSP4 and giantin signals (center and left panels) indicated NSP4 was absent from the Golgi at 24 hpi and agreed with the recent report of NSP4-EGFP and giantin lacking colocalization (Berkova et al., 2006). Although NSP4 was found both in isolated PM caveolae and associated with caveolin-1 at the cell periphery at 24 hpi, previous studies indicate that the initial association of NSP4 with DRM occurs between 6 and 18 hpi (Cuadras and Greenberg, 2003; Sapin et al., 2002). To evaluate the NSP4-caveolin-1 association at this earlier time point, the subcellular distributions of both proteins were evaluated at 7.5 hpi. The fluorescent signals of NSP4 and caveolin-1 (Fig. 13E, center and left panels) overlapped at this early time point with greater than 50% of NSP4 colocalizing with caveolin-1. However the subcellular sites of overlap were different from those observed at 24 hpi. At 7.5 hpi, colocalizing pixels of approximately the same fluorescent intensities were present at the cell periphery, but were primarily in cytoplasmic and perinuclear sites (Fig. 13E, right panel). While caveolin-1 traffics directly between the ER and PM caveolae in specific chaperone complexes, the only experimentally defined caveolin-1 vesicular pathway transits through the Golgi and buds from the trans-Golgi network (TGN) (Dupree et al., 1993; Uittenbogaard et al., 1998; Scheffele et al., 1998). Therefore the subcellular distributions of NSP4 and TGN-localized golgin-97 were examined at 7.5 hpi (Fig. 13F center and left panels). The absence of signal overlap (13F, right panel) confirmed NSP4 was absent from the Golgi at 7.5 and 24 hpi in MDCK cells. Further, there was no detectable Golgi contaminant in CSC caveolae (Fig. 14).
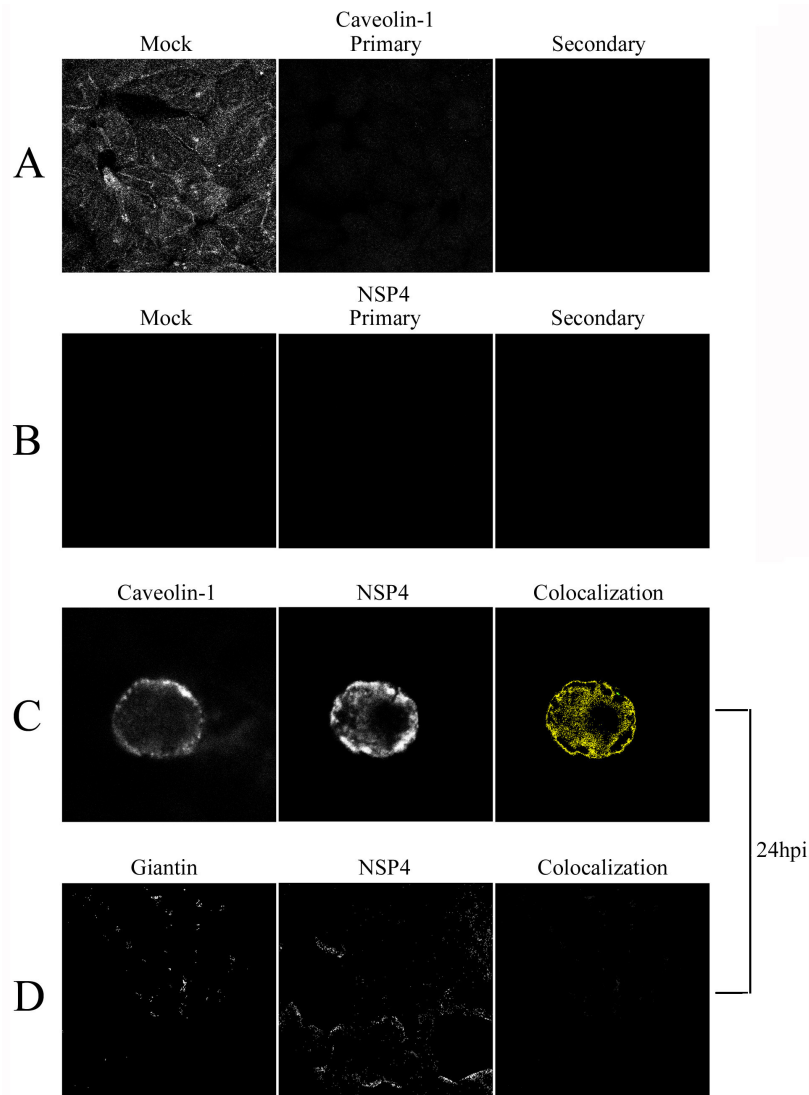
Fig. 13. Association of NSP4 with Caveolin-1 during Early and Late Infection. Fluorescently-tagged secondary antibodies were imaged with 488 nm then 568 nm excitation sources to capture FITC or TR data respectively and to control for FITC signal bleed into the TR images. Images from mock or RV-infected cells in the absence of either primary or secondary antibodies were used to control for stain specificity and non-specific binding of each antibody set (representative [**A**] caveolin-1 and [**B**] NSP4 images at 7.5 hpi shown). For each primary antibody set, the overlapping pixels of approximately equal intensities for FITC and TR were highlighted to identify subcellular distribution of signal colocalization (right panels). (**C**) Images captured at 24 hpi revealed that caveolin-1 (left) and NSP4 (center) colocalized at perinuclear, cytoplasmic, and peripherial sites (right). (**D**) There is an absence of colocalization (right) between Golgi-localized giantin (left) and NSP4 (center) at 24 hpi.

Caveolin-1	NSP4	Colocalization

E

Golgin-97	NSP4	Colocalization

F

7.5hpi
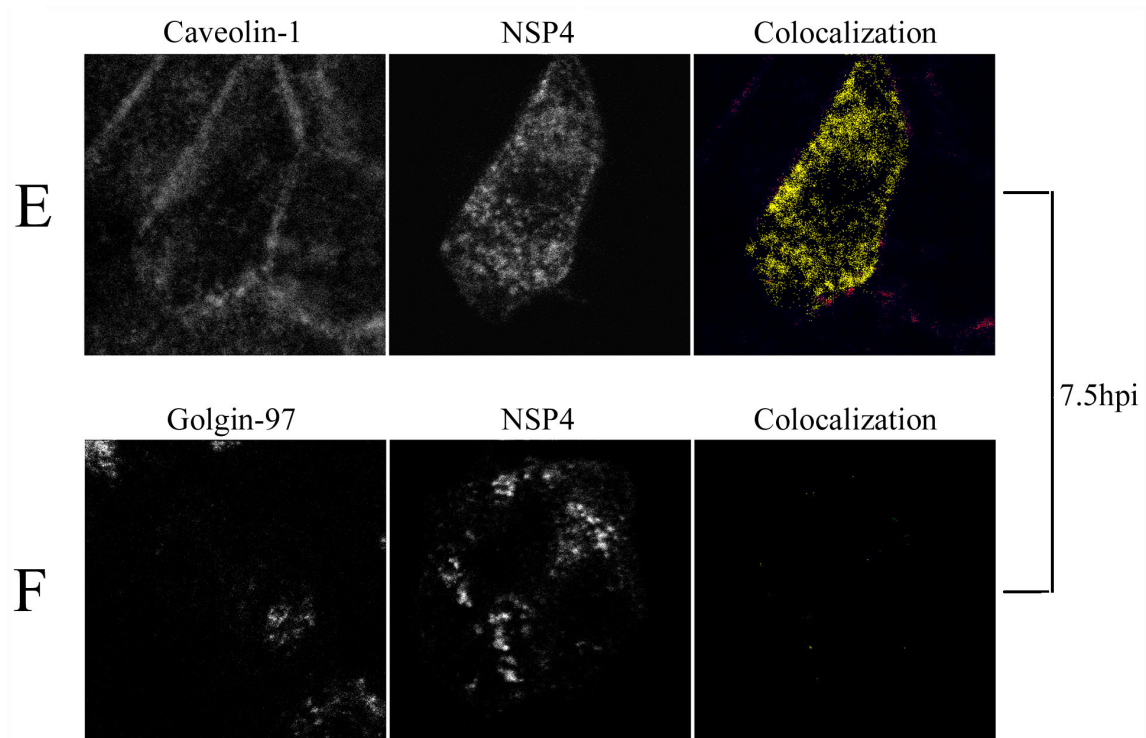
Fig. 13 cont. Fluorescently-tagged secondary antibodies were imaged with 488 nm then 568 nm excitation sources to capture FITC or TR data respectively and to control for FITC signal bleed into the TR images. For each primary antibody set, the overlapping pixels of approximately equal intensities for FITC and TR were highlighted to identify subcellular distribution of signal colocalization (far right panels). (**E**) At 7.5 hpi, caveolin-1 (left) and NSP4 (center) colocalized predominately at punctuate, cytoplasmic sites with weak perinuclear staining (right). (**F**) At the same time post infection, images of NSP4 (center) and the *trans*-Golgi-localized Golgin-97 (left) showed an absence of colocalization (right).
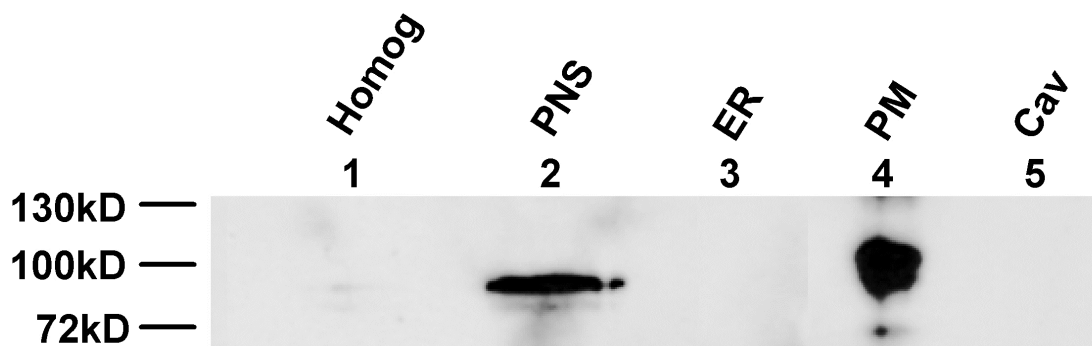
Fig. 14. Distribution of Golgin-97 in CSC-Isolated Membrane Fractions. Equal amounts of total protein from homogenate (Homog), post-nuclear supernatant (PNS), ER, PM, and caveolae (Cav) fractions isolated from RV-infected MDCK cells by CSC isolation (lanes 1-5 respectively) were assayed for the presence of the TGN marker golgin-97 (Table I). Using marker-specific antisera, golgin-97 was undetectable in the CSC caveolae fraction by Western blot.

DISCUSSION

Utilizing a newly developed raft membrane isolation protocol and RV-infected cells, our data show the presence of full-length, high-mannose glycosylated NSP4 in PM caveolae that lack ER marker, but contain caveolin-1, flotillin-1 and G_{M1}. Several reports have implicated the association of NSP4 with lipid rafts. First, a preferential interaction between NSP4 and $NSP4_{114-135}$ with anionic, cholesterol-rich, caveolae-like model membranes has been shown by circular dichroism and a filter-binding assay (Huang et al., 2001 and 2004). Second, RV particles, VP4 (the RV spike protein), and NSP4 are associated with DRM in RV-infected cells (Sapin et al., 2002). Third, infectious RV particles are detected in Triton X-100 insoluble fractions and sensitive to drugs that compromise lipid raft integrity (Cuadras and Greenberg, 2003). Fourth, NSP4 directly binds caveolin-1 with the binding site mapping to NSP4 residues 114-135 (Parr et al., 2006). Taken together, these data strongly indicate an association of raft membranes with RV and NSP4 for intracellular transport from the ER.

There are several reported raft/caveolae isolation protocols that have been extensively utilized to study the composition and interactions specific to raft membrane microdomains (Pike, 2003). For our purposes, it was critical to isolate PM caveolae free of even a trace of ER contamination. ER is a known reservoir of NSP4 during RV infection (Bergmann et al., 1989) and the presence of ER membranes could non-specifically introduce NSP4 into caveolae in the absence of NSP4-raft association. We recognize this concern may be unique to NSP4 and other ER-localized proteins such that a trace of ER contamination would not influence the conclusions of other studies.

A recent report has confirmed that NSP4 bypasses the Golgi in route from the ER to the cell periphery using a NSP4-EGFP fusion protein (Berkova et al., 2006). In that study, the NSP4-EGFP fusion protein fails to localize with Golgi marker, giantin, but colocalizes with the autophagosomal marker LC3 and accumulates close to, but not within, the PM cytoplasmic leaflet. In the present study, we show fully glycosylated, EndoH-sensitive NSP4 in CSC caveolae. This discrepancy in PM localization may be due to inherent differences in virally expressed NSP4 versus expression of a NSP4-EGFP fusion protein and the use of different cell lines. Nonetheless our data agree with that of Berkova et al. (2006) on several key points, including the presence of NSP4 in cytoplasmic, vesicular structures that bypass the Golgi in transport to the PM and the presence of non-ER NSP4 intracellular pools with apparently distinct functions.

Caveolae can function as vesicular carriers containing key fusion complex proteins that mediate vesicle formation, docking and fusion, including GTPases, annexins, N-ethylmaleimide (NEM)-sensitive fusion factor (NSF), soluble NSF attachment proteins (SNAP), and SNAP receptors (SNARE) found on vesicles (vSNARE) or target membranes (tSNARE) (Schnitzer et al., 1995; Razaui et al., 2002). It remains unclear if CSC caveolae interact with fusion-competent caveolae vesicles. The autophagosomes carrying NSP4 apparently do not fuse with other membranes such as the PM. Hence distinct pools of functionally divergent NSP4 may be uniquely transported.

NSP4 and caveolin-1 colocalized at multiple sites within the infected cells (this study and Parr et al., 2006). Although colocalizations via merged confocal images are widely used to determine if two or more molecules are in close proximity, the resolution of these colocalized molecules is approximately 250 nm (McIntosh et al., 2003). Given that caveolae are 50-100 nm in diameter, imaging data alone are inconclusive, necessitating a second, confirmatory technique (Manders et al., 1993).

Caveolin-1 and G_{M1} are established markers for raft/caveolae fractions (Smart et al., 1995; Souto et al., 2003; Rothberg et al., 1992). Flotillin-1, a 45kD membrane-associated protein enriched in isolated lipid rafts as defined by Triton X-100-extracted DRM (Bickel et al., 1997; Morrow et al., 2002), also is detected in high pH, sodium carbonate-extracted 'caveolae', but is absent from immunopurified 'caveolae' (Bickel et al., 1997; Souto et al., 2003). In our hands, flotillin-1 was present in CSC caveolae along with the other two caveolae markers, although the protein markers were not enriched in CSC caveolae when compared to their respective PM levels. Our focus was on obtaining 'pure', ER-negative PM caveolae rather than acquiring large quantities of raft membranes. We discovered there was a trade off between purity and recovery with a probable loss of PM caveolae during processing or extraction of the caveolae subset. Alternatively, the brief sonication used to disrupt the large membrane sheets before ConA-affinity isolation may have sheared a portion of the peripheral and membrane associated protein populations. With these shearing conditions, the presence of full-length NSP4 in CSC caveolae suggests NSP4 crosses the PM bilayer rather than interact by a peripheral association. Additional studies are needed to distinguish the precise protein-lipid interaction.

To ensure the presence of NSP4 in CSC caveolae was not due to co-isolation of a contaminant membrane, calnexin, Golgin-97, clathrin, and Na/K-ATPase α marker proteins were examined. These proteins are commonly utilized to indicate the presence of the corresponding membrane (Drenan et al., 2004; Kirchhausen, 2000; Lisanti et al., 1994). The resultant marker profiles indicate CSC caveolae is void of detectable ER, Golgi, and clathrin-coated membranes, as well as non-raft PM domains and therefore

appropriate for determining the presence of NSP4 in PM caveolae. Optimization of the CSC caveolae isolation to extract a final membrane fraction devoid of detectable Na/K-ATPase α from PM enriched in the same markers resulted in extraction of predominantly PM caveolae, but potentially could be an enriched subset of the cell caveolae population.

The recent identification of NSP4 in DRM isolated from RV RF-infected colon cells (Sapin et al., 2002) prompted us to define the composition of identical DRM isolated from MDCK cells and provide further insight into the presence of NSP4 in lipid rafts and caveolae. While clathrin was not detected in MDCK DRM, significant amounts of the ER and non-raft PM markers were present. Due to the ER and non-raft PM contaminants, previous identification of NSP4 in DRM is indicative, but not conclusive, of NSP4 caveolae localization.

The critical intracellular receptor function of NSP4 in RV morphogenesis stresses the importance of a NSP4 pool in the ER during infection (Au et al., 1989; Bergmann et al., 1989; Chan et al., 1988). NSP4 in CSC caveolae extracted from a PM-enriched material devoid of detectable ER contamination indicates the presence of a second pool of NSP4 that is transported to PM caveolae during infection. A third and fourth pool have been implicated in LC3-containing autophagosomes (Berkova et al., 2006) and radiating from the ERGIC along microtubules (Xu et al., 2000). It is reasonable to propose the RV multifunctional enterotoxin is transported by multiple cellular pathways to different intracellular locations for distinct purposes. More than one pathway may direct NSP4 to the same intracellular site dependent on the infecting viral strain, time post infection, and differences in techniques.

In summary, NSP4 is a multifunctional, complex glycoprotein that uniquely interacts with host cell molecules. The data presented herein confirms the presence of full-length NSP4 in PM caveolae and the lack of Golgi association in transport to the PM. Additional studies are needed to determine if NSP4 transport is dependent on caveolin-1 or caveolae intracellular movement and to fully elucidate the many roles of NSP4 during infection.

MATERIALS AND METHODS

Antibodies and Reagents. Antibodies directed against Na/K-ATPase α (mouse anti-sheep Na/K-ATPase α; Affinity BioReagents, Inc., Golden, CO), calnexin (rabbit anti-canine calnexin aa 575-593; Stressgen Biotech, Victoria, BC Canada), Golgin-97 (mouse anti-human golgin-97; Molecular Probes, Eugene, OR), giantin (rabbit anti-human giantin aa 1-469, Covance Research Products, Inc, Princeton, JN), flotillin-1 (mouse anti-mouse flotillin-1 aa 312-428) and clathrin (mouse anti-rat clathrin heavy chain aa 4-171; BD Transduction Lab, Lexington, KY), and cholera toxin (rabbit anti-Vibrio cholerae toxin; Sigma Aldrich, Saint Louis, MO) were purchased from the indicated commercial sources. Horseradish peroxidase (HRP; goat anti-rabbit and anti-mouse IgG*HRP; Southern Biotech Assoc, Inc, Birmingham, AL), alkaline phosphatase (AP; goat anti-rabbit IgG*AP; Sigma Aldrich) and fluorescent (goat anti-mouse IgG-Texas Red [TR]; Rockland Immunochemicals, Inc, Gilbertsville, PA; goat anti-rabbit IgG-fluorescein [FITC]; KPL, Inc, Gaithersburg, MD) conjugated antibodies also were purchased commercially. Anti-caveolin-1 peptide (aa 2-31 deduced from the human caveolin-1 sequence) and anti- NSP4 peptide (aa 150-175 deduced from the simian rotavirus SA11 NSP4 sequence) were generated in rabbits and mice using peptide crosslinked to keyhole limpet hemocyanin (KLH) as antigen (Parr et al., 2006). $NSP4_{150-175}$-specific antibodies were affinity purified before use in confocal micrcroscopy. Purified cholera toxin B subunit (Sigma Aldrich), 5-bromo-4-chloro-3'-indolyphosphate p-toluidine (BCIP)/nitro-blue tetrazolium chloride (NBT) premixed electrophoresis reagent (Sigma Aldrich), Concanavalin A-Sepharose 4B (ConA, Amersham Pharmacia Biotech, Piscataway, NJ), α-methyl-D-mannopyranoside (Acros Organics/Fisher Sci Intl, Inc, Hampton, NH), endo-β-N-acetylglucosaminidase H (EndoH; New England BioLabs, Ipswich, MA), protease inhibitor cocktail set III (Calbiochem, Darmstadt, Germany), and 0.45μ pure nitrocellulose (GE Osmonics Labstore, Minnetonka, MN) were acquired from commercial sources.

Cultured Cells and Virus. Madin Darby Canine Kidney cells (MDCK; ATCC, Manassas, VA) were grown in maintenance media (Dulbecco's Modification of Eagle's

media (D-MEM) with 4.5 g/L glucose, L-glutamine, and sodium pyruvate; Mediatech, Inc., Herndon, VA) supplemented to 2 mM L-glutamine (200 mM; BioWhittaker/Cambrex), 1 mM sodium pyruvate (100 mM; Cambrex), 0.1 mM non-essential amino acids (10 mM; Mediatech, Inc.), 100 U/L penicillin (pen), 100 µg/L streptomycin (strep), 0.25 µg/L Fungizone (10,000 U pen/10,000 strep/25 ug/L Fungizone; Cambrex), 43.9 mM sodium bicarbonate (Grand Island Biologicals Co), 5% fetal bovine serum, and 5% Serum Supreme (Cambrex) at 37^oC in 5% CO_2. Cells stocks were maintained in 175 cm^2 flasks and expanded into 500 cm^2 trays or 2 cm^2 multiwell plates (Corning, Inc, Corning, NY). MDCK cells were infected with SA11 clone 4F (gift of Mary Estes, Baylor College of Medicine, Houston, TX) at an MOI of 2. Briefly, the virus was sonicated (5min using a cuphorn attachment ice bath in a Misonix Sonicator 3000; Misonix, Inc, Farmingdale, NY) and incubated in serum-free D-MEM with 5 µg/ml trypsin for 30 min at 37^oC, then incubated with the activated inoculum for 1h at 37^oC in 5% CO_2. The inoculum was replaced with serum-free D-MEM supplemented with 1µg/ml trypsin and the cells incubated for an additional 7.5 or 24 h.

DRM Isolation. DRM were isolated from MDCK cells as previously described (Sapin et al., 2002). Briefly, four 500 cm^2 trays of cells were grown to confluency (~ $6x10^7$ cells/tray), washed with phosphate buffered saline (PBS), and scraped into a 4ml final volume of TNE buffer (20 mM Tris-HCl pH 7.4, 150 mM NaCl, 1 mM EDTA, 0.2 µM PMS-F and 1% Triton X-100). The suspended cells were passed 10 times through a 22-guage needle and the homogenate incubated for 30 min at 4^oC before mixing with 2.5 M sucrose to a density of 40%. A 40%, 35%, 5% discontinuous sucrose density gradient was centrifuged at 180,000 X g, 4^oC for18 h (Beckman SW41Ti rotor and Optima LE-80k Ultracentrifuge) and the DRM were recovered from the 35%/5% interface. For Western blot analysis, the DRM and DSM proteins (40% gradient layer) were further processed by ultracentrifugation (190,000 X g, 1.5 h, Beckman SW41Ti rotor) in Tris buffer (10 mM Tris, 1 mM EDTA), suspended in PBS for protein quantification or in PBS containing 0.2 µM PMS-F and 1 µl/ml protease inhibitor cocktail set III for cold storage at -80^oC. All membrane isolations were completed on ice unless otherwise noted.

CSC Caveolae Isolation. PM-derived caveolae were isolated with a sucrose gradient followed by ConA affinity chromatography (CSC) as described (Gallegos et al., 2006). Briefly, MDCK cells were grown in 4-8 trays (500 cm^2), washed twice with PBS, and scraped into 8 ml final volume. Cells were pelleted for 5 min at 1,000 X g at room temperature (RT), suspended in 2 ml of 0.25 M sucrose, 1 mM EDTA, 20 mM Tris-base, pH 7.8, and homogenized by nitrogen gas cavitation (15 min at 40 psi). The nuclei and remaining intact cells were pelleted by centrifugation for 10 min at 1,000 X g RT. Original cell supernatant and PNS were floated on a discontinuous sucrose density gradients (0.5 ml 55%, 1.5 ml 40%, 1.5 ml 35%, 1.5 ml 32%, 1.5 ml 29%, 1.5 ml 27%, and 1.5 ml 20%; all w/v in 1 mM EDTA, 20 mM Tris-base pH 7.8), and centrifuged for 90 min at 192,000 X g 4°C. ER-enriched fractions (35%/40% and 40%/55% interface bands) from the cell supernatant gradient were pooled, pelleted for 2 h at 190,000 X g 4°C, and suspended in PBS containing 0.2 µM PMS-F and 1 µl/ml protease inhibitor cocktail set III for storage at -80°C. The PNS-derived PM fractions (27%/29%, 29%/32%, and 32%/35% interface bands) were pooled, sonicated briefly (three 1 sec pulses at 5 sec intervals in a Misonix Sonicator with cuphorn attachment at power level 3) and added to a slurry of ConA-sepharose 4B prewashed in Buffer 1 (0.14 M KCl, 0.01 M HEPES, 1 mM MgCl$_2$, 1 mM MnCl$_2$, pH 7.8 with KOH). The PM-containing slurry was mixed for 2 min by nitrogen bubbling, incubated for 10 min at RT for binding, transferred to a glass preparative column and washed with 75 ml of Buffer 1. Buffer 2 (0.5 M α-methyl-mannopyranoside in buffer 1) was added, mixed by nitrogen bubbling and the ConA-binding material drained from the column. A total of six sequential 14 ml Buffer 2 washes were collected, centrifuged for 14 h at 111,000 X g 4°C, and the resulting caveolar membrane pellets suspended in small volumes of Buffer 2 for protein quantification or Buffer 2 containing 0.2 µM PMS-F and 1µl/ml protease inhibitor cocktail set III for storage at -80°C. See Appendix B for further details.

Protein Quantification. Micro BCA^{TM} Protein Assay and SilverSNAP Stain II kits (Pierce, Rockford, IL) were used to quantify the protein concentration of the isolated membrane fractions. The Micro BCA kit was used with BSA standards per

manufacturer's protocol to calculate an initial protein concentration for each membrane fraction. To ensure the differences in sample solvents did not alter the analysis of marker enrichment, equivalent amounts of each fraction as calculated above were resolved by SDS-PAGE and silver stained using SilverSNAP. Densitometry scans of the stained proteins in each lane were used to correct the BCA protein concentrations based on the fold difference from the lysate (Triton X-100 fractions) or homogenate (CSC fractions) absorption units per lane.

Electron Microscopy of Isolated Caveolae. CSC caveolae were negatively stained with 2% phosphotungstic acid (PTA), pH 7.0, as described with slight alterations (Gelderblom et al., 1991) and examined by electron microscopy, Zeiss EM 10C. In brief, CSC caveolae were adsorbed onto a Formvar coated film grid (Electron Microscopy Sciences, Fort Washington, PA) for 1hr at RT. The adsorbed objects were stained with PTA and images captured at 8,000 fold magnification. The captured images were scanned and processed with ImageJ (developed at NIH and is available at http://rsb.info.nih.gov/ij) for scale (3 fold digital zoom for a resolution of 1.52 pixels per nm), threshold, and manual discrete object separation. The processed images were analyzed in Adobe Photoshop by Feret's function to quantify the maximal diameter of visible discrete membranes.

Endoglycosidase Reactions. For EndoH cleavage, 1μg aliquots of total protein from fractionated caveolae isolated from uninfected and RV-infected (MOI of 2, 24 hpi) MDCK cells were used. The gylcoprotiens were denatured and diluted per manufacturer's protocol (New England Biolabs). Either 1 μl of sterile water (mock cleavage) or 1 μl of EndoH was added to the control/sample set from mock and infected cells. The cleavage reaction was performed for 1 h at 37°C and the proteins resolved by SDS-PAGE and Western blot.

Western Blot Analyses. A series of Western blots were utilized to monitor enrichment of specific organelle markers in each of the isolated membrane fractions, and to identify those fractions containing NSP4. Two μg total protein from each fraction (or 1 μg of each glycosidase cleaved sample) was resolved on 12% polyacrylamide minigels

and transferred to nitrocellulose filters (0.45 μ pure nitrocellulose; GE Osmonics) according to the manufacturer (Mini-PROTEAN II and Trans-Blot respectively; BioRad). The filters were blocked in 10% (w/v) non-fat dry milk in PBS (10% blotto) for 1 h at RT and reacted with the primary antibody (1° Ab) in 2.5% blotto for 14 h at 4^oC with rocking. The filters were incubated an additional 1h at RT with 1° Ab, then washed once in 0.5% blotto, twice in 0.5% blotto with 0.05% Tween-20, and once in 0.5% blotto with rocking (10 min per wash). Secondary antibodies (2° Ab) were diluted in 2.5% blotto and incubated with the filters for 1 h at RT with rocking. The filters were washed as above, rinsed with PBS, and reacted with SuperSignal West Pico or Femto chemiluminescent substrates as per manufacturer's protocols (Pierce). The marker-specific bands were visualized by exposure to and development of x-ray film and the resulting signals were analyzed by densitometry scan.

Cholera Toxin G_{M1} Binding Assay. A dilution series of purified G_{M1} (0 to 100 ng) and equivalent amounts of total protein from each isolated fraction were spotted onto nitrocellulose filters, air dried, and rinsed twice in PBS. The filters were blocked in 3% (w/v) BSA in PBS for 30 min at RT, rinsed twice gently with PBS, and incubated with 1 μg/ml cholera toxin subunit B (CT-B) in PBS for 2 h at RT. Excess CT-B was removed with 2 PBS rinses and the filters were incubated with 1:500 rabbit anti-CT-B in PBS for 1 h at RT. Following two rinses with PBS, the filters were incubated with goat anti-rabbit IgG conjugated to alkaline phosphotase in PBS (1:7,500) for 30 min at RT, and rinsed twice in PBS. The filters were washed in AP reaction buffer (1 M Tris, 0.1 mM NaCl, 10.5 mM $MgCl_2$ pH 9.0) for 5 min at RT and the G_{M1}:CT-B signals developed in BCIP/NBT. The filters were rinsed twice in water, dried, and laminated before analysis of the resulting signals by densitometry scan.

Confocal Microscopy. Mock and SA11-infected MDCK cells grown on glass coverslips were processed at 7.5 or 24 hpi for fluorescent imaging. Mock and infected cells were rinsed in PBS, fixed and permeabilized in methanol:acetone (1:1, v/v) for 10 min at -20^oC. Non-specific binding sites were blocked with 3% blotto/PBS for 45 min at RT and cells incubated with primary antibodies diluted in 1% blotto/PBS at RT for 45

min. The cells were washed in 0.5% blotto/PBS four times, 10 min each and incubated with TR or FITC labeled secondary antibodies diluted in 1% blotto/PBS for 45 min in the dark. The cells were washed again as above (in the dark), twice in PBS, and mounted with fluorescent mounting media (KPL) onto glass slides. The resulting fluorescent images were captured with a MRC-124MP BioRad laser scanning confocal microscopy (LSCM) system (BioRad, Hercules, CA) using a Zeiss inverted Axiovert microscope (Carl Zeiss, Inc., Thronwood, NY), a 63X Zeiss oil Apochromat objective, and the 488 and 568 nm excitation lines of an argon/krypton ion laser source. LaserSharp 3.0 (BioRad), Confocal Assistant 4.02 (Brelje TC/BioRad) and Adobe Photoshop 7.0 (Adobe Systems Inc., San Jose, CA) were used to capture the pixilated fluorescent data, to calculate colocalization values and to adjust contrast curves to construct the final images respectively.

CHAPTER IV

EXTRACELLULAR EXPOSURE OF THE CARBOXYL TERMINUS OF FULL-LENGTH NSP4 ON THE PLASMA MEMBRANE OF ROTAVIRUS-INFECTED MDCK CELLS

INTRODUCTION

Rotavirus (RV) nonstructural protein 4 (NSP4) is a multifunctional glycoprotein initially defined as an endoplasmic reticulum (ER)-localized receptor critical for virion morphogenesis at the ER (Ericson et al., 1982; Au et al., 1989; Bergmann et al., 1989). However, the calcium (Ca^{2+})-mediated chloride secretion and diarrhea induced by this nonstructural protein at the PM indicate that NSP4 can function outside of the ER (Ball et al., 1996). In NSP4-enhanced green fluorescent protein (EGFP)-transfected HEK293 cells, a portion of the fusion protein is localized at the cell periphery, but not within the plane of the PM (Berkova et al., 2006). Yet a carboxyl (C)-terminal NSP4 fragment has been identified in the media of RV-infected MA104 and HT-29 cultures and colocalization of C-terminal NSP4 epitopes with extracellular matrix proteins at the basement membranes of RV-infected mouse pup intestinal epithelium has been reported (Zhang et al., 2000; Boshuizen et al., 2004). In this study, laser scanning confocal microscopy (LSCM) confirmed both the presence of NSP4 at the PM and exposure of the NSP4 C-terminus on the exofacial surface of RV-infected epithelial cells. Cell surface-specific biotinylation and subsequent analysis of the biotin-labeled proteins confirmed NSP4 exposure and revealed that the exposed enterotoxin was full-length and high-mannose glycosylated.

RESULTS

LSCM Analysis of NSP4 Presence at the PM. To determine if NSP4 trafficked to the PM, we assessed the association of the enterotoxin with PM-localized Na/K-ATPase in SA11-infected MDCK cells at 24 hpi. While the microdomain distribution of Na/K-ATPase is still under debate, the integral membrane protein's presence at the PM of

kidney and absorptive epithelia cells, as well as that of MDCK cells, has been documented (Almers and Stirling, 1984; Deppe et al., 2002). In the characterization of CSC cavolae 'purity' (see CHAPTER II), Na/K-ATPase was used as a marker for non-raft membranes. However, it is a quintessential marker for identifying the PM in fluorescent and confocal microscopy. The resolution of the laser scanning confocal system used in this study was approximately 250 nm per pixel. As PM caveolae are defined morphologically as 50 – 100 nm diameter membrane invaginations, it is possible for a protein within a caveolae microdomain (NSP4) to be present within the same pixel (colocalize) as a protein in the non-raft portion of the PM (Na/K-ATPase). Our confocal imaging indicated that $37.3 \pm 1.5\%$ (n=3) of the NSP4 signal present in MDCK cells late during infection (Fig 15A) overlaps with the Na/K-ATPase staining of the PM (Fig 15B). The overlapping pixels in which both signals are present at similar intensities appear to distribute near or at the surface of the infected cells (Fig 15C).

To confirm the presence of NSP4 at the cell surface, we first had to ensure our staining of intact cells did not detect intracellular proteins. Due to its Golgi-specific localization and the lack of previous association with RV or NSP4, giantin-specific antibodies were used to test for PM permeability (Linstedt and Hauri, 1993; Berkova et al., 2006). MDCK cells fixed and permeabilized as above displayed significant punctate and reticular giantin signal (Fig 16A). However, when the cells were incubated with giantin-specific antibodies and fixation without permeabilization, the Golgi staining was absent (Fig 16B). While giantin staining of the Golgi was visible in RV-infected cells as well, the number and size of these structures were reduced and seldom within the same plane as a majority on the NSP4 signal (data not shown). As earlier observed, a predominately peripheral and cytoplasmic NSP4 signal distribution was found in RV-infected MDCK cells fixed and permeabilized at 24 hpi (Fig 16C). However in intact cells, NSP4-specific staining appeared in thin peripheral patches at 24 hpi (Fig 16D). Similar, albeit smaller, patching of lipid raft proteins has been observed at the PM of other cell types and the surface NSP4 distribution is suggestive, but not conclusive of enterotoxin segregation into PM microdomains (Harder et al., 1998).
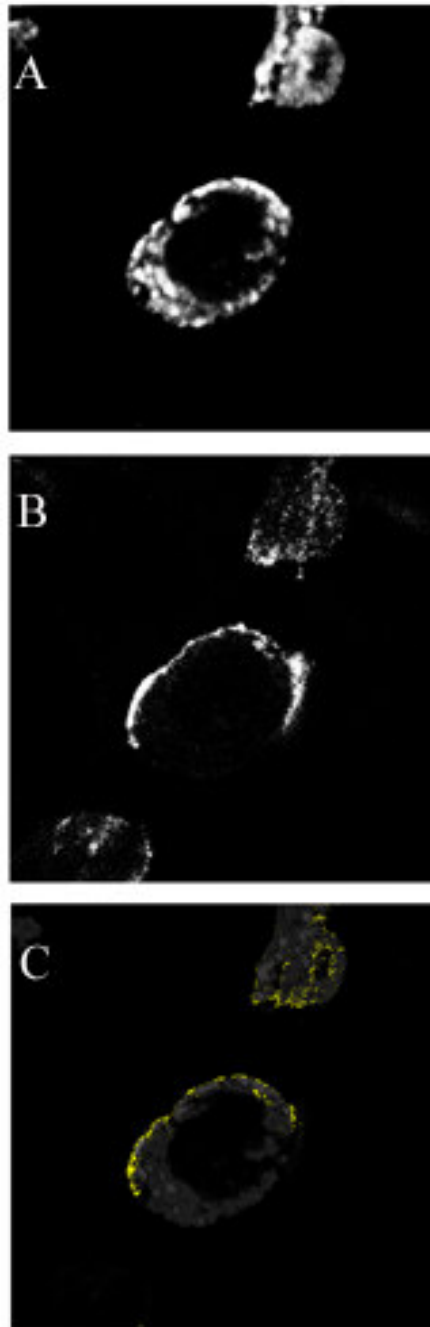
Fig. 15. NSP4 Colocalization with Na/K-ATPase at the PM. RV-infected MDCK cells fixed and permeabilized at 24 hpi were stained for (**A**) NSP4 (rabbit anti-NSP4 aa 150-175) and (**B**) Na/K-ATPase α. (**C**) Overlapping pixels of equivalent intensities were primarily distributed at the cell periphery.
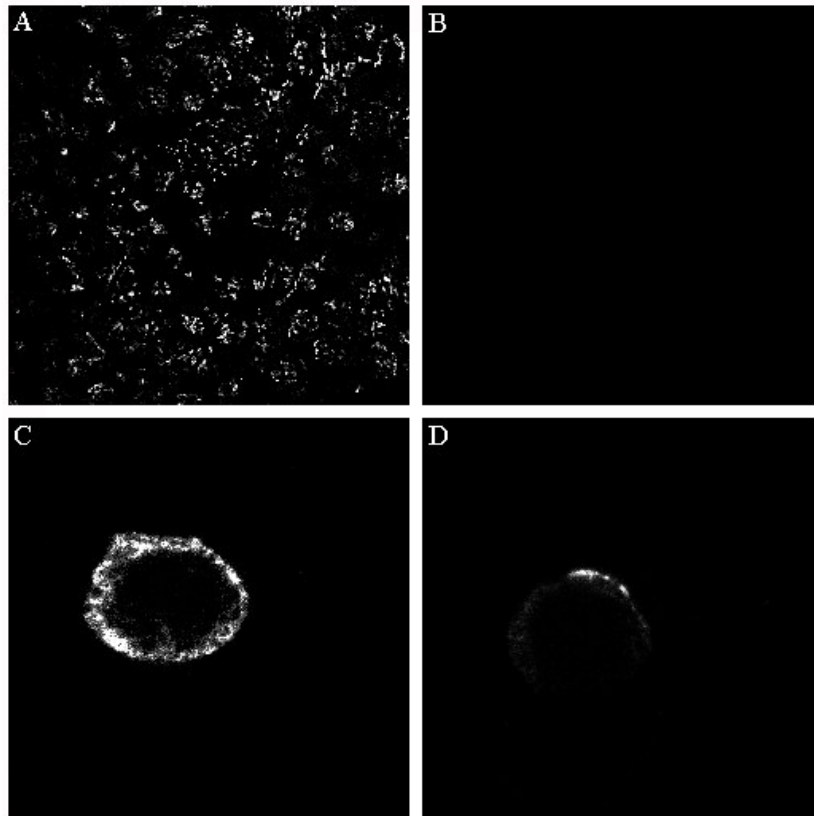
Fig. 16. Exposure of the NSP4 C-Terminus on the Cell Surface. At 24 h post mock infection, MDCK cells were stained for giantin and NSP4 (aa 150-175) after (**A**) fixation and permeabilization or (**B**) before only fixation to characterize permeability-dependent staining. As the intracellular protein giantin was only observed in permeabilized cells, RV-infected MDCK cells were processed in the same manor at 24 hpi. The resulting staining patterns show a marked difference in NSP4 distribution between (**C**) permeabilized and (**D**) intact MDCK cells during infection.

Characterization of Exposed NSP4. Three distinct NSP4 bands of approximately 28, 24, and 20 kD in molecular weight were found in lysates derived from RV-infected MDCK at 24 hpi (Fig 17 lane 2). The altered molecular weights are a result of different NSP4 glycosylation states (double-, single-, and unglysocylated respectively) with each glycan characterized as a high-mannose, EndoH-sensitive moiety (Ericson et al., 1982). Biotinylation of cell surface proteins and streptavidin-agarose extraction allowed isolation of polypeptides exposed on the surface on MDCK cells through their biotin modification. Surface proteins extracted from RV-infected MDCK cells at 24 hpi included the 28 kD (double-glycosylated) form of NSP4 (Fig 17, lane 7). The shift in molecular weight to unglycosylated (20 kD) observed after EndoH digestion of this surface protein extract confirms that the glycans are high-mannose moieties. The molecular weight of NSP4 determined by comparison to SDS-PAGE markers, the presence of specific staining using antibodies to a NSP4 C-terminal epitope, and the presence of amino terminal-localized glycosylations together confirm that NSP4 exposed on the surface of RV-infected MDCK cells is full-length in nature.

DISCUSSION

The focus of this study was to determine if NSP4 was present in the PM of RV-infected epithelial cells. To address this we used LSCM for analysis of NSP4 colocalization with a PM marker protein and NSP4 fluorescence on the surface on intact cells during RV infection. Our results indicated that NSP4 is present at and exposed on the extracellular surface of the PM on RV-infected MDCK cells. Characterization of the exposed NSP4 after isolation via surface biotinylation revealed that the enterotoxin was full-length and high-mannose glycosylated.
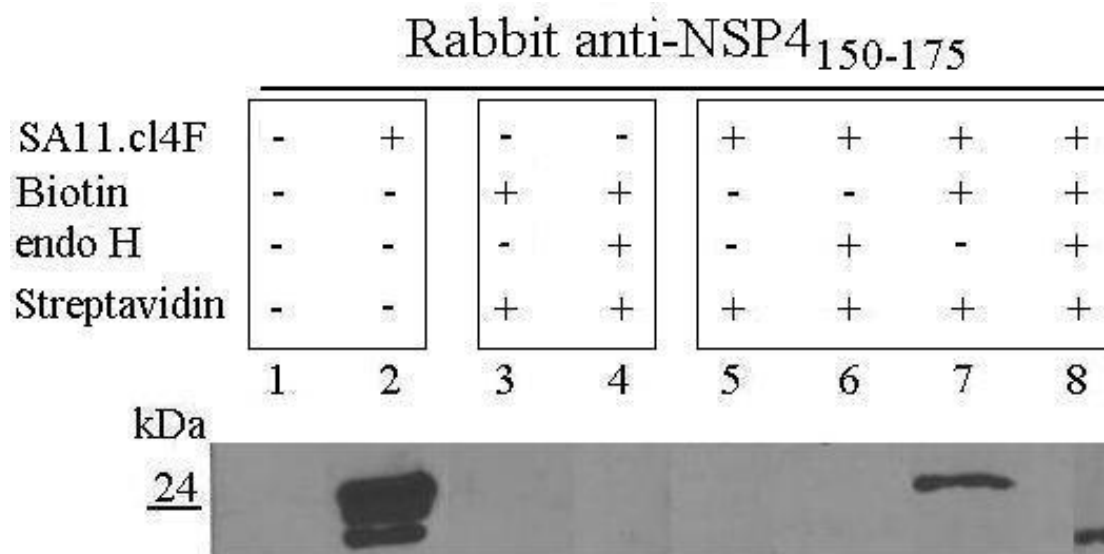
Rabbit anti-NSP4$_{150-175}$

	1	2	3	4	5	6	7	8
SA11.cl4F	-	+	-	-	+	+	+	+
Biotin	-	-	+	+	-	-	+	+
endo H	-	-	-	+	-	+	-	+
Streptavidin	-	-	+	+	+	+	+	+

kDa

24

Fig. 17. Full-Length, High-Mannose Glycosylated NSP4 Exposed at the PM. Lysates and cell surface proteins extracted as indicated from mock and RV-infected MDCK cells (taken at 24 hpi) were mock or EndoH digested, resolved by SDS-PAGE, and Western blotted with anti-NSP4 peptide (aa 150-175) antibodies. Mock and infected lysates (lanes 1 and 2 respectively) confirmed the presence of double-, single-, and unglycosylated (28, 24, 20 kD) forms of NSP4 in RV-infected MDCK cells. Cell surface proteins extracted from cells at 24 h post mock infection (lanes 3 and 4) and mock extracted cell surface proteins from RV-infected cell 24 hpi (lanes 5 and 6) were mock (lanes 3 and 5) or EndoH (lanes 4 and 6) digested to control for specificity of NSP4 staining. Cell surface proteins extracted from RV-infected cells (lane 7) indicated the presence of the 28 kD form of NSP4 which was shown to be high-mannose glycosylated by virtue of its shift in molecular weight after EndoH digestion (lane 8).

This is the first report specifically identifying the full-length enterotoxin within the PM of infected cells. Though this appears to be in opposition to the previously reported absence of NSP4 within the plane of the PM, this previous study used NSP4-EGFP-transfected HEK293 cells rather than defining NSP4 subcellular distribution during RV infection (Berkova et al., 2006). While not sufficient to confirm the enterotoxin's specific PM microdomain distribution, the exposure of full-length, EndoH-sensitive NSP4 in 'patches' at the PM is of particular interest with our previous identification of this same NSP4 form in isolated PM caveolae. Caveolae, a subset of lipid rafts, are defined morphologically as flask-shaped PM microdomains and

functionally as foci of cellular signaling (Pike, 2003). The presence of giantin staining in fixed and permeabilized cells and its absence in intact cells indicated that the patching observed with NSP4 staining on the PM surface was not due to clustering and endocytosis of the primary or secondary antibodies. The absence of fluorescent patches on the surface of uninfected cells, regardless of the cold treatment used (data not shown), confirmed that the signals were the authentic surface distribution of NSP4 and not a product of antibody endocytosis. The presence of the NSP4 C-terminus exposed at the PM of infected cells (shown here), particularly if exposed in caveolae, would expose the NSP4 enterotoxic domain (aa 114-135) to surface receptors on the PM of both infected cells and neighboring, uninfected cells (Ball et al., 1996). Also of interest is the full-length nature of NSP4 exposed on the surface of infected cells.

To date, the only form of NSP4 identified released from infected cells is the C-terminal (aa 112-175) enterotoxic cleavage fragment (Xu et al., 2000). The site and mechanism of this cleavage are unknown, but the presence of full-length NSP4 in PM caveolae and exposed on the cell surface suggests that the cleavage may occur directly on the PM. While beyond the scope of this study, characterizing the potential localization of exposed NSP4 in PM caveolae, the induction of Ca^{2+} mobilization in uninfected neighboring cells, and the cleavage mechanism of NSP4 at the PM would provide a unique link between the enterotoxin's location and function during RV infection.

MATERIALS AND METHODS

Antibodies and Reagents. An antibody directed against the C-terminus of NSP4 was raised in mice against a 25 aa peptide, deduced from the simian rotavirus SA11 clone 3 NSP4 sequence (aa 150-175), crosslinked to keyhole limpet hemocyanin (KLH) and affinity purified with the $NSP4_{150-175}$ peptide before use in LSCM. Rabbit anti-giantin (Convance Research Products, Inc., Princeton, NJ), mouse anti-sheep sodium/potassium (Na/K)-ATPase α (Affinity BioReagents, Inc., Golden, CO), goat anti-rabbit IgG conjugated to horseradish peroxidase (HRP; Southern Biotech Assoc,

Inc, Birmingham, AL), goat anti-mouse IgG conjugated to Texas Red (TR; Rockland Immunochemicals, Inc., Gilbertsville, PA), and goat anti-rabbit IgG conjugated to fluorescien (FITC; KPL, Inc., Gaithersburg, MD) were obtained from the commercial sources indicated. EZ-Link® Sulfo-NHS-SS-Biotin and streptavidin-agarose (Pierce, Rockford, IL), endo-β-N-acetylglucosaminidase H (EndoH; New England BioLabs, Ipswich, MA), protease inhibitor cocktail set III (Calbiochem, Darmstadt, Germany), and 0.45 μ pure nitrocellulose (GE Osmonics Labstore, Minnetonka, MN) were also purchased from commercial sources.

Cell Lines, Virus, and Culture Media. Madin Darby Canine Kidney (MDCK; American Type Culture Collection, Manassas, VA) cells were grown in maintenance media (Dulbecco's Modification of Eagle's media (D-MEM) with 4.5 g/L glucose, L-glutamine, and sodium pyruvate; Mediatech, Inc., Herndon, VA) supplemented to 2mM L-glutamine (200mM; Cambrex Corporation, East Rutherford, NJ), 1 mM sodium pyruvate (100 mM; Cambrex), 0.1 mM non-essential amino acids (10 mM; Mediatech, Inc., Holly Hill, FL), 100 U/L penicillin (pen), 100 μg/L streptomycin (strep), 0.25 μg/L Fungizone (10,000 U pen/10,000 U strep/25 ug/L Fungizone; Cambrex), 43.9 mM sodium bicarbonate (tissue culture grade; Invitrogen Corporation, Carlsbad, CA), 5% fetal bovine serum (Cambrex), and 5% Serum Supreme (Cambrex) at 37°C in 5% CO_2. MDCK cells were infected with SA11 clone 4F (gift of Mary Estes, Baylor College of Medicine, Houston, TX) at an MOI of 2. Briefly, the virus inoculum was sonicated (5 min using a cuphorn attachment ice bath in a Misonix Sonicator 3000; Misonix, Inc, Farmingdale, NY) and incubated in serum-free D-MEM with 5 μg/ml trypsin for 30 min at 37°C, then incubated with the activated inoculum for 1h at 37°C in 5% CO_2. The inoculum was replaced with serum-free D-MEM supplemented with 1 μg/ml trypsin and the cells incubated for an additional 24 h.

Immunofluorescent Microscopy. Mock and SA11-infected MDCK cells grown on glass coverslips were processed 24 hours post inoculation for fluorescent imaging. For colocalization of NSP4 with the PM marker Na/K-ATPase, mock and infected cells were fixed and permeabilized at -20°C in methanol:acetone (1:1, v/v) for 10 min. The cells

were then briefly dried, rinsed twice with sterile PBS, and incubated for 30 min in 3% (w/v) non-fat dry milk (blotto) in PBS (blotto/PBS) to block non-specific antibody binding. Primary antibodies in 1% blotto/PBS were incubated on the cells for 45 min, then removed with four washes of 0.5% blotto/PBS (10 min each). Fluorescently-labeled secondary antibodies in 1% blotto/PBS were then incubated on the cells for 45 min in the dark, removed by washing as above, before rinsing the cells twice in PBS and mounting with fluorescent mounting media (KPL) onto glass slides.

For NSP4 exposure on intact cells, mock and infected cells were rinsed with serum-free D-MEM, incubated for 30 min with serum-free D-MEM supplemented with 1% (w/v) non-fat dry milk (blotto/D-MEM) at 4^oC, then incubated for 45 min with primary antibodies diluted in 1% blotto/D-MEM at 4^oC. The labeled cells were rinsed twice with PBS, cold treated with methanol only for 10 min at -20^oC, then rinsed twice with PBS. Finally, the cells were incubated for 45 min with fluorescently-labeled secondary antibodies diluted in 1% blotto/D-MEM at 4^oC in the dark, washed five times with 0.5% blotto/PBS (5 min per wash, in the dark) at 4^oC, washed twice in PBS, and mounted with fluorescent mounting media (KPL) onto glass slides. Fixed and permeabilized control cells were processed as above, but the cold treatment was carried out before addition of the primary antibodies and used 10 min with methanol:acetone (1:1, v/v) at -20^oC.

All of the resulting fluorescent image data were captured with a MRC-124MP BioRad laser scanning confocal microscopy (LSCM) system (BioRad, Hercules, CA) using a Zeiss inverted Axiovert microscope (Carl Zeiss, Inc., Thronwood, NY), a 63X Zeiss oil Apochromat objective, and the 488 and 568 nm excitation lines of an argon/krypton ion laser source. LaserSharp 3.0 (BioRad) to, Metamorph 4.0 (Molecular Devices Corporation, Sunnyvale, CA), and Adobe Photoshop 7.0 (Adobe Systems Inc., San Jose, CA) were used to capture the pixilated fluorescent data and calculate colocalization values, convert the image data to tiff format, and adjust for contrast curves to construct the final images, respectively.

Biotinylation and Isolation of Cell Surface Proteins. Mock and infected cells grown in 6 well plates (9.5 cm^2 per well) as above then washed three times with ice-cold PBS-CM (PBS supplemented with 0.1 mM CaCl$_2$ and 1 mM MgCl$_2$) directly before labeling. Surface proteins were biotinylated with a 30 min incubation in 0.5 mg/ml solution of Sulfo-NHS-SS-Biotin (2.5 µl of 200 mg/ml NHS-SS-Biotin in DMSO per ml of ice-cold PBS-CM) at 4°C. Exess biotin was quenched with an equal volume of cold cell culture maintenance media (D-MEM with serum), the cells were washed three times with ice-cold PBS-CM, and lysed in 0.8 ml SDS-free RIPA buffer (150 mM NaCl, 50 mM Tris-base, 10% NP40, 0.5% DOC, pH 8.0) with protease inhibitors (1:1000 protease inhibitor cocktail set III, Calbiochem) per 9.5 cm^2 culture surface area for 20 min at 4°C. Cells were then scraped into prechilled siliconized tubes, the plates incubated with an additional 0.2 ml lysis buffer for 10 min at 4°C, and the corresponding lysates pooled. To extract the biotin-labeled surface proteins, 30 µl of streptavidin-agarose slurry (6% solution stock, Pierce) per ml lysate was incubated at 4°C for approximately 14 h with constant rotation and the agarose-bound proteins pelleted at 12,000 Xg for 20 min at 4°C. Each pellet was washed 3 times with 1 ml of lysis buffer, the supernatants carefully removed, and the remaining pellet suspended in lysis buffer supplemented with 1% SDS. Surface proteins were removed from the agarose by boiling for 10 min, centrifugation at 12,000 Xg for 20 min at 4°C, and surface protein supernatants were transferred to new tubes for protein quantification. Mock biotinylated (less NHS-SS-Biotin) and mock pull-down (less streptavidin-agarose) samples from both mock and infected MDCK were used to control for non-specific binding of proteins to the agarose beads.

Protein Quantification. The Micro BCA^{TM} Protein Assay kit (Pierce, Rockford, IL) was used with a BSA standard curve as per manufacturer's protocol to quantify the protein concentration of the isolated surface protein samples and controls.

Endoglycosidase Reactions. For EndoH cleavage, 1 µg aliquots of total protein from each biotinylation sample and control were denatured and diluted per manufacturer's protocol (New England Biolabs). Either 1 µl of sterile water (mock cleavage) or 1 µl of EndoH was added to each control/sample set from mock and

infected cells. The cleavage reaction was performed for 1 h at 37°C and the proteins resolved by SDS-PAGE and Western blot.

Western Blot Analyses. Western blot analysis was used to identify both the presence of NSP4 and the potential shift in NSP4 molecular weight after EndoH digestion in each cell surface protein sample and control. Each surface protein cleavage reaction (approximately 1 µg total per lane) was resolved on 12% polyacrylamide minigels and transferred to nitrocellulose filters (0.45 µ pure nitrocellulose; GE Osmonics) according to the manufacturer (Mini-PROTEAN II and Trans-Blot respectively; BioRad). The filters were blocked in 10% blotto/PBS for 1h at RT and reacted with rabbit anti-NSP4$_{150-175}$ in 2.5% blotto/PBS for 14 h at 4°C with rocking. The filters were incubated an additional 1 h at RT with anti-NSP4, then washed once in 0.5% blotto/PBS, twice in 0.5% blotto/PBS with 0.05% Tween-20 (v/v), and once in 0.5% blotto/PBS with rocking (10 min each). The HRP-labeled secondary antibody was diluted in 2.5% blotto/PBS and incubated with the filters for 1 h at RT with rocking. The filters were washed as above, rinsed with PBS, and reacted with SuperSignal Femto chemiluminescent substrates as per manufacturer's protocols (Pierce). The marker-specific bands were visualized by exposure to and development of x-ray film.

CHAPTER V
PROBLEMS

While controls and complementary methods were used to confirm the results of this study, there are inherent weaknesses in the individual protocols. Membrane isolations use two specific strategies to produce a fraction enriched in the desired membranes: removal of undesired structures and specific extraction or pull-down of desired structures. In this study, the specific densities of the membrane structures present after cell cavitation were used to remove remaining whole cells, intact nuclei, and soluble cytoplasmic contents. Sucrose density gradient centrifugation both removed structures such as mitochondria, lysosomes, and peroxisomes, but also specifically extracted larger structures which were predominately ER- and PM-derived microsomes. ConA chromatography further extracted specific membranes that contained glyco-proteins and -lipids with terminal mannose or glucose residues. As the marker composition indicates, enrichment of the PM using the size and specific density of the PM-derived microsomes produced the desired Na/K-ATPase α- and clathrin heavy chain-enriched membrane fraction. However, there is a corresponding presence of both the ER marker calnexin and Golgi marker giantin. These contaminants are removed during ConA chromatography, but the resulting CSC caveolae fraction could contain Golgi-derived raft/caveolae membranes. The EndoH-sensitivity of caveolar NSP4 and its corresponding lack of colocalization with Golgi-localized markers confirmed NSP4 was not present in the Golgi making this potential contamination a moot point (van Vliet et al., 2003). As ConA extraction is dependent on the presence of glycosylated proteins and lipids, there is a possibility of isolating either glycoprotein/lipid-enriched non-caveolar PM microdomains and/or losing glycoprotein/lipid-poor PM caveolae membranes. It was of interest to note that three of the caveolae/raft markers used only the membrane-inserted lipid G_{M1} was enriched in CSC caveolae from its homogenate and PM levels. G_{M1} has previously been used to quantify caveolae enrichment in isolated membranes and the EM analysis of CSC caveolae confirmed that the isolated membranes were

similar to morphological caveolae. In spite of this, as caveolin-1 is the defining marker of caveolae the absence of its enrichment is puzzling. It is possible that the sonication used to disrupt the large microsomes present in the CSC PM sheared a portion of the membrane-associated protein populations from the membranes. Indeed, the greater relative loss of flotillin-1 (peripheral membrane protein) than caveolin-1 (membrane associated) appears to favor this explanation. There is also the possibility that the glycol-proteins/lipids bound by the ConA column are enriched in non-caveolar rafts so that the raft marker G_{M1} is enriched, but caveolae markers caveolin-1 and flotillin-1 are diluted in the final CSC caveolae fraction. The colocalization of NSP4 with caveolin-1 at the PM was confirmed with confocal microscopy. While this method cannot differentiate between caveolin-containing pre-caveolae rafts, caveolae, and caveolae subsets, it does confirm the enterotoxin's association with the key caveolae structural protein at the PM.

The membrane fluidity measurements reported in this study for each of the isolated raft/caveolae fractions were based on the polarization changes in the fluorescent signals from a panel of lipid probes. However, this change or anisotropy can be a result of two separate types of lipid movement: lateral across the plane of the membrane and rotational within the plane of the membrane. Thus our polarization measurements quantified the average relative fluidity of each membrane, but cannot identify which type(s) of movement occurred.

Of the NSP4-specific bands found in RV-infected cell homogenates and CSC caveolae, our Western blot analysis was unable to completely identify the 16 kD NSP4 band. Our results suggest it is an unglycosylated, C-terminal NSP4 fragment. However, as full-length NSP4 dimers at higher molecular weights were still present even after prolonged boiling in sample buffer with β-mercaptaethanol (data not shown) we could not differentiate between a single 16 kD polypeptide or a dimer of the NSP4 aa 112-175 secreted fragment (~7.5 kD monomer molecular weight). Additionally, there are reports that the EndoH substrate specificity may include select hybrid glycosylations in addition to the ER-derived high-mannose glycans (Ballou L et al., 1990). The previous characterization of NSP4 glycans with radiolabeled carbohydrates and EndoH confirmed

the high-mannose nature of NSP4 during RV infection and allowed us to confirm the presence of these glycans through endoglycosidase cleavage (Ericson et al., 1982).

In determining the distribution of NSP4 at the PM in this study, laser scanning confocal microscopy (LSCM) was a powerful complementary methodology. However, the resolution of colocalization with the LSCM system used in this study was approximately 250 nm. As morphological caveolae are 50 – 100 nm in diameter, colocalization of NSP4 with caveolin-1 was sufficient to suggest that NSP4 trafficked from the ER to the PM in association with caveolin-1-containing structures, but could not by itself conclusively localize the enterotoxin to PM caveolae. The lack of a negative control for the cellular markers also made differentiation of diffuse cytoplasmic staining and background fluorescence difficult. As such, the reported subcellular distribution of NSP4-caveolin-1 colocalization may have excluded the presence of NSP4 in caveolin-1-containing chaperone complexes within the cytoplasm. The focus on NSP4 trafficking in RV-infected MDCK cells leaves two further issues unresolved. First, while this study confirms that NSP4 associates with caveolin-1 at internal sites early and exposed at the PM surface later in infection, it cannot confirm if NSP4 is competent and sufficient of itself to use this caveolin-1-associated transport pathway (i.e. without other RV proteins). NSP4 has been previously identified in lipid rafts as defined by DRM in transfected cells so the enterotoxin can enter a similar membrane microdoamin subgroup by itself. Yet with the data presented here, it is unclear if NSP4 is able to traffic specifically to PM caveolae or the exofacial PM surface in the absence of other viral proteins. Secondly, MDCK are kidney-derived. These cells have been the basis of numerous intracellular trafficking studies including caveolae/caveolin subcellular movement, but they are not the primary cell infected by RV during a natural host infection (Rodriguez-Boulan et al., 2000). As such, the results of this study are invaluable in furthering our understanding of NSP4 trafficking and the potential link between NSP4 localization and function during RV infection, but further experimentation is needed to both resolve the subcellular transport pathways of NSP4 during host infection and determine both the orientation and function of NSP4 at the PM.

CHAPTER V1
DISCUSSION/CONCLUSION

The focus of this study is to determine if rotavirus (RV) non-structural protein 4 (NSP4) traffics from the ER to PM caveolae during infection. To address this, we used compositional analysis of PM caveolae and confocal microscopy to define the subcellular distribution of NSP4 in RV-infected cells. Our results reveal that full-length, high-mannose glycosylated NSP4 traffics to PM caveolae during RV infection. While NSP4 associates with the key caveolae structural protein caveolin-1 at both early and late stages of infection, the lack of NSP4 association with Golgi-localized proteins at both stages indicates that the enterotoxin's ER to PM caveolae transport pathway bypasses the Golgi apparatus. Additionally, at least the carboxyl-terminus of the enterotoxin is exposed on the exofacial PM leaflet of infected cells.

In characterizing the transport of RV NSP4, this work also revealed unique characteristics in the structure and function of isolated cellular lipid rafts and caveolae. Raft and caveolae composition is experimentally defined through the analyses of isolated membrane subdomains and via microscopy. To determine if NSP4 traffics to PM caveolae, we first examined caveolae isolated from RV-infected cells for the presence of entertoxic protein. The detergent insolubility of lipid rafts, including caveolae, is the traditional characteristic exploited to isolate these membrane microdomains from the cellular membrane pool (Pike, 2003). Our analysis of these detergent-resistant membranes (DRM) isolated from MDCK cells suggests that while NSP4 was found previously in a similar type of isolated material (Sapin et al., 2002), there are several inherent problems with using DRM to approximate PM caveolae for the localization of NSP4.

First, DRM are isolated from whole cell lysates. As lipid rafts have been previously identified in several intracellular organelle and vesicle membranes in addition to the PM, a portion of the rafts fractionated into DRM will not be of PM origin (van Vliet et al., 2003). While identification of NSP4 in this membrane fraction would

provide an association between the enterotoxin and this class of membrane subdomain in MDCK cells, it is not appropriate to the focus of this project.

Secondly, the use of detergents to separate membrane fractions may alter the structure and sterol exchange dynamics of the membrane (Pike, 2003). Analysis of the DRM extracted from MDCK cells revealed the presence of a significant amount of crystalline sterol which under physiological conditions is only observed in peroxisome membranes (McIntosh et al., 2003; Tabas, 1997). Also, these DRM have a high membrane fluidity and small difference between the exo- and cytofacial membrane leaflets in spite of the crystalline sterol presence. The high initial sterol exchange rate and it's relative insensitivity to the presence of a sterol carrier protein also indicates that DRMs do not retain functional similarity to intact PM. Determining whether these alterations were artifacts of the isolation methodology or due to non-raft membrane contaminants are subjects of future studies. However, we did confirm that these differences were not due to the presence of detergents in the DRM fraction as no detergents were present in the DRM fraction itself.

Finally, as DRMs are isolated from whole cell lysates rather than a pre-isolated PM fraction, there is a greater probability for inclusion of non-raft membrane contaminants in the final raft extract. Compositional analysis of the DRM fraction confirms that the membrane extract is enriched in both lipid (G_{M1}) and protein (caveolin-1, flotillin-1) markers reported to be concentrated in lipid rafts. However, the analysis also indicates that DRMs contain significant amounts of ER membrane (calnexin) and non-raft PM (Na/K-ATPase α). As NSP4 is known to be present in the ER during RV infection, the presence of this membrane in the DRMs strongly indicates that this material is not appropriate for use in determining if NSP4 traffics out of the ER to PM caveolae. Based on these problems, the DRM method was replaced with non-detergent raft/caveolae method to isolate the membrane microdomains from the PM of MDCK cells without ER or non-raft PM contamination.

Introduced as a non-detergent alternative method for caveolae extraction, the Percoll and OptiPrep gradient-based procedure of Smart et al. (1995) begins with pre-

isolation of a rough PM fraction. The non-detergent, raft/caveolae (NDCR) membranes extracted from this PM fraction were analyzed for membrane structure, sterol exchange function, and the presence of contaminating membranes. Results indicate that NDCR do not contain detectable crystalline sterol, yet they have lower relative membrane fluidity than DRM. The elevated membrane leaflet fluidity gradient and sterol-carrier protein-sensitive sterol transfer rate indicate that the NDCR fraction is closer to sharing the structure and sterol exchange dynamics of intact PM than the DRM. However, the compositional analysis revealed the presence of both ER and non-raft PM contamination in the NDCR fraction. While the membrane structural and functional characteristics of the NDCR appear to provide a closer approximation of PM caveolae than the DRM, the ER contaminant endemic in both isolated raft fractions indicates that neither procedure is appropriate for addressing the presence of NSP4, an ER resident, in PM caveolae.

We developed a sucrose gradient- and concanavalin A (ConA) affinity chromatography-based method specifically optimized to isolate a caveole/raft (ACR) fraction from a MDCK cell-derived, PM-enriched material. The ACR fraction contains the same raft/caveolae lipid and protein markers as the NDCR and DRM extracts, but without detectable ER or non-raft PM markers. EM analysis of the ACR membranes revealed a predominately vesicular physical shape similar to PM caveolae invaginations. Structurally, ACR shares many characteristics with NDCR membranes, including a lack of crystalline sterol, relatively low membrane fluidity, and a high relative fluidity gradient between the endo- and exofacial membrane leaflets. The cholesterol exchange between ACR fractions is similar to that observed with NDCR material. Both have relatively low initial exchange rates that are sensitive to the presence of a sterol carrier protein. The compositional and structural analyses of the ACR fraction indicate that these membranes share several similarities with the NDCR material, but lack the ER contamination endemic in NDCR and DRMs. For the purposes of our study, the ACR membranes provide a close approximation of the PM raft/caveolae appropriate for the determining if NSP4 traffics to these membrane subdomains during RV infection.

These data provide the first comparison of lipid raft/caveolae fractions from three separate lipid raft/caveolae extraction methods for the presence of non-raft membrane contaminants, membrane structure, and function as it relates to sterol movement. The structural results revealed that each isolated membrane contains unique characteristics that, while related to each other, highlight the current problem in defining both cellular lipid raft and caveolae composition. Earlier reports using DRM analysis to identify lipid raft resident proteins and lipids were invaluable in both optimizing subsequent isolation methodologies and in identifying potential raft markers for use in both immunomicroscopy of lipid rafts and association of viruses with cellular rafts. In this instance, however, the presence of non-raft PM and specifically ER membrane contamination in both DRM and NDCR indicates that any NSP4 protein found in these membranes may be an artifact of the isolation technique rather than the true presence on the RV enterotoxin in the lipid raft/caveolae membrane microdomains. The sucrose gradient- and affinity chromatography-based method presented here for the first time allows analysis of a PM-derived raft/caveolae extract for the presence of proteins known to traffic through the ER. This is of specific importance for both NSP4 and the RV structural protein VP7 are present as ER glycoproteins during infection (Kabcenell and Atkinson, 1985). Moreover, this lack of contamination will also allow for analysis of other viral and cellular proteins trafficking between the ER and PM rafts/caveolae.

In applying this technique to RV SA11 clone 4F-infected MDCK cells at 24 hpi, we unexpectedly found full-length, glycosylated NSP4 in isolated PM caveolae membranes. Previously, only a secreted NSP4 C-terminal fragment (NSP4 residues 112-175) has been identified outside of infected cells (Zhang et al., 2000). However, the identification of NSP4 aa 114-135 and aa 120-147 at the basement membranes of RV EDIM-infected intestinal cells confirms the presence of the NSP4 carboxyl-terminus at the PM and indicates that the full-length enterotoxin may also be present (Boshuizen et al., 2004). Presence of the full-length viral protein in CSC caveolae confirms that along with the enterotoxic domain, the transmembrane domain and glycosylation sites of NSP4 are transported to the PM microdomains. The presence of full-length NSP4 in caveolae

suggests unique characteristics of the protein's transport for the ER to the PM and/or of its orientation and potential function at the PM.

NSP4 and the NSP4 enterotoxic domain, aa 114-135, induce chloride secretion and water accumulation in mouse pup intestines through mobilization of intracellular calcium (Ball et al., 1996). When applied exogenously, both NSP4 and $NSP4_{114-135}$ initiate a phoshpolipase C (PLC)-dependant increase in cytoplasmic calcium concentration through release of intracellular calcium stores and calcium influx at the PM (Dong et al., 1997). Expression of the enterotoxin however induces a similar increase in cytoplasmic calcium levels even in the presence of a PLC inhibitor (Berkova et al., 2003). As PM caveolae are enriched in molecules that regulate cellular calcium homeostasis (i.e. the PM calcium pump, IP3 receptors, and PIP2), the presence of NSP4 in these PM microdomains provides a potential link between the enterotoxin's subcellular distribution and enterotoxic function (Fujimoto et al., 1992; Fujimoto, 1993; Hope and Pike, 1996; Pike and Casey, 1996). Alternately, NSP4 association with PM caveolae and caveolin-1 may function primarily as a transport mechanism to deliver other viral proteins, progeny virions, and/or just NSP4 from the ER to the PM for secretion or subsequent diffusion into other membrane domains. It is of interest to note however, that the binding site of caveolin-1 maps to NSP4 aa 112-140, a site neatly overlapping the NSP4 enterotoxic domain (aa 114-135) (Parr et al., 2006). While this study does confirm that NSP4 specifically associates with caveolin-1 as early as 7.5hpi, examination of NSP4-mediated virion protein, secondary transport/diffusion, and caveolin-1 mediation of NSP4 enterotoxic function are subjects for interesting future studies.

Inclusion of the NSP4 N-terminal transmembrane (TM) domain on caveolar NSP4 at the PM suggests that transport of the enterotoxin between the ER and PM may be membrane-mediated through vesicular structures. In addition, it also indicates the potential for NSP4 insertion in the PM bilayer exposing the enterotoxin on the exofacial surface of infected cells. Analyses of NSP4 colocalization with caveolin-1 both early and late in infection confirm that NSP4 traffics to the cell periphery in caveolin-1-associated

punctate structures. While this does not rule out NSP4 transport via the caveolin-1-containing cytoplasmic chaperone complex, the reproducible and pervasive punctate patterns strongly suggest a caveolin-1-positive, vesicular transport mediator. Colocalization of NSP4 with the PM marker Na/K-ATPase α confirms that the peripheral NSP4 staining was associated with the PM during infection.

The exposure of the enterotoxin on the exofacial surface of RV-infected MDCK cells was also confirmed. Confocal analysis of intact, SA11 clone 4F-infected MDCK cells specifically identified the extracellular exposure of at least $NSP4_{150-175}$. If the viral protein passes through the PM bilayer at its TM domain, these results would suggest that the NSP4 enterotoxic domain is present on the surface of infected cells, exposing uninfected neighboring cells to effects of exogenous NSP4. Further characterization of the exposed NSP4 with membrane impermeate biotinylation and streptavidin pull-down revealed that the exposed enterotoxin was full-length and glycosylated. While these results cannot confirm that NSP4 exposed on the surface of infected cells is localized in caveolae microdomains, the patching of NSP4 signals observed during confocal analysis does suggest that the exposed full-length enterotoxin localizes to some type of microdomain within the PM.

Both caveolar NSP4 and NSP4 exposed at the cell surface also share a similar glycosylation pattern. In both instances, the viral protein was predominately double glycosylated with EndoH-sensitive carbohydrate moieties. While blocking N-linked glycosylation during RV infection was previously shown to inhibit infectious virus release and virion association with DRM, glycosylation has been shown to be unnecessary for NSP4 transport into the DRM fraction (Delmas et al., 2004). The EndoH-sensitivity of NSP4 glycans at the PM, however, does suggest a unique, Golgi-bypassing aspect of NSP4 ER to PM transport (Ericson et al., 1982). The only experimentally defined Golgi-bypassing caveolin-1 transport pathway between the ER and PM is mediated by a cytoplasmic chaperone complex rather than vesicular structures (Uittenbogaard et al., 1998). The cellular protein secretory transport chain also traffics a variety of transmembrane glycoproteins from the ER to the PM, but it too transits

through the ERGIC and Golgi apparatus (van Vliet et al., 2003). Similar to this secretory mechanism, the membrane-mediated transport of caveolin-1 initiates at the ER and transits through the ERGIC and the Golgi where the protein buds from the TGN in caveolae-like vesicles for subsequent transport to the PM (Liu et al., 1999). As entry of NSP4 into the caveolin-1-enriched DRM fraction is reported to occur between 7 and 18 hpi, we examined NSP4 association with both caveolin-1 and Golgi marker proteins at early (7.5 hpi) and late (24 hpi) stages of infection to determine if NSP4 used one of these known membrane/vesicle- mediated transport mechanisms for its ER to PM movement (Cuadras and Greenberg, 2003; Sapin et al., 2002). Colocalization of NSP4 with caveolin-1 at 7.5 hpi coincided with a specific lack of NSP4 association with TGN-localized golgin-97. This confirms that while the enterotoxin associates with caveolin-1-positive vesicular structures early in infection, it was not present in the Golgi, specifically the TGN where caveolae vesicles are though to bud. Colocalization of NSP4 with caveolin-1 late in infection indicated that the NSP4-containing, caveolin-1-positive structures had moved from a predominately cytoplasmic distribution to a peripheral localization. The lack of NSP4 colocalization with the Golgi-localized giantin confirmed results reported in an earlier work with NSP4-EGFP and confirmed our results indicating that the predominant ER to PM transport pathway used by NSP4 is not one of the currently defined secretory or caveolin-1/caveolae mechanisms (Berkova et al., 2006). This Golgi-bypassing, caveolin-1-associated vesicular transport pathway and the pools of NSP4 it appears to supply at the PM, both in PM caveolae and exposed on the cell surface, identify a new feature of NSP4 transport and potential function during infection.

As NSP4 intracellular transport, subcellular distribution, and functions have been identified, several distinct spatial and functional pools of NSP4 have begun to take shape. Initially, lack of Golgi-specific processing to NSP4 glycans, immunolocalization of NSP4 to the ER, and the critical receptor function played by NSP4 at the ER during virion morphogenesis were though to characterize the only NSP4 pool, at the ER, during RV infection (Kabcenell and Atkinson, 1985). However, recent publications identified two additional NSP4 pools: one vesicular and ERGIC/microtubule-associated and the

other also vesicular, but LC3/viroplasm-associated. The first is characterized by punctate NSP4 staining that colocalizes with redistributed ERGIC-53 (an ERGIC marker) and β-COP (a COP-I-positive transport vesicle marker), but not Sec13p (a COP-II-positive transport vesicle marker) in transfected cells (Xu et al., 2000). In addition, the data reported by Xu et al. also suggest that these vesicles are associated with microtubules and radiate out along linear tracks toward the cell periphery.

The second pool was defined by NSP4 colocalization with the autophagosome marker microtubule-associated protein 1 light-chain 3 (LC3) using laser confocal microscopy in NSP4-EGFP-transfected and RV SA11-infected cells (Berkova et al., 2006). Autophagy is an essential cellular degredative process defined by the sequestration of cytoplasmic constituents, including structures as large as entire organelles, into double-membrane-bound vesicles that subsequently fuse with lysosomes. While little is known about the composition of these apparently ER-derived autophagosomes, the process of autophagy itself proceeds through three distinct stages: induction, sequestration, and maturation. Pertinent to the NSP4 pool, when LC3 is covalently modified with phosphotidylethanolamine it redistributes from the cytoplasm into preautophagic, crescent-shaped vesicles. LC3 remains in these structures as they engulf portions of the cytoplasm forming distinct autophagic vesicles and through maturation in which these vesicles fuse with lysosome-associated membrane protein (LAMP) 1 and 2-containing endosomes/lysosomes (Kirkegaard et al., 2004). NSP4-EGFP was shown to associate with LC3, but not Golgi-localized giantin, endosome-localized Rab-9, or lysosome-localized LAMP1 in transfected cells. In infected cells, these LC3- and NSP4-containing bodies formed "cap-like structures" associated with NSP5-positive 'viroplasms' suggesting that they may play a role in creation, stability, or subcellular localization of the viroplasm during RV infection (Berkova et al., 2006). The smaller viroplasm size and apparent partial loss of viroplasm/ER association observed with NSP4 silencing during RV infection support these potential roles for this pool of NSP4 during infection (Lopez et al., 2005). The final pools of NSP4 concern the presence and distribution of the enterotoxin at the PM during infection.

This work shows for the first time that NSP4 is present in PM caveolae and exposed at the cell surface as a full-length, high-mannose glycosylated protein during RV infection. Through trafficking to the PM in caveolin-1-positive vesicular structures, NSP4 in PM caveolae provides a potential link between the enterotoxin's subcellular localization and its calcium-based toxicity in infected cells. While not necessarily localized to PM caveolae, NSP4 exposed at the surface of infected cells indicates that both endogenous and exogenous NSP4-induced signaling can occur within an infected cell and uninfected, neighboring cells can also be exposed to exogenous NSP4. Uncharacterized in this study, the presence of a ~16 kD unglycosylated, C-terminal NSP4 fragment in CSC caveolae suggests that the aa 112-175 NSP4 cleavage product (a dimer of which should be approximately 15 kD in molecular weight) may be present in PM caveolae (Zhang et al., 2000). Currently the subcellular site of the cleavage event and the mechanism of its secretion are unknown. The presence of full-length NSP4 and the NSP4 fragment in PM caveolae, as well as the exposure of the C-terminus of full-length NSP4 on the cell surface, suggests the enticing possibility of NSP4 cleavage and release directly at the PM exofacial leaflet. Unfortunately, the identity of the ~16 kD NSP4 fragment has yet to be confirmed. The resolution limitations of the techniques used (in this and previous studies) and the lack of a comprehensive spatial and temporal analysis of NSP4 subcellular distribution make identifying overlaps between the different NSP4 pools difficult. However, each new piece of the complex NSP4 transport puzzle has given us a deeper understanding of the multifunctional nature of this once dogmatically ER-imprisoned viral glycoprotein.

CHAPTER VII
FURTHER EXPERIMENTS

To further define the pool of NSP4 localized at the PM, we first need to refine our understanding of the ER to PM transport of the enterotoxin. LSCM colocalization with NSP4 and an expanded marker panel (Table 6) in RV-infected MDCK and an intestinal-derived cell line, Caco-2 or HT-29, would identify the organelles, transport vesicles, and chaperone complexes involved in NSP4 subcellular movement. The resolution of each colocalization can also be focused from about 250nm to under 10nm using fluorescent resonance energy transfer (FRET). This method uses pairs of fluorophores chosen so that emission of the donor probe excites the acceptor probe only when the fluorophores are less than 10 nm from each other. Both the increase of donor emission in the photobleaching of the acceptor probe and the emission of the acceptor after donor excitation can be used to calculate the distance between the fluorophores with the radius depending upon the probe pair used. Defining the temporal association of NSP4 with each colocalizing marker will also allow for identification of the individual transport pathways used by the enterotoxin during RV infection.

LSCM colocalization can further define the association of NSP4 ER to PM movement with cellular caveolin/caveolae transport. While Fischer rat thyroid (FRT) cells do not express caveolin-1, DRMs have been isolated from these cells. Time course colocalization of NSP4 with the panel of intracellular markers in RV-infected FRT cells would identify any alterations in NSP4 transport. By transfecting the FRT cells with a caveolin-1 expression vector and repeating the colocalization analysis, the specific dependence of NSP4 transport on caveolin-1 trafficking could be determined. Additional characterization of the dependence of NSP4 transport on cellular raft and cholesterol trafficking can be determined by time course colocalization in MDCK cells in the presence of transport inhibitors (Table 7).

Each treatment will disrupt a different aspect of intracellular cholesterol distribution, resulting in both altered caveolin/caveolae trafficking and decreased

presence of caveolae at the PM (Gumbleton et al., 2000). Concatenate alteration to NSP4 transport is indicative that the treatment disrupted a transport mechanism required for NSP4 movement in infected cells. Cyclosporin A and rapamycin disrupt immunophilin chaperone complexes inhibiting chaperone-mediated caveolin-1 ER to PM caveolae transport. Progesterone treatment also inhibits ER to PM movement of cholesterol resulting in accumulation of caveolin-1 in the ER. Cholesterol oxidase, filipin, and cyclodextrin selectively remove cholesterol from the PM resulting in a decreased presence of PM caveolae invaginations and internalization of caveolin-1 to the ER. Dose response curves of each treatment will control for potential toxicity and determine the conditions required to alter caeolin-1 trafficking in MDCK and Caco-2 cells before RV infection. FRT cells can also be used with Fura-2, a fluorescent Ca^{2+} indicator, to determine caveolin-1-dependence of the intracellular Ca^{2+} mobilization induced by exogenous and endogenous NSP4. While caveolin-2 is present, FRT cells do not express caveolin-1 or have morphological PM caveolae. FRT and caveolin-1-transfected FRT cells will be exposed to purified NSP4 or transfected for NSP4 expression to determine if either form of exposure specifically requires caveolin-1 to mediate its Ca^{2+} - mediated signaling.

Table 6. Subcellular Markers and Their Locations.

Marker	Location	Other
Caveolin-1	PM caveolae	ER, Golgi, raft vesicles
G_{M1}	Caveolae/lipid rafts	
Flotillin-1	Caveolae/lipid rafts	
Calnexin	ER (transmembrane)	
Calreticulin	ER (soluble)	ER to Golgi intermediate complex (ERGIC), Golgi
Sec23p	COP-II$^+$ vesicles	ERGIC, ER
ERGIC-53	ERGIC	
β-COP	COP-I$^+$ vesicles	ERGIC, Golgi
Giantin	cis/medial Golgi	
Golgin-97	trans Golgi network (TGN)	
Clathrin heavy chain	PM coated-pits	TGN, endosomes
Na/K-ATPase α	Non-raft PM	
Transferin receptor	Non-raft PM	
LC3	Autophagosomes (lipidated)	Cytoplasmic (unmodified)
HSP-56	Cytoplasmic	part of caveolin-1$^+$ complex
Cyclophilin 40	Cytoplasmic	part of caveolin-1$^+$ complex
Cyclophilin A	Cytoplasmic	part of caveolin-1$^+$ complex

Table 7. Agents Used for Altering Cholesterol and/or Caveolin-1 Trafficking.

Agent	Effect
Cholesterol Oxidase	Induces PM to ER to Golgi translocation of caveolin-1 without altering caveolae-mediated cholesterol trafficking
Filipin	Decreases the number of invaginated PM caveolae via cholesterol binding
Progesterone	Inhibits ER to PM transport of newly synthesized cholesterol and retains caveolin-1 in the ER
Cyclodextrin	Binds and solubilizes cholesterol depleting PM levels when applied directly or enriching PM levels when preincubated with free cholesterol
Cyclosporin A	Disrupts cyclophilin-containing chaperone complexes resulting in loss of soluble caveolin-1 ER to PM caveolae transport

REFERENCES

Almers W and Stirling C (1984) Distribution of transport proteins over animal cell membranes. *J Membr Biol* **77**: 169-186.

Anderson RGW (1998) The caveolae membrane system. *Annu Rev Biochem* **67**: 199-225.

Atshaves BP, Starodub O, McIntosh AL, Roths JB, Kier AB, and Schroeder F (2000) Sterol carrier protein-2 alters HDL-mediated cholesterol efflux. *J Biol Chem* **275**: 36852-36861.

Atshaves BP, Gallegos AM, McIntosh AL, Kier AB, and Schroeder F (2003) Sterol carrier protein-2 selectively alters lipid composition and cholesterol dynamics of caveolae/lipid raft vs. non-raft domains in L-cell fibroblast plasma membranes. *Biochem* **42**: 14583-14598.

Au KS, Chan WK, Burns JW, and Estes MK (1989) Receptor activity of rotavirus nonstructural glycoprotein NS28. *J Virol* **63**: 4553-4562.

Ball JM, Tian P, Zeng C, Morris AP, and Estes MK (1996) Age-dependent diarrhea is induced by a rotavirus nonstructural glycoprotein. *Science* **272**: 101-104.

Ballou L, Hernandez LM, Alvarado E, and Ballou CE (1990) Revision of the oligosaccharide structures of yeast carboxypeptidase Y. *Proc Natl Acad Sci USA* **87**: 3368-3374.

Bergeron RJ and Scott J (1982a) Fluorescent lipoprotein probe. *Anal Chem* **119**: 128-134.

Bergeron RJ and Scott J (1982b) Cholestatriene and ergostatetraene as *in vivo* and *in vitro* membrane and lipoprotein probes. *J Lipid Res* **23**: 391-404.

Bergmann CC, Maass D, Poruchynsky MS, Atkinson PH, and Bellamy AR (1989) Topology of the non-structural rotavirus receptor glycoprotein NS28 in the rough endoplasmic reticulum. *EMBO J* **8**: 1695-1703.

Berkova ZA, Morris AP, and Estes MK (2003) Cytoplasmic calcium measurement in rotavirus enterotoxin-enhanced green fluorescent protein (NSP4-EGFP) expressing cells loaded with Fura-2. *Cell Calcium* **34**: 55-68.

Berkova ZA, Crawford SE, Trugnan G, Yoshimori T, Morris AP, and Estes MK (2006) Rotavirus NSP4 induces a novel vesicular compartment regulated by calcium and associated with viroplasms. *J Virol* **80**: 6061-6071.

Berthouex PM and Brown LC (1994a) Assessing the difference of proportions. In: *Statistics for Environmental Engineers* (Berthouex PM and Brown LC, Eds.) pp 115-122, CRC Press, Boca Raton, FL.

Berthouex PM and Brown LC (1994b) Multiple paired comparisons of k averages. In: *Statistics for Environmental Engineers* (Berthouex PM and Brown LC, Eds.) pp 123-128, CRC Press, Boca Raton, FL.

Bickel PE, Scherer PE, Schnitzer JE, Oh P, Lisanti MP, and Lodish HF (1997) Flotillin and epidermal surface antigen define a new family of caveolae-associated integral membrane proteins. *J Biol Chem* **272**: 13793-13802.

Boesze-Battaglia K, Clayton ST, and Schimmel RJ (1996) Cholesterol redistribution within human platelet plasma membrane: evidence for a stimulus-dependent event. *Biochem* **35**: 6664-6673.

Boshuizen JA, Rossen JWA, Sitaram CK, Kinenai FFP, Simons-Oosterhuis Y, Lafferber JA, Büller HA, and Einerhand AWC (2004) Rotavirus enterotoxin NSP4 binds to the extracellular matrix proteins laminin-β3 and fibronectin. *J Virol* **78**: 10045-10053.

Both GW, Siegman LJ, Bellamy AR, and Atkinson PH (1983) Coding assignment and nucleotide sequence of simian rotavirus SA11 gene segment 10: location of glycosylation sites suggests that the signal peptide is not cleaved. *J Virol* **48**: 335-339.

Brown DA and London E (1998) Functions of lipid rafts in biological membranes. *Annu Rev Cell Dev Biol* **14**: 111-136.

Chan WK, Au KS, and Estes MK (1988) Topography of the simian rotavirus nonstructural glycoprotein (NS28) in the endoplasmic reticulum membrane. *Virol* **164**: 435-442.

Cha SH, Jung N-H, Kim B-R, Kim H-W, and Kwak J-O (2004) Evidence of cyclooxygenase-1 association with caveolin-1 and -2 in cultured human embryonic kidney (HEK293) cells. *IUBMB Life* **56**: 221-227.

Ciarlet M and Estes MK (2001) Interactions between rotavirus and gastrointestinal cells *Curr Opin Microbiol* **4**: 435-441.

Colles SM, Wood WG, Myers-Payne SC, Igbavboa U, Avdulov NA, Joseph J, and Schroeder F (1995) Structure and polarity of mouse brain synaptic plasma membrane: effects of ethanol *in vitro* and *in vivo*. *Biochem* **34**: 5945-5959.

Crabb NT and Persinger HE (1964) Determination of polyoxyethylene nonionic surfactants in water at parts per million level. *J Amer Oil Chem Soc* **41**: 752-755.

Cuadras MA and Greenberg HB (2003) Rotavirus infectious particles use lipid rafts during replication for transport to the cell surface *in vitro* and *in vivo*. *Virology* **313**: 308-321.

Cuadras MA, Bordier BB, Zambrano JL, Ludert JE, and Greenberg HB (2006) Dissescting rotavirus particle-raft interactions with small interfering RNAs: insights into rotavirus transit through the secretory pathway. *J Virol* **80**: 3935-3946.

Daleke DL and Lyles JV (2000) Identification and purification of aminophospholipid flippases. *Biochim Biophys Acta* **1486**: 108-127.

Davidson GP, Gall DG, Petric M, Butler DG, and Hamilton JR (1977) Human rotavirus enteritis induced in conventional piglets. Intestinal structure and transport. *J Clin Investig* **60**: 1403-1409.

Deppe CE, Heering PJ, Tinel H, Kinne-Saffran E, Grabensee B, and Kinne RK (2002) Effect of cyclosporine A on Na+/K(+)-ATPase, Na+/K+/2Cl- cotransporter, and H+/K(+)-ATPase in MDCK cells and two subtypes, C7 and C11. *Exp Nephrol* **5**: 471-480.

Delseth C, Kashman Y, and Djerassi C (1979) Ergosta-5,7,9(11),22-tetraen-3beta-ol and its 24epsilon-ethyl homolog, two new marine sterols from the red sea sponge *Biemna fortis*. *Helv Chim Acta* **62**: 2037-2045.

Dong Y, Zeng CQ-Y, Ball JM, Estes MK, and Morris AP (1997) The rotavirus enterotoxin NSP4 mobilizes intracellular calcium in human intestinal cells by stimulating phospholipase C-mediated inositol 1,4,5-triphosphate production. *Proc Natl Acad Sci USA* **94**: 3960-3965.

Drenan RM, Liu X, Bertram PG, and Zheng XFS (2004) FKBP12-rapamycin-associated protein or mammalian target of rapamycin (FRAP/mTOR) localization in the endoplasmic reticulum and the Golgi apparatus. *J Biol Chem* **279**: 772-778.

Dudeja PK, Harig JM, Wali RK, Knaup SM, Ramaswamy K, and Brasitus TA (1991) Differential modulation of human small intestinal brush-border membrane hemileaflet fluidity affects leucine aminopeptidase activity and transport of D-glucose and L-glutamate. *Arch Biochem Biophys* **284**: 338-345.

Dupree P, Parton RG, Raposo G, Kurzchalia TV, and Simons K. (1993) Caveolae and sorting in the trans Golgi network of epithelial cells. *EMBO J* **12**: 1597-1605.

Eckert GP, Igbavboa U, Muller W, and Wood WG (2003) Lipid rafts of purified mouse brain synaptosomes prepared with or without detergent reveal different lipid and protein domains. *Brain Res* **962**: 144-150.

Edidin M (2003) The state of lipid rafts: from model membranes to cells. *Annu Rev Biophy Biomol Struct* **32**: 257-283.

Ericson BL, Graham DY, Mason BB, and Estes MK (1982) Identification, synthesis, and modifications of simian rotavirus SA11 polypeptides in infected cells. *J Virol* **42**: 825-839.

Farthing MJ (2000) Diarrhoea: a significant worldwide problem. *Int J Antimicrob Agents* **14**: 65-69.

Fischer RT, Stephenson FA, Shafiee A, and Schroeder F (1985) Structure and dynamic properties of dehydroergosterol, delta 5,7,9(11),22-ergostatetraen-3 beta-ol. *J Biol Phys* **13**: 13-24.

Florine-Casteel K and Feigenson GW (1988) On the use of partition coefficients to characterize the distribution of fluorescent membrane probes between coexisting gel and fluid lipid phases: an analysis of the partition behavior of 1,6-diphenyl-1,3,5-hexatriene. *Biochim Biophys Acta* **941**: 102-106.

Foster LJ, de Hoog CL, and Mann M (2003) Unbiased quantitative proteomics of lipid rafts reveals high specificity for signaling factors. *Proc Natl Acad Sci USA* **100**: 5813-5818.

Fra AM, Masserini M, Palestini P, Sonnino S, and Simons K (1995) A photo-reactive derivative of ganglioside $_{GM1}$ specifically cross-links VIP21-caveolin on the cell surface. *FEBS Letters* **375**: 11-14.

Frolov A, Petrescu A, Atshaves BP, So PTC, Gratton E, Serrero G, and Schroeder F (2000) High density lipoprotein mediated cholesterol uptake and targeting to lipid droplets in intact L-cell fibroblasts. *J Biol Chem* **275**: 12769-12780.

Fuchs M, Hafer A, Muench C, Kannenberg F, Teichmann S, Scheibner J, Stange EF, and Seedorf U (2001) Disruption of the sterol carrier protein 2 gene in mice impairs biliary lipid and hepatic cholesterol metabolism. *J Biol Chem* **276**: 48058-48065.

Fujimoto T, Nakade S, Miyawaki A, Mikoshiba K, and Ogawa K (1992) Localiation of inositol 1,4,5-triphosphate receptor-like protein in plasmalemmal caveolae. *J Cell Biol* **119**: 1507-1513.

Fujimoto T (1993) Calcium pump of the plasma membrane is localized in caveolae. *J Cell Biol* **120**: 1147-1157.

Gallegos AM, Atshaves BP, Storey SM, Starodub O, Petrescu AD, Huang H, McIntosh AL, Martin G, Chao H, Kier AB, and Schroeder F (2001a) Gene structure, intracellular localization, and functional roles of sterol carrier protein-2. *Prog Lipid Res* **40**: 498-563.

Gallegos AM, Atshaves BP, Storey SM, McIntosh AL, Petrescu AD, and Schroeder F (2001b) Sterol carrier protein-2 expression alters plasma membrane lipid distribution and cholesterol dynamics. *Biochem* **40**: 6493-6506.

Gallegos AM, McIntosh AL, Atshaves BP, and Schroeder F (2004) Structure and cholesterol domain dynamics of an enriched caveolae/raft isolate. *Biochem J* **382**: 451-461.

Gallegos AM, Storey SM, Kier AB, Schroeder F, and Ball JM (2006) Structure and cholesterol dynamics of caveolae/raft plasma membrane domains. *Biochem* In press.

Gaus K, Gratton E, Kable EPW, Jones AS, Gelissen I, Kritharides L, and Jessup W (2003) Visualizing lipid structure and raft domains in living cells with two-photon microscopy. *Proc Natl Acad Sci USA* **100**: 15554-15559.

Gelderblom HR, Renz H, and Özel M (1991) Negative staining in diagnostic virology. *Micron and Microscopica Acta* **22**: 435-447.

Ge M, Field KA, Aneja R, Holowka D, Baird B, and Freed JH (1999) Electron spin resonance characterization of liquid ordered phase of detergent resistant membranes from RBL-2H3 cells. *Biophys J* **77**: 925-933.

Gimpl G and Fahrenholz F (2000) Human oxytocin receptors in cholesterol-rich vs. cholesterol-poor microdomains of the plasma membrane. *Eur J Biochem* **267**: 2483-2497.

Greff RA, Setzkorn EA, and Leslie WD (1965) A colorimetric method for determination of parts/million of nonionic surfactants. *J Amer Oil Chem Soc* **42**: 180-185.

Gumbleton M, Abulrob AG, and Campbell L (2000) Caveolae: an alternative membrane transport compartment. *Pharm Res* **17**: 1035-1048.

Gustavsson J, Parpal S, Karlsson M, Ramsing C, Thron H, Borg M, Lindroth M, Peterson KH, Magnusson K-E, and Strålfors P (1999) Localization of the insulin receptor in caveolae of adipocyte plasma membrane. *FASEB J* **13**: 1961-1971.

Hale JE and Schroeder F (1982) Asymmetric transbilayer distribution of sterol across plasma membranes determined by fluorescence quenching of dehydroergosterol. *Eur J Biochem* **122**: 649-661.

Harder T, Scheiffele P, Verkade P, and Simons K (1998) Lipid domain structure of the plasma membrane revealed by patching of membrane components. *J Cell Biol* **141**: 929-942.

Heerklots H, Szadkowska H, Anderson T, and Seelin J (2003) The sensitivity of lipid domains to small perturbations demonstrated by the effect of Triton. *J Mol Biol* **329**: 793-799.

Hope HR and Pike LJ (1996) Phosphoinositides and phosphoinositide-utilizing enzymes in detergent-insoluble lipid domains. *Mol Biol Cell* **7**: 843-851.

Huang H, Schroeder F, Zeng C, Estes MK, Schoer JK, and Ball JM (2001) Membrane interactions of a novel viral enterotoxin: rotavirus nonstructural glycoprotein NSP4. *Biochem* **40**: 4169-4180.

Huang H, Schroeder F, Estes MK, McPherson T, and Ball JM (2004) Interaction(s) of rotavirus non-structural protein 4 (NSP4) C-terminal peptides with model membranes. *Biochem J* **380**: 723-733.

Jackson MR, Nilsson T, and Peterson PA (1990) Identification of a consensus motif for retention of transmembrane proteins in the endoplasmic reticulum. *EMBO J* **9**: 3153-3162.

John K, Kubelt J, Muller P, Wustner D, and Herrmann A (2002) Rapid transbilayer movement of the fluorescent sterol dehydroergosterol in lipid membranes. *Biophys J* **83**: 1525-1534.

Kabcenell AK and Atkinson PH (1985) Processing of the rough endoplasmic reticulum membrane glycoproteins of rotavirus SA11. *J Cell Biol* **101**: 1270-1280.

Kabeye Y, Mizushima N, Ueno T, Yamamoto A, Kirisako T, Noda T, Kominami E, Ohsumi Y, and Yoshimori T (2000) LC3, a mammalian homologue of yeast Apg8p, is localized in autophagosome membranes after processing. *EMBO J* **19**: 5720-5728.

Kavecansky J, Joiner CH, and Schroeder F (1994) Erythrocyte membrane lateral sterol domains: a dehydroergosterol fluorescence polarization study. Biochem 33: 2880-2890.

Kirchhausen T (2000) Three ways to make a vesicle. *Nat Rev* **1**: 187-198.

Kirkegaard K, Taylor MP, and Jackson WT (2004) Cellular autophagy: surrender, avoidance, and subversion by microorganisms. *Nat Rev: Micro* **2**: 301-314.

Linstedt AD and Hauri HP (1993) Giantin, a novel conserved Golgi membrane protein containing a cytoplasmic domain of at least 350kDa. *Mol Biol Cell* **4**: 679-693.

Lisanti MP, Scherer PE, Vidugiriene J, Tang Z, Hermanowski-Vosatka A, Tu YH, Cook RF, and Sargiacomo M (1994) Characterization of caveolin-rich membrane domains isolated from an endothelial-rich source: implications for human disease. *J Cell Biol* **126**: 111-126.

Liu P, Li W-P, Manchleidt T, and Anderson RGW (1999) Identification of caveolin-1 in lipoprotein particles secreted by exocrine cells. Nat Cell Biol **1**: 369-375.

London E and Brown DA (2000) Insolubility of lipids in Triton X-100: physical origin and relationship to sphingolipid/cholesterol membrane domains (rafts). *Biochim Biophys Acta* **1508**: 182-195.

Lopez T, Camacho M, Zayas M, Najera R, Sanchez R, Arias CF, and Lopez S (2005) Silencing the morphogenesis of rotavirus, *J Virol* **79**:184-192.

Lu L, Tai G, and Hong W (2004) Autoantigen Golgin-97, an effector of Arl1 GTPase, participates in traffic from the endosome to the trans-Golgi network. *Mol Biol Cell* **15**: 4426-4443.

Lyle JM, Bullitt E, Bienz K, and Kirkegaard K (2002) Visualization and functional analysis of RNA-dependent RNA polymerase lattices. *Science* **296**: 2218-2222.

Manders EMM, Verbeck FJ, and Aten JA (1993) Measurement of colocalization of objects in dual-color confocal images. *J Microsc* **169**: 375-382.

Marnett LJ, Rowlinson SW, Goodwin DC, Kalgutkar AS, and Lanzo CA (1999) Arachidonic acid oxygenation by COX-1 and COX-2. Mechanisms of catalysis and inhibition. *J Biol Chem* **274**: 22903-22906

Mayer S and Maxfield FR (1995) Insolubility and redistribution of GPI-anchored proteins at the cell surface after detergent treatment. *Mol Biol Cell* **6**: 929-944.

McIntosh AL, Gallegos AM, Atshaves BP, Storey SM, Kannoju D, and Schroeder F (2003) Fluorescence and multiphoton imaging resolve unique structural forms of sterol in membranes of living cells. *J Biol Chem* **278**: 6384-6403.

Mebus JC (1989) Reovirus-like calf enteritis. *Amer Digest Disease* **21**:592-599.

Meyer JC, Bergmann CC, and Bellamy AR (1989) Interaction of rotavirus cores with the nonstructural glycoprotein NS28. *Virol* **171**: 98-107.

Morrow IC, Rea S, Martin S, Prior IA, Prohaska R, Hancock JF, James DE, and Parton RG (2002) Flotillin-1/Reggie-2 traffics to surface raft domains via a novel Golgi-independent pathway. *J Biol Chem* **277**: 48834-48841.

Murata M, Peranen J, Schreiner R, Wieland F, Kerzchalia TV, and Simons K (1995) VIP21/caveolin is a cholesterol-binding protein. *Proc Natl Acad Sci USA* **92**: 10339-10343.

Murphy TV, Gargiullo PM, Massoudi MJ, Nelson DB, Jumaan AO, Okoro CA, Zanardi LR, Setia S, Fair E, LeBaron CW, Wharton M, and Livingood JR (2001) Intussusception among infants given an oral rotavirus vaccine. *New Engl J Med* **344**: 564-572.

Ovchinnikov YA, Luneva NM, Arystarkhova EA, Gevondyan NM, Arzamazova NM, Kozhich A, Nesmeyanov VA, and Modyanov NN (1988) Topology of Na$^+$, K$^+$-ATPase: identification of the extra- and intracellular hydrophilic loops of the catalytic subunit by specific antibodies. *FEBS Letters* **227**: 230-234.

Palandino S, Sarnataro D, Pillich R, Tivodar S, Nitsch L, and Zurzolo C (2004) Protein oligomerization modulates raft partitioning and apical sorting of GPI-anchored proteins. *J Cell Biol* **167**: 699-709.

Parr RD and Ball JM (2003) New donor vector for generation of histidine-tagged fusion proteins using the Gateway Cloning System. *Plasmid* **49**: 179-183.

Parr RD, Storey SM, Mitchell DM, McIntosh AL, Zhou M, Mir KD, and Ball JM (2006) The rotavirus enterotoxin NSP4 directly interacts with the caveolar structural protein caveolin-1. *J Virol* **80**: 2842-2854.

Parton RG (1994) Ultrastructural localization of gangliosides; $_{GM1}$ is concentrated in caveolae. *J Hist Cytochem* **42**: 155-166.

Pike LJ and Casey L (1996) Localization and turnover of phosphatidylinositol 4,5bisphosphate in caveolin-enriched membrane domains. *J Biol Chem* **271**: 26435-26456.

Pike LJ, Han X, Chung KN, and Gross RW (2002) Lipid rafts are enriched in arachidonic acid and plasmenylethanolamine and their composition is independent of caveolin-1 expression: a quantitative electrospray ionization/mass spectrometric analysis. *Biochem* **41**: 2075-2088.

Pike LJ (2003) Lipid rafts: bringing order to chaos. *J Lipid Res* **44**: 655-667.

Pike LJ (2004) Lipid rafts: heterogeneity on the high seas. *Biochem J* **378**: 281-292.

Prashar UD, Hummelman EG, Bresee JJ, Miller, MA and Glass RI (2003) Global illnesses and deaths caused by rotavirus disease in children. *Emerg Inf Dis* **9:**565-572.

Radeva G and Sharom FJ (2004) Isolation and characterization of lipid rafts with different properties from RBL-2H3 (rat basophilic leukaemia) cells. *Biochem J* **380**: 219-230.

Rajagopalan S, Xu Y, and Brenner MB (1994) Retention of unassembled components of integral membrane proteins by calnexin. *Science* **263**: 387-390.

Razani B, Woodman SE, and Lisanti AP (2002) Caveolae: from cell biology to animal physiology. *Pharmacol Rev* **54**:431-467.

Rossen JWA, Buoma J, Roatgeep RHC, Büller HA, and Einerhand AWC (2004) Inhibition of cyclooxygenase activity reduces rotavirus infection at a post binging step. *J Virol* **78**: 9721-9730.

Rothberg KG, Heuser JE, Donzell WC, Ying Y-S, Glenney JR, and Anderson RGW (1992) Caveolin, a protein component of caveolae membrane coats. *Cell* **68**: 673-682.

Sapin C, Colard O, Delmas O, Tessier C, Breton M, Enouf V, Chwetzoff S, Ouanich J, Cohen J, Wolf C, and Trugnan G (2002) Rafts promote assembly and apical targeting of a non-enveloped virus, rotavirus, in Caco-2 cells. *J Virol* **76**: 4591-4602.

Scheffele P. Verkade P, Fra AM, Virla H, Simons K, and Ikonen E (1998) Caveolin-1 and -2 in the exocytic pathway of MDCK cells. *J Cell Biol* **140**: 795-806.

Scherer PE, Lewis RY, Volonté D, Engelman JA, Galbiati F, Couet J, Kohtz S, van Donselaar E, Peters P, and Lisanti MP (1997) Cell-type and tissue-specific expression of caveolin-2: caveolins 1 and 2 co-localize and form stable hetero-oligomeric complexes *in vivo*. *J Biol Chem* **272**: 29337-29346.

Schmid S (1997) Clathrin-coated vesicle formation and protein sorting: an integrated process. *Annu Rev Biochem* **66**: 511-548.

Schnitzer JE, McIntosh DP, Dvorak AM, Liu J, and Oh P (1995) Separation of caveolae from associated microdomains of GPI-anchored proteins. *Science* **269**: 1435-1439.

Schnitzer JE, Lichtenberg D, and Kozlov MM (2003) Temperature dependence of the solubilization of dipalmitoylphosphatidylcholine (DPPC) by the non-ionic surfactant Triton X-100, kinetic and structural aspects. *Chem Phys Lip* **126**: 55-76.

Schoer J, Gallegos AM, Starodub O, Petrescu A, Roths JB, Kier AB, and Schroeder F (2000) Lysosomal membrane cholesterol dynamics: role of sterol carrier protein-2 gene products. *Biochem* **39**: 7662-7677.

Schroeder F and Soler-Argilaga C (1983) Calcium modulates fatty acid dymanics in rat liver plasma membranes. *Eur J Biochem* **132**: 517-524.

Schroeder F (1984) Fluorescent sterols: probe molecules of membrane structure and function. *Prog Lipid Res* **23**: 97-113.

Schroeder F, Morrison WJ, Gorka C, and Wood WG (1988) Transbilayer effects of ethanol on fluidity of brain membrane leaflets. *Biochim Biophys Acta* **946**: 85-94.

Schroeder F and Nemecz G (1990) Transmembrane cholesterol distribution. In: *Advances in Cholesterol Research* (Esfahami M and Swaney J, Eds.) pp 47-87, Telford Press, Caldwell, NJ.

Schroeder F, Jefferson JR, Kier AB, Knittell J, Scallen TJ, Wood WG, and Hapala I (1991) Membrane cholesterol dynamics: cholesterol domains and kinetic pools. *Proc Soc Exp Biol Med* **196**: 235-252.

Schroeder R, London E, and Brown D (1994) Interactions between saturated acyl chains confer detergent resistance on lipids and glycosylphosphatidylinositol (GPI)-anchored proteins: GPI-anchored proteins in liposomes and cells show similar behavior. *Proc Natl Acad Sci USA* **91**: 12130-12134.

Schroeder F, Hubbell T, Colles SM, and Wood WG (1995) Expression of liver fatty acid binding protein in L-cells: plasma membrane response to ethanol. *Arch Biochem Biophys* **316**: 343-352.

Schroeder F, Frolov AA, Murphy EJ, Atshaves BP, Jefferson JR, Pu L, Wood WG, Foxworth WB, and Kier AB (1996) Recent advances in membrane cholesterol domain dynamics and intracellular cholesterol trafficking. *Proc Soc Exp Biol Med* **213**: 150-177.

Schroeder F, Frolov A, Schoer J, Gallegos AM, Atshaves BP, Stolowich NJ, Scott AI, and Kier AB (1998) Intracellular sterol binding proteins, cholesterol transport and membrane domains. In: *Intracellular Cholesterol Trafficking* (Chang TY and Freeman DA, Eds.) pp 213-234, Kluwer Academic Publishers, Boston.

Schroeder F, Gallegos AM, Atshaves BP, Storey SM, McIntosh AL, Petrescu AD, Huang H, Starodub O, Chao H, Yang H, Frolov A, and Kier AB (2001a) Recent advances in membrane cholesterol microdomains: rafts, caveolae, and intracellular cholesterol trafficking. *Exp Biol Med* **226**: 873-890.

Schroeder F, Wood WG, and Kier AB (2001b) Lipid domains and biological membrane function. In: *Cell Physiology Sourcebook: A Molecular Approach*. (Sperelakis N, Ed.) pp 81-94, Academic Press, New York.

Schroeder F, Gallegos AM, Atshaves BP, McIntosh AL, Petrescu AD, Huang H, Chao H, Yang H, Frolov A, and Kier AB (2001c) Recent advances in membrane microdomains: rafts, caveolae and intracellular cholesterol trafficking. *Exp Biol Med* **226**: 873-890.

Schroeder F, Atshaves BP, Gallegos AM, McIntosh AL, Liu JC, Kier AB, Huang H, and Ball JM (2005) Lipid rafts and caveolae organization. In: *Advances in Molecular and Cell Biology* (Frank PG and Lisanti MP, Eds.) pp 3-36, Elsevier, Amsterdam.

Sica D, Boniforti L, and DiGiacomo G (1982) Sterols of *Candida tropicalis* grown on n-alkanes. *Phytochem* **21**: 234-236.

Simons K and Ikonen E (1997) Functional rafts in cell membranes. *Nature* **387**: 569-572.

Simons K and Vaz WL (2004) Model systems, lipid rafts, and cell membranes. *Annu Rev Biophys Biomol Struct* **33**: 269-295.

Skwarek M (2004) Recent controversy surrounding lipid rafts. *Arch Immunol Theor Exp* **52**: 427-431.

Smart EJ, Ying Y-S, Mineo C, and Anderson RGW (1995) A detergent-free method for purifying caveolae membrane from tissue culture cells. *Proc Natl Acad Sci USA* **92**: 10104-10108.

Smart EJ, Graf GA, McNiven MA, Sessa WC, Engelman JA, Scherer PE, Okamoto T, and Lisanti MP (1999) Caveolins, liquid-ordered domains, and signal transduction. *Mol Cell Biol* **19**: 7289-7304.

Smart EJ (2005) Caveolae and the regulation of cellular cholesterol homeostasis. In: *Advances in Molecular and Cell Biology* (Lisanti MP and Frank PG, Eds.) pp 35, Elsevier B.V., Amsterdam.

Song KS, Scherer PE, Tang ZL, Okamoto T, Li S, Chafel M, Chu C, Kohtz DS, and Lisanti MP (1996) Expression of caveolin-3 in skeletal, cardiac, and smooth muscle cells: caveolin-3 is a component of the sarcolemma and co-fractionates with dystrophin and dystrophin-associated glycoproteins. *J Biol Chem* **271**: 15160-15165.

Sot J, Collado MI, Arrondo JLR, Alanso A, and Goui FM (2002) Triton X-100-resistant bilayers: effects of lipid composition and relevance to the raft phenomenon. *Langmuir* **18**: 2828-2835.

Souto RP, Vallega G, Wharton J, Vinten J, Tranum-Jensen J, and Pilch PF (2003) Immunopurification and characterization of rat adipocyte caveolae suggest their dissociation from insulin signaling. *J Biol Chem* **278**: 18321-18329.

Spink CH, Yeager M, and Feigenson GW (1990) Partitioning behavior of indocarbocyanine probes between coexisting gel and fluid phases in model membranes. *Biochim Biophys Acta* **1023**: 25-33.

Stoorvogel W, Oorschot V, and Geuze HJ (1996) A novel class of clathinr-coated vesicles budding from endosomes. *J Cell Biol* **132**: 21-33.

Suhy DA, Giddings TH Jr, and Kirkegaard K (2002) Remodeling the endoplasmic reticulum by poliovirus infection and by individual viral proteins: an autophagy-like origin for virus-induced vesicles. *J Virol* **74**: 8953-8965.

Sweet WD and Schroeder F (1986a) Plasma membrane lipid composition modulates action of anesthetics. *Biochim Biophys Acta* **861**: 53-61.

Sweet WD and Schroeder F (1986b) Charged anaesthetics alter LM-fibroblast plasma-membrane enzymes by selective fluidization of inner or outer membrane leaflets. *Biochem J* **239**: 301-310.

Sweet WD, Wood WG, and Schroeder F (1987) Charged anesthetics selectively alter plasma membrane order. *Biochem* **26**: 2828-2835.

Sweet WD and Schroeder F (1988a) Polyunsaturated fatty acids alter sterol transbilayer domains in LM fibroblast plasma membrane. *FEBS Letters* **229**: 188-192.

Sweet WD and Schroeder F (1988b) Lipid domains and enzyme activity. In: *Advances in Membrane Fluidity: Lipid Domains and the Relationship to Membrane Function* (Aloia RC, Cirtain CC, and Gordon LM, Eds.) pp 17-42, Alan R. Liss, Inc., New York.

Tabas I (1997) Free cholesterol-induced cytotoxicity. *Trends Cardiovasc Med* 7: 256-263.

Talloczy Z, Jiang W, Virgin HW IV, Leib DA, Scheuner D, Kaufman RL, Eskelinen E-L, and Levine B (2002) Regulation of starvation and virus-induced autophagy by elF2α kinase signaling pathway. *Proc Natl Acad Sci USA* **99**: 190-195.

Thomas JL, Holowka D, Baird B, and Webb WW (1994) Large scale co-aggregation of fluorescent lipid probes with cell surface proteins. *J Cell Biol* **125**: 795-802.

Uittenbogaard A, Ying Y-S, and Smart EJ (1998) Characterization of a cytosolic heat-shock protein-caveolin chaperone complex. *J Biol Chem* **273**: 6525-6532.

Uittenbogaard A, Everson WV, Mafveev SV, and Smart EJ (2002) Cholestryl ester is transported from caveolae to internal membranes as part of a caveolin-annexin II lipid-protein complex. *J Biol Chem* **277**: 4925-4931.

van Vliet C, Thomas EC, Merino-Trigo A, Teasdale RD, and Gleeson PA (2003) Intracellular sorting and transport of proteins. *Prog Biophys Mol Biol* **83**: 1-45.

Williams BRG (2001) Signal integration via PKR. *Sci Sig Transd Knowl Environ* **89-re2**: 1-10.

Wood GW, Schroeder F, Igbavboa U, Avdulov NA, and Chochina SV (2002) Brain membrane cholesterol domains, aging and amyloid beta-peptides. *Neurobiol Aging* **23**: 685-694.

Xu A, Bellamy AR, and Taylor JA (2000) Immobilization of the early secretory pathway by a virus glycoprotein that binds to microtubules. *EMBO J* **19**: 6465-6474.

Yarbrough TL, Lu T, Lee H-C, and Shibata EF (2004) Localization of cardiac sodium channels in caveolae-rich membrane domains: regulation of sodium current amplitude. *Circ Res* **90**: 443-449.

Zhang M, Zeng CQ-Y, Morris AP, and Estes MK (2000) A functional NSP4 enterotoxin peptide secreted from rotavirus-infected cells. *J Virol* **74**: 11663-11670.

Zhang W, McIntosh AL, Xu H, Wu D, Gruninger T, Atshaves BP, Liu JCS, and Schroeder F (2005) Structural analysis of sterol distribution in the plasma membrane of living cells. *Biochem* **44**: 2864-2984.

APPENDIX A

STRUCTURAL ANALYSIS SUMMARY OF ISOLATED MEMBRANE MICRODOMAINS

outer leaflet
inner leaflet

Non-raft   DRM   NDCR   ACR
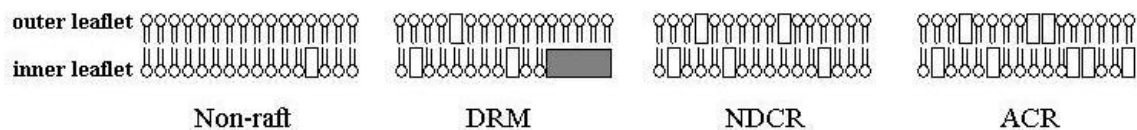
⌂ = phospholipid

☐ = cholesterol/sterol

▨ = cholesterol/sterol crystal

Fluidity Trends:
1. Sterol: Non-raft > DRM > NDCR > ACR
2. Non-raft acyl chain: Non-raft, DRM > NDCR > ACR
3. Raft acyl chain: Non-raft > DRM > NDCR > ACR
4. General acyl chain: Non-raft > DRM > NDCR > ACR
5. Inner leaflet acyl chain: Non-raft, DRM > NDCR > ACR
6. Outer leaflet acyl chain: Non-raft > DRM > NDCR > ACR

APPENDIX B

CSC FRACTIONATION OF CAVEOLAE FROM EPITHELIAL CELLS

Briefly, cells were washed and scraped in cold PBS before being centrifuged. Cell pellet was suspended in 2 ml 0.25 M sucrose, 1 mM EDTA, 20 mM Tris-base, pH 7.8, and cavitated under nitrogen to produce a cell homogenate. The homogenate was centrifuged, then the post nuclear supernatant (PNS) was separated from the cell debris and clarified by high speed centrifugation. The clarified PNS (supernatant) and debris pellet were loaded onto separate discontinuous sucrose density gradients, centrifuged, and the proteins bands at specific gradient layers extracted. The 35/40 and 40/55 interface bands taken from the supernatant gradient were pooled, centrifuged, and the pellet retained as an ER-enriched fraction. The 27/29, 29/32, and 32/35 bands were pooled to produce a PM-enriched fraction, sonicated briefly three times to disrupt the large membrane sheets, and mixed with sepharose bead-bound concanavilin A in column buffer 1 (0.14 M KCl, 0.01 M HEPES, 1 mM $MgCl_2$, 1 mM $MnCl_2$, pH 7.8 with KOH) . The material was mixed via nitrogen bubbling, allowed to bind for 10min, then transferred to a gravity column and allowed to settle for 15 min. The settled column was drained to the bead bed level before being washed multiple times with two bed volumes of column buffer 1 and drained back to the top of the column bed. Individual 12ml aliquots of column buffer 2 (0.5 M α-methyl-mannopyranoside in buffer 1) were then added to the column and allowed to displace the bound material for 10min before being drained into individual centrifuge tubes. The buffer 2 washes were repeated six times before the eluted material was centrifuged and the caveolae-enriched pellet was suspended in small volumes of buffer 2 with protease inhibitors.
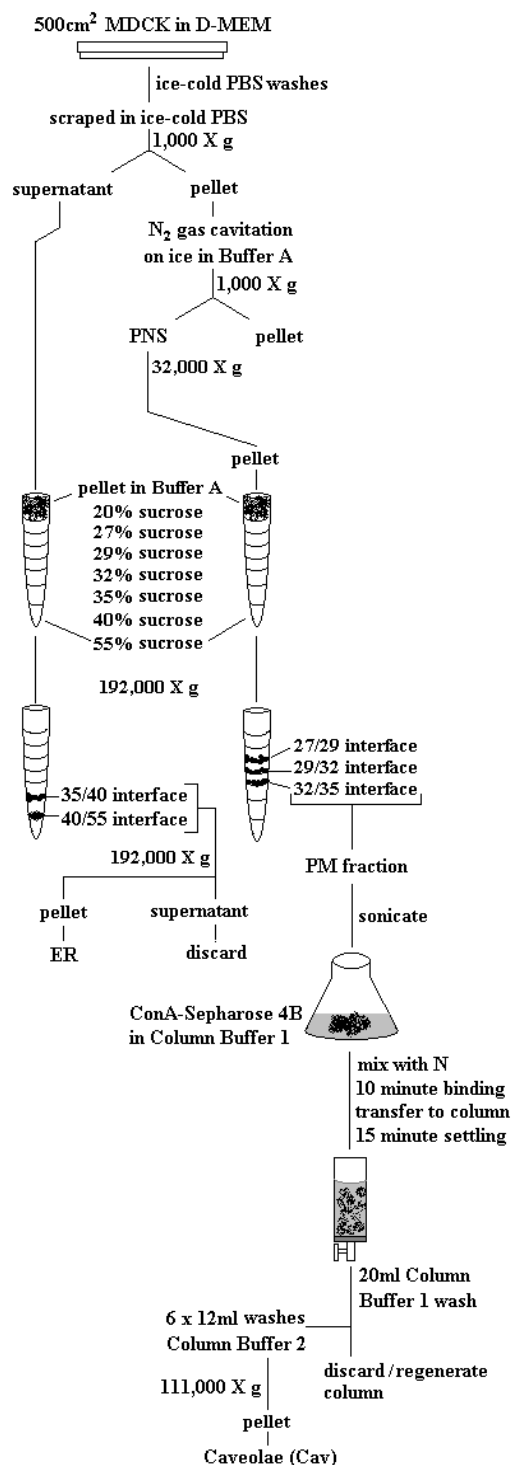
VITA

Name:	Stephen Michael Storey
Address:	Texas A&M University College of Veterinary Medicine Department of Veterinary Pathobiology MS 4467 College Station, TX 77843
Email Address:	sstorey@cvm.tamu.edu
Education:	B.S., Genetics, Texas A&M University at College Station, 1996 Ph.D., Veterinary Microbiology, Texas A&M University at College Station, 2006